Human alternatives to foetal bovine serum for the expansion of human adipose-derived stem cells

Written by

Aurona Gerber

12179206

Submitted in fulfilment of the degree

MSc: Medical Immunology

at the Faculty of Health Sciences

Department of Immunology

University of Pretoria

2021

Supervisor

Prof. Michael S. Pepper

Institute for Cellular and Molecular Medicine (ICMM), Department of Immunology

Faculty of Health Sciences, University of Pretoria

Declaration of original authorship

I, Aurona Gerber, hereby declare that this dissertation, which I hereby submit in fulfilment of the requirements for the degree MSc: Medical Immunology at the University of Pretoria, is my own work and has not been previously submitted for a degree at this or any other university.

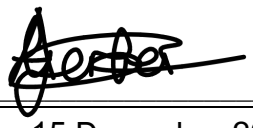

Date: 15 December 2021

Faculty of Health Sciences

Department of Immunology

Institute for Cellular and Molecular Medicine

University of Pretoria

South Africa

Acknowledgements

I would like to thank my supervisor Prof Michael S Pepper for providing me the opportunity to complete this work in his laboratory and the ongoing support towards bettering myself as a scientist.

Thank you to lab manager Candice Murdoch and Dr Chrisna Durant for always be available and willing to help with planning and technicalities of the experiments.

Thank you to SANBS and Esmé van Wyk at the STS division. Without your willingness to help and provide blood products this project would not have succeeded.

Thank you to the staff at the CRU who helped with the blood product collection

Thank you to the National Research Foundation and ICMM for your continued financial support throughout the completion of this degree.

To my lab colleagues Candice Herd, Elize Wolmarans, Juanita Mellet Potgieter, and Jamie Mollentze for all the office lunch hours and the willingness to add some fun into the long days where science happened even though you planned. May we never see fungus again. Thank you Simoné for the random facetime calls to have long chats I didn't realise I needed. Thank you for slogging through the mud with me. We made it.

Thank you to my family for their unwavering support and their steadfast belief that I can do this. It helps to have someone believe in you who knows the struggles of academia.

Thank you to my husband, Ruco, for the endless motivation and support during the long lab days, the cranky writing days, the whiny fungus days, and the wonderful smooth-sailing days. Thank you for reminding me that baby steps will get me there in the end. Thank you for the coffee in bed and for the food and wine all the times I needed to take a step back from it all.

Lastly, I thank God for His faithful guidance on this difficult journey. To Him goes all the glory.

I dedicate this work to:

My parents for always reminding me that the mountain in front of me is not that huge if you take one step at a time.

My husband for his unwavering belief in my perseverance.

Executive summary

The use of human adipose derived stem/stromal cells (hASCs) in a therapeutic setting is has increased research in the field with various clinical trials currently being conducted (1). However, the use of foetal bovine serum (FBS) as a standard hASC culture media supplement poses challenges towards a good manufacturing practices (GMP) compliant therapeutic hASC product. Human blood component alternatives to FBS for cell culture serum supplementation were investigated for compliance to good manufacturing practices (GMP) when considering hASCs for therapeutic use.

A head-to-head comparison of five human alternatives to FBS for hASC culture medium supplementation was completed. hASCs were expanded in five human alternatives and FBS, and the morphology, proliferation, viability, and retention of adipogenic potential of ASCs were investigated and compared. All human alternatives resulted in faster proliferation compared to FBS. Pooled human platelet lysate (pHPL) and platelet-rich-plasma (PRP) were identified as the best alternatives for hASC expansion *in vitro* as they resulted in faster hASC proliferation than human serum (HS), fresh-frozen plasma (FFP), platelet-poor plasma (PPP), and FBS.

hASCs were able to differentiate into adipocytes in pHPL and PRP (the two human alternatives resulting in the fastest proliferation) and FBS. The study results lead to a conclusion that it is possible to use human alternatives to FBS for *in vitro* hASC expansion as the first step towards producing a GMP compliant hASC product for use in regenerative medicine and cellular therapy approaches.

Keywords: adipose-derived stromal/stem cells; good manufacturing practices, foetal bovine serum; platelet-rich plasma, platelet-poor plasma, platelet lysate, human serum

Table of Contents

List of abbreviations

Abbreviation	Definition
7AAD	7-Amino-actinomycin
ASC	Adipose-derived stromal/stem cells
BAT	Brown adipose tissue
BP	Band pass
CAL	Calibration factor
CAR	Chimeric antigen receptor
CD42a	Cluster of differentiation 42a
CD61	Cluster of differentiation 61
CGM	Complete growth medium
CRU	Clinical Research Unit
DAPI	4',6-diamidino-2-phenylindole
DMEM	Dulbecco's Modified Eagles Medium
DMSO	Dimethyl sulfoxide
dsDNA	Doube stranded DNA
EGF	Epidermal growth factor
ESCs	Embryonic stem cells
FBS	Foetal bovine serum
FFP	Fresh frozen plasma
FGF	Fibroblast growth factor
FITC	Fluorescein isothiocyanate
FL	Fluorescent detector channels
FS	Forward scatter
GCCP	Good cell culture practise
GMP	Good manufacturing practices
hASCs	Human adipose-derived mesenchymal stem/stromal cells
HLA	Human leukocyte antigen
HS	Human serum
IFATS	International Federation for Adipose Therapeutics and Science
iPSCs	Induced pluripotent stem cells
ISCT	International Society for Cellular Therapy
LP	Long pass

MSCs	Mesenchymal stromal/stem cells
MuSCs	Muscle satelite/stem cells
nPRP	Non-activated platelet rich plasma
OD	Optical density
p/s	Penicillin-streptomycin
PBS	Phosphate buffer saline
PCs	Platelet concentrates
PDGF	Platelet-derived growth factor
PE	Phycoerythrin
pHPL	Pooled human platelet lysate
PI	Propidium iodide
PLTs	Platelets
PPP	Platelet-poor plassma
PRP	Platelet-rich plasma
PS	Phosphatidylserine
PSCs	Pluripotent stem cells
QC	Quality control
RT	Room temperature
SANBS	South African National Blood Service
SP	Short pass
SRB	Sulforhodamine B
SS	Side scatter
STS	Specialised Therapeutics Services
SVF	Stromal vascular fraction
TCA	Trichloroacetic acid
TGF-β	Transforming growth factor-β
tPRP	Thrombin-activated platelet rich plasma
UP	University of Pretoria
VDC Ruby	Vybrant® DyeCycle™ Ruby
VEGF	Vascular endothelial growth factor
WAT	White adipose tissue
WBC	White blood cell
α-MEM	Minimum Essential Medium Eagle – Alpha Modification

List of figures

List of tables

Chapter 1: Introduction

This chapter, Chapter 1, is the introductory chapter to this dissertation that reports on a study investigating which of five human alternatives produced from various components of whole blood is a suitable replacement to foetal bovine serum (FBS) for *in vitro* culture of human adipose derived stromal/stem cells (hASCs).

Cellular therapy and regenerative medicine have increased interest in using stem cells for treatments across various fields such as bone and cartilage repair, ischaemic diseases, transplantation, and cancer treatments (2–6). The unique regenerative capacity of stem cells has been investigated for use in cell-based treatments in transplantation and tissue engineering. Several clinical trials with promising results are currently underway (1,2,7–9).

Mesenchymal stromal/stem cells (MSCs) are present in adult tissues, including bone marrow, adipose tissue, umbilical cord blood, and dental pulp. Their widespread availability makes them attractive for regenerative medicine (10–14). One of the major types of MSCs currently being investigated is adipose-derived stromal/stem cells (ASCs). ASCs can be obtained by minimally invasive means and are isolated from routinely discarded adipose tissue where they are present in abundance (12,14,15). ASCs have been found to differentiate reproducibly into a variety of cell types *in vitro.* Additionally, they are good candidates for autologous and allogeneic therapeutic use as they can differentiate into multiple cell types (are multipotent), will not elicit an inflammatory or immune response in the host after transplant (are immunoprivileged), and can alter the immune response through various means as discussed in section 2.2 (immunomodulatory) (16,17).

Some concerns remain before ASC-based therapy can be considered for routine treatment. Traditionally, ASCs are expanded and differentiated in a medium containing FBS (18–20). Before *ex vivo* expanded and differentiated cells can be considered for therapeutic products, a crucial requirement is their adherence to good manufacturing practice (GMP) guidelines (21–25). The presence of xenogeneic substances like FBS in ASC culture media poses several challenges in terms of their safety as a cell product due to possibly eliciting an immune response to the foreign antigens of bovine origin (xeno-immunisation), batch to batch variation, and potential contamination with prions,

mycoplasma, or viruses (19,26–28). Various alternatives of human and chemical origin have been investigated. Still, little consensus has been reached as to which is the superior FBS replacement. hASCs expanded *in vitro* in media containing human alternatives have been found to have a better morphology and proliferate faster while retaining their immunophenotype compared to FBS (28,29,38–41,30–37). According to the author's knowledge, current studies have mainly focused on one or two alternatives to FBS, with no studies comparing all the human alternatives used in this study side-by-side. To determine a suitable replacement for FBS from human blood products, ASCs expanded in the different human alternatives must adhere to previously published guidelines by Bourin et al. (2013), namely: 1) adherence to plastic; 2) expression of a specific cell surface immunophenotype; 3) retention of trilineage differentiation ability.

This study investigated which of five human alternatives produced from various components of whole blood is a suitable replacement to FBS while adhering to the published guidelines. The study had four objectives. The first was to obtain and perform quality control measurements on five blood products chosen as human alternatives to FBS, namely pooled human platelet lysate (pHPL), human serum (HS), fresh frozen plasma (FFP), platelet-poor plasma (PPP), and platelet-rich plasma (PRP)). The second objective was to use cryopreserved hASCs to investigate the proliferation and morphology of the hASCs expanded and maintained in human alternatives compared to FBS. The third objective was to investigate cell number, immunophenotype, cell cycle, and viability of hASCs expanded and maintained in the human alternatives compared to FBS using flow cytometry. The last objective was to investigate the retention of adipogenic differentiation potential of hASCs expanded and maintained in human alternatives and FBS.

A study to ensure GMP compliance of a therapeutic cell product is complex and vast. Inherent variability is a natural consequence when using biological products, such as primary cells and blood product donations. Therefore, the scope of this study was limited to comparing the human alternatives to FBS. Furthermore, due to time limitation the investigation of ASC differentiation potential was limited to the retention of adipogenic potential as a characteristic of ASC adherence to published guidelines.

The remainder of this document is structured as follows: Chapter 2 is the literature review, Chapter 3 presents an overview of the experimental procedures used throughout this study. The production of the human alternatives and results from quality control measurements (the first objective) are described in Chapter 4. Chapter 5 focuses on the proliferation and morphology of ASCs in human alternatives compared to FBS (the second objective). The third objective investigated hASC cell counts, immunophenotype, cell cycle, and cell viability in the different culture media, discussed in the main flow cytometry study in Chapter 6. The last objective, retention of adipogenic differentiation potential of hASCs in the various media, is investigated in Chapter 7. Lastly, the future perspectives and concluding remarks from this study are discussed in Chapter 8.

Chapter 2: Literature review

2.1 Stem cells, regenerative medicine, and cell-based therapy

Stem cells are defined as a clonal population of self-renewing, multipotent cells able to generate more than one cell type (13). Clonal expansion refers to the ability of cells to grow in number during culture from a single self-renewing cell. Self-renewal is a functional characteristic of stem cells that refers to their ability to produce two daughter cells identical to the mother cell seemingly indefinitely without undergoing cell cycle arrest or entering senescence (13). Potency refers to the potential of stem cells to produce a variety of differentiated cell lineages from a progenitor cell type. Stem cells may produce multiple differentiated cell types (multipotency or pluripotency) or give rise to a single cell type (unipotency) (13).

Stem cells are present throughout human development and can be isolated from tissues at the earliest stages of embryogenesis through to adulthood. During embryonic development, three cell layers (inner endoderm, middle mesoderm, and outer ectoderm) form the germ layer from which all adult tissue cells develop (13). The endoderm develops into tissues in the gut and internal organs such as the lungs, liver, and pancreas. Bone marrow, blood, and muscle, among others, develop from the mesoderm with the ectoderm giving rise to nervous tissue and skin (13). Embryonic stem cells (ESCs) are pluripotent as they are isolated from the inner cell mass at the blastocyst or morula stage during embryogenesis (13,42,43) and contribute to the development of all somatic lineages (13). Ethical concerns surrounding the point where life begins limit the utility of ESCs and research using these cells is not permitted in many countries, including South Africa (44). Stem cells isolated from fully developed tissues are considered adult stem cells. Adult stem cells can be pluripotent, multipotent, or unipotent and function in the daily rejuvenation of tissues through *in situ* differentiation (13). This includes haematopoietic stem cells found in the bone marrow that form all blood and immune cells in the body, mesenchymal stem/stromal cells that form multiple cell lineages including bone, cartilage, and fat, and various types of tissue-specific progenitors such as muscle satellite cells (12,13,16). Haematopoietic

stem cells and mesenchymal stem/stromal cells for research purposes are abundant in medical waste products such as umbilical cord and cord blood, lipoaspirate and solid fat tissue, and dental pulp (12,13). Towards a sustainable, ethically uncontroversial therapeutic product, researchers have found a way to create pluripotent stem cells (PSCs) (called induced pluripotent stem cells (iPSCs)) from terminally differentiated cells through the transduction of these cells using four transcription factors associated with pluripotency (45).

2.1.1 Regenerative medicine and cell-based therapy

Regenerative medicine may include multiple treatments ranging from surgery and surgical implants to cell- or gene-based therapies and organ transplants (46). The uncertainty regarding what regenerative medicine entails may be clarified by the definition of Mason & Dunnill (2008). These authors defined regenerative medicine as follows: “Regenerative medicine replaces or regenerates human cells, tissue or organs, restoring or establishing normal function”. This definition therefore includes the use of gene therapies, tissue engineering and new tissue generation, small molecule drugs (47), and stem cells in cell-based therapies and tissue regenerating treatments (46,47).

Cell therapy uses cells as medicine to treat certain conditions. Similarly, gene therapy comprises genetic supplementation or correction through gene-delivery mechanisms, such as viral vectors (47). Cell and gene therapy may also be combined to obtain a specified treatment. Instead of delivering the gene product directly to patient cells *in vivo*, the gene product is delivered into patient cells *ex vivo*, where extracted cells are modified and expanded *in vitro* prior to transplantation. An example of this scenario would be the use of iPSCs where readily available somatic cells are reverted to the pluripotent stem cell state (2,45). In all these scenarios, cells and genes are used as medicine instead of conventional drugs. Most cell therapies currently involve the isolation and transplantation of cells after a period of *in vitro* expansion. Implantation of whole tissues or organs obtained from tissue engineering that contain donor cells may also be considered a form of cell therapy (47). It is important to note that cell and gene therapies are currently not standard forms of treatment but are mainly experimental in nature, except for chimeric antigen receptor (CAR) T-cell therapy (47).

CAR T-cell treatment of cancer, specifically $CD19^+$ B-cell malignancies, is currently the best example of a combination of cell- and gene therapy (Figure 2.1). In short, it requires the collection of patient T-cells (autologous T-cells) through leukapheresis. The obtained white blood cell product is enriched for T lymphocytes by removing myeloid cells, red blood cells, natural killer cells, and malignant cancer cells (7). Transgenes that encode a synthetic receptor targeting surface antigens on malignant cells are delivered to the T-lymphocytes via transduction of a viral vector. These steps are followed while patients undergo conditional chemotherapy. Before transplantation, *ex vivo* expansion of the engineered T-cells takes place to obtain clinically relevant cell numbers. This strategy allows the reprogramming of one's own T-lymphocytes to express the CAR targeting surface markers on malignant cells leading to destruction of the malignant cells by T-lymphocytes (7,8).

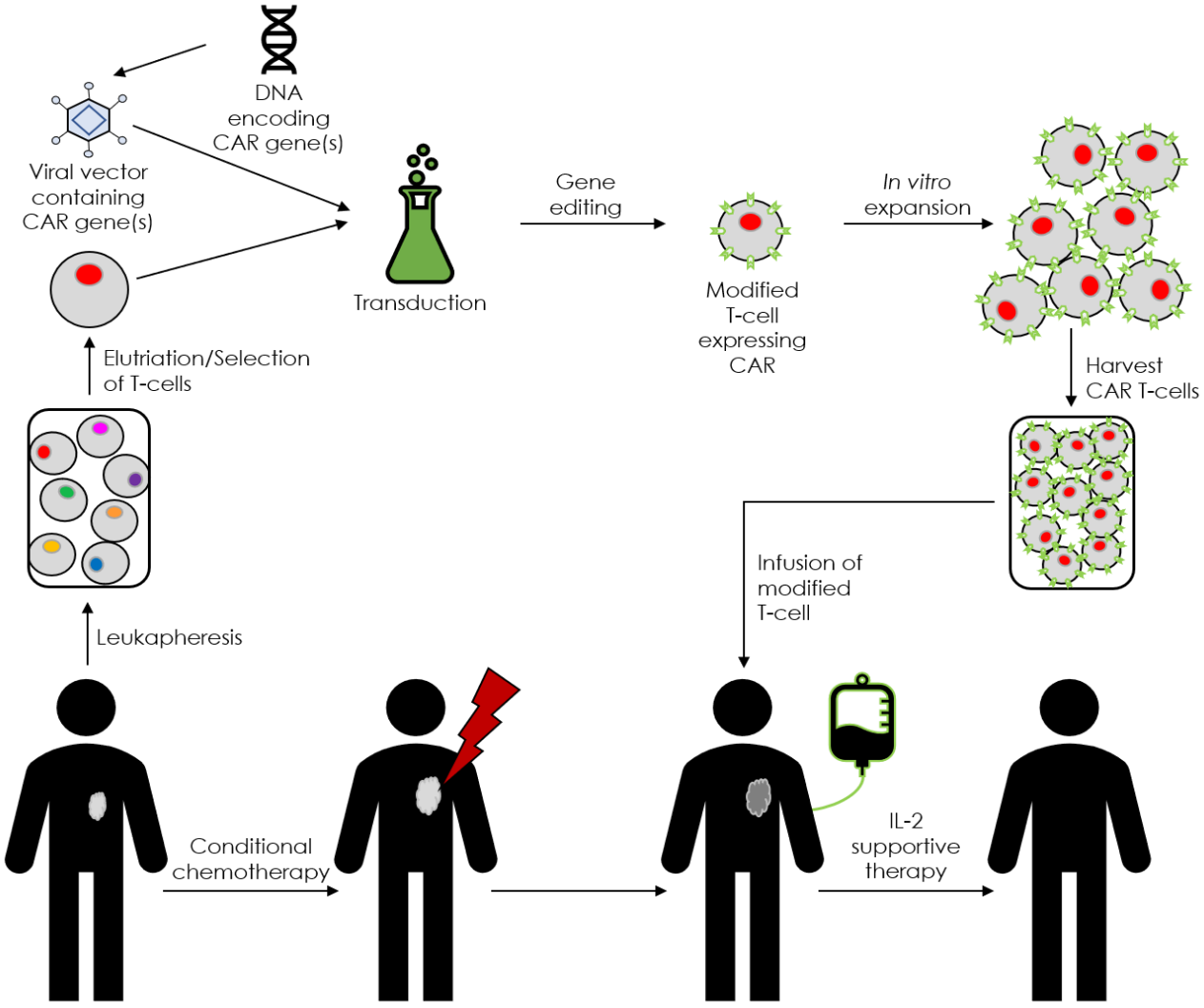

Figure 2.1: CAR T-cell production.
Description of CAR T-cell production where patient T-lymphocytes are harvested, genetically modified to target malignant cells, and expanded ex vivo before transplantation. (used and adapted with permission from Lipowska-Bhalla, Gilham, Hawkins, & Rothwell, 2012)

Apart from cell therapy to treat cancer, interest in the use of cell therapy for bone and cartilage repair (3,4), treatment of ischaemic diseases (48), soft tissue growth (49), wound healing (50,51) and immune disorders (52–54) is increasing globally. A combination of cell and gene therapies has been used to treat disease but many challenges still remain (2). Junctional epidermolysis bulbosa, a hereditary disease of the skin that causes blistering due to gene mutations affecting the extracellular matrix of skin cells, has been treated with a combination of cell and gene therapy (2,55). The authors obtained autologous epidermal keratinocyte stem cells from the epithelia present in the affected patient's skin from a biopsy specimen that did not present with

blistering. The cells present in this specimen were genetically engineered to express normal laminin. A normal skin graft was produced (termed holoclones) and transplanted, obtaining an 80% generation of healthy skin in the patient (2,47,55).

Similarly, cell therapy has been used to treat cardiac muscle loss after an event such as a myocardial infarction. Human ES cell-derived cardiac progenitor cells have been shown to engraft and re-muscularise the myocardium after being injected into rodents shortly after an infarct (2,56). A concern when using ESCs is that the cells from the inner mass of a blastocyst can differentiate into all cell types in the body (ESCs are nascent) and as such, could form tumours containing various types of tissues (termed teratomas) when used as a treatment in cell therapy. Furthermore, the allogeneic nature of these cells may pose a risk for an immunological response (47), aside from the ethical concerns raised earlier (44).

Additional to cardiac muscle, treating skeletal muscle disorders such as Duchenne's muscular dystrophy with a combination of cell and gene therapy has been investigated. Autologous myogenic precursor cells (myoblasts) have been used in the treatment of Duchenne's. Still, treatment efficiency was low due to their inability to replenish the muscle stem cell reservoir and poor engraftment. Subsequently, cell therapy using human adult muscle stem cells (MuSCs, also known as muscle satellite cells) has been attempted. MuSCs are challenging to expand in culture due to a loss of stem cell potential and are in short supply, limiting this therapy's clinical potential (2,57–59).

PSCs have been used *in vitro* and in murine models to generate a variety of blood cells. PSCs may be differentiated into megakaryocytes for platelet supply, haematopoietic stem cells to produce any leukocyte lineage or even T-cells for CAR T-cell therapy (60–64). These approaches enable enhanced safety and predictability of blood supply, the possibility of ready to use products when patients require bone marrow transplants or treatment for cancer, as well as treatment for sickle-cell anaemia and life-threatening haemorrhaging (2).

iPSCs may contribute towards basic research regarding certain diseases because iPSCs may be produced from a patient's cells containing the disease-causing mutation. The effects of the mutation and the potential gene therapy approaches can be investigated *in vitro*. iPSCs are especially advantageous in diseases of a neurological

nature, as it is challenging to obtain biopsies from patients for *in vitro* studies (65). In treating these types of conditions, gene therapy may be used to rectify the genetic defect before transplantation back into the patient (47). These cells will be an autologous treatment which reduces potential immune rejection present in ESC or allogeneic cell therapy; however, there are still concerns regarding the possible generation of tumours when using iPSCs (47).

The wide range of diseases that may potentially be treated using stem cell and cell-based therapies has increased expectations regarding cell replacement and regenerative medicine. Research in the fundamental biology of stem cells and their mechanisms of differentiation has subsequently been promoted (2,66). This growing knowledge and the continually increasing use of stem cells in clinical applications mean that issues of safety, efficacy, reproducibility, and quality are at the forefront of research in this field (67). Stem cell culture and isolation procedures, legislation, and terminology must be standardised globally to ensure GMP and clarity when stem cells are considered for use in patients (15,51,68,69).

2.2 Mesenchymal stromal/stem cells

MSCs are heterogeneous adult stem/stromal cells found in several adult tissues (70). There is some confusion regarding their nomenclature. The International Society for Cellular Therapy (ISCT) has proposed that cells isolated from mesenchymal tissue with the ability to adhere to plastic be called “mesenchymal stromal cells”. The term “mesenchymal stem cells” is proposed for plastic adherent, self-renewing, and multipotent cells (16). MSCs have conventionally been isolated from bone marrow and were described as non-phagocytic fibroblast cells able to form adherent colonies in culture (70,71). It has since become apparent that MSCs are present in various tissues, including adipose tissue, umbilical cord, dental pulp, and Wharton’s jelly (10,15,70). In a joint statement, the ISCT and International Federation for Adipose Therapeutics and Science (IFATS) recommended that MSCs isolated from adipose tissue be termed adipose-derived stromal cells (abbreviated ASCs) while MSCs isolated from bone marrow remain MSCs (17). The procedure used to isolate MSCs from adult bone marrow is invasive and yields low stem cell counts compared to ASCs extracted from adipose tissue (16,69). ASCs can be obtained in high numbers from lipoaspirate with minor donor site morbidity and thus are an excellent alternative source of MSCs to bone marrow-derived MSCs (69). MSCs lack a unique identifying stem cell marker but can be identified by an expressed surface phenotype as proposed by the ISCT and IFATS, described in detail in 2.3.2.1 below (13,16,17,70).

Besides the stem cell characteristics, MSCs have various immunomodulatory properties resulting from secreted factors and cell-to-cell interactions, increasing their attraction for cell therapy (13,69,70,72). MSCs reduce the mobilisation of neutrophils, macrophages, and dendritic cells to damaged tissue (70,72). MSCs also play a role in inhibiting neutrophil apoptosis, reduce endothelial tissue binding, and stimulate neutrophil cytokine secretion (70). The immunomodulatory effects of MSCs on mast cells involve limiting degranulation and reducing chemotaxis (70,72). MSCs also modulate lymphocytes as they inhibit lymphocyte proliferation, reduce pro-inflammatory cytokine release from lymphocytes, and promote the release of anti-inflammatory cytokines (72). Natural killer cell activation is inhibited along with a

decrease in their cytotoxic ability by MSCs, among other described immunomodulatory effects (72).

Furthermore, MSCs play a role in tissue regeneration by migration to the site of injury or inflammation (6,73), cell-to-cell contact, and secretion of trophic factors to create a reparative milieu. In cooperation with immunomodulation, MSCs promote tissue repair by promoting angiogenesis, having an antiapoptotic effect, reducing fibrosis at the site of tissue repair, and promoting proliferation (70,72,74–76). Initially, regeneration of damaged tissue by transplanted MSCs was thought to be dependent on engraftment at the injury site. Further research revealed tissue regeneration without engraftment, which is postulated to result from MSCs' ability to create a microenvironment promoting self-regeneration in damaged tissues (70,72).

The characteristics of MSCs outlined above make their use in regenerative medicine attractive. More than 1200 clinical trials in multiple stages are currently registered worldwide on clinicaltrials.gov (1), for treatments ranging from diabetic nephropathy to knee osteoarthritis and respiratory distress syndrome.

2.3 Adipose-derived stromal/stem cells

ASCs can be isolated from adipose tissue or lipoaspirate routinely discarded as medical waste after surgical procedures such as lipoplasty and abdominoplasty. Enzymatic digestion, by collagenase, dispase, trypsin, or similar enzymes, of minced adipose tissue releases the stromal vascular fraction (SVF) from the extracellular matrix, which contains 15-30% adipose-derived stromal cells (17). The SVF is heterogeneous containing various cell types including ASCs, endothelial cells, lymphocytes, fibroblasts, and pericytes, among others (17). Seeding the SVF in culture medium allows for the enrichment of ASCs in the heterogeneous cell mixture through plastic adherence. The resulting adherent ASC population *in vitro* in cell culture is by no means homogenous but is less heterogeneous than SVF, and can differentiate into osteoblasts, chondrocytes, myocytes, and adipocytes (17).

In vitro cell culture requires that the culture medium contain the necessary nutritional components needed for cell growth including amino acids, monosaccharides, vitamins, inorganic ions and trace elements (26). Basal culture media such as Dulbecco's Modified Eagle Medium (DMEM) contain inorganic salts, amino acids and vitamins (77).

A basal medium such as DMEM is supplemented with serum produced from plasma. Serum is added to medium to provide essential nutrients such as amino acids, vitamins, salt, and nucleic acid derivatives. Serum also contains components promoting adherence such as fibronectin and laminin that allow cells to adhere to culture vessels and expand using the extracellular matrix. The production of serum from plasma means that serum contains various hormones and growth factors such as insulin and fibroblast growth factor that allow cell proliferation. The composition of serum and its addition to culture medium maintains a physiological balance for cell growth *in vitro* (26,78). Natural medium is usually derived from animal tissue, with animal-derived serum being the most widely used addition for tissue culture. The current standard serum used in *in vitro* tissue culture is bovine serum (26).

2.3.1 Proliferation, cell cycle, cell death

Cell proliferation is the increase in cell number observed after a period in culture, whereas cell growth is related to the changes in size, shape and internal complexity of cells. Cell proliferation, growth, and death are intricately linked by progression through the cell cycle (78–81), which can be affected by the external environment, such as culture medium, and medium additions like serum or other factors (78).

The progression of cells through the cell cycle, resulting proliferation, and potential cell death are important factors to consider when assessing the safety and quality of cells intended for therapeutic use. Faster proliferation in culture is desired to reduce the time needed for *in vitro* expansion, but uncontrolled proliferation or cell death may indicate that cells fail to complete essential cell cycle processes or that the internal or external environment is unfavourable.

The cell cycle consists of four phases (summarised in Figure 2.2) governed by a series of restriction points or "checkpoints" which determine whether the cell can move to the next phase. The increase in cell number (progenitor cells) observed during proliferation results from the M phase during the cell cycle. The M phase consists of two significant events, nuclear division (mitosis) and cytoplasmic division (cytokinesis). Mitosis consists of prophase, metaphase, anaphase, and telophase, during which chromosomes segregate and the nucleus divides into two daughter nuclei. The cytoplasm divides in two during cytokinesis which usually happens at the same time as telophase, resulting in two genetically identical daughter cells (80). Following the M phase, the cell enters the first gap (G_1) phase (80). The checkpoint near the end of the G_1 phase is crucial as this allows the cell to enter the senescence or G_0 (resting) phase due to unfavourable external conditions or other cell signals. Senescence refers to cell cycle arrest due to aging as opposed to quiescence that refers to cell cycle arrest due to unfavourable external conditions such as insufficient growth factors or nutrition (82). Cells can remain in G_0 for an extended time before resuming proliferation and progressing through the cell cycle. The two gap phases (G_1 and G_2) are more than just delays in the cell cycle. This allows the cell to grow in size, accumulate mass, and monitor its internal and external environment ensuring optimal conditions for proliferation (80). If the G_1 checkpoint is passed, cells commit to proliferation and enter

the S (synthesis) phase, where the genome is replicated. The duplicated DNA integrity is assessed at another checkpoint, after which the cell progresses to the second gap (G_2) phase before entering the M phase again. The G_1, S, and G_2 phases together make up interphase. Interphase and the M phase together complete the cell cycle.

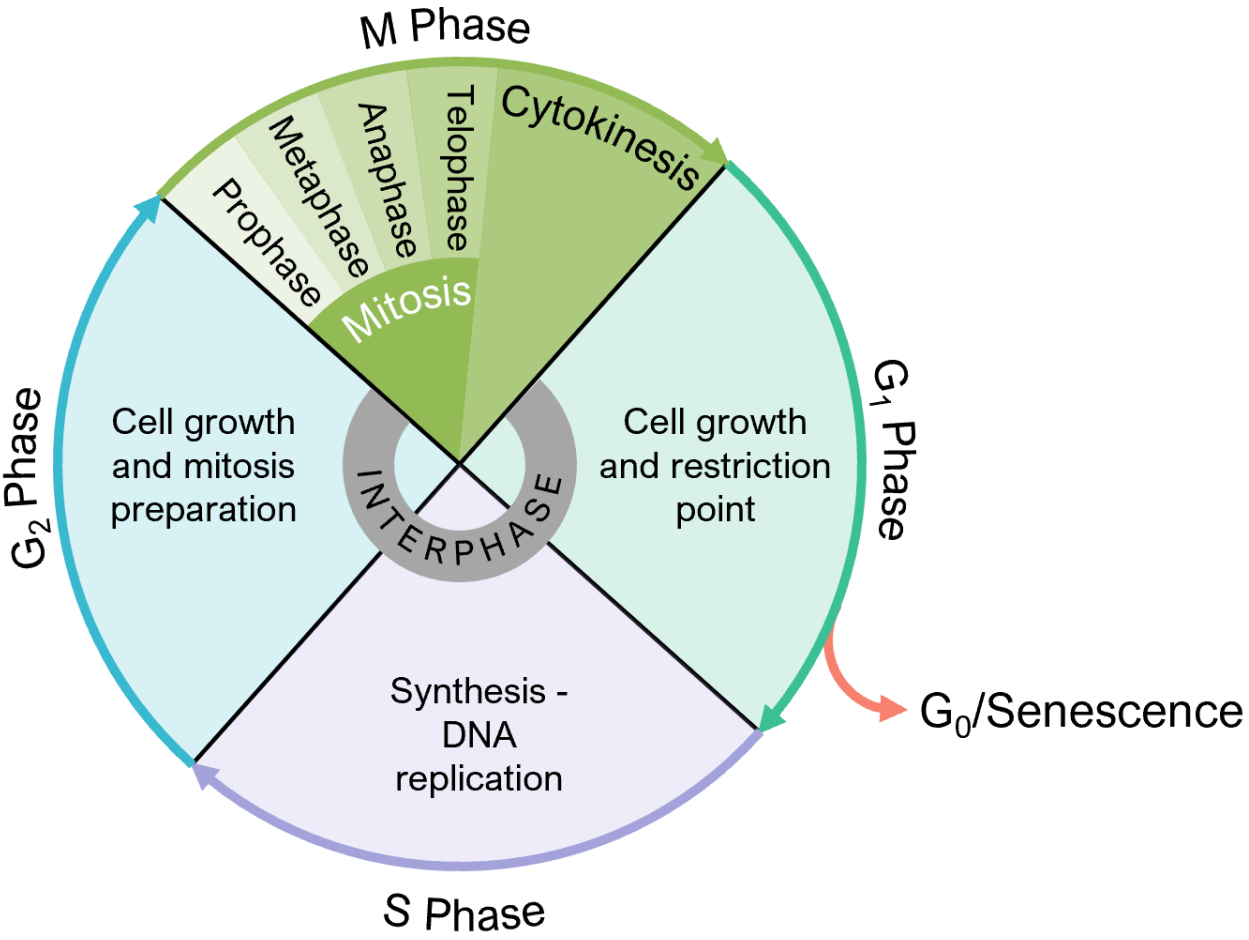

Figure 2.2: Cell cycle summary
The four phases of the cell cycle, M, G_1, S, and G_2. The decision for a cell to continue with proliferation or remain senescent (G_0) occurs at the restriction point near the end of G_1. DNA is replicated during the S phase before entering the last growth phase (G_2) and continuing to nuclear and cytoplasmic division in the M phase. Figure made by candidate.

Progression through the cell cycle is a tightly regulated process. The restriction point is the checkpoint where the cell commits to proliferation independent of environmental signals. Other critical checkpoints are DNA structure checkpoints, where cell cycle arrest occurs due to incomplete DNA replication or insufficient DNA integrity (83). Table 2.1 summarises each phase and its respective features.

Table 2.1: Cell cycle phases and features summary.

State	Phase	Description
Senescent or resting	Gap 0 (G_0)	The cell has exited the cell cycle and has stopped growth and proliferation. Terminally differentiated or undifferentiated cells can stay senescent for extended periods.
Interphase	Gap 1 (G_1)	Cell mass, volume, and size increase (growth) during the growth phase. The cell prepares for DNA replication. The DNA content is 2N. The G_1 checkpoint ensures that the cell is ready for the S phase. After the restriction checkpoint is passed, the cell commits to the cell cycle.
	Synthesis (S)	The genome is duplicated during DNA replication; histones are produced. The DNA content is variable; between 2N-4N
	Gap 2 (G_2)	Cell growth occurs along with microtubule and cell content production in preparation for cell division. The G_2 checkpoint ensures the cell is ready to enter the M phase. DNA content is 4N.
Cell division	Mitosis (M)	Growth is arrested, sister chromatids (4N) are separated (prophase, metaphase, anaphase) followed by nuclear (telophase/karyokinesis) and cytoplasmic (cytokinesis) division resulting in two identical daughter cells (2N).

Compiled from Alberts et al., 2017; Alenzi, 2004; Bertoli et al., 2013; Björklund, 2019.

Any disruption of the orderly progression through the cell cycle may activate cell death signalling pathways. Uncontrolled proliferation or overproduction of progenitor cells is usually associated with high levels of cell death (81). Various pathways leading to cell death have been identified that may be initiated by pre-programming or in response to environmental factors, namely, apoptosis, autophagy, oncosis, necrosis, and pyroptosis, to name a few (84–87). For this study, focus will be on apoptosis and necrosis, since it may occur as a result of environmental changes, as is taking place

when serum additions in culture media are changed and protocols to study these pathways are well defined (summarised in Table 2.2).

Table 2.2: Summary of apoptosis and necrosis features

	Apoptosis	**Necrosis**
Process	Physiological, active	Pathological, passive
Morphology	Chromatin aggregation. Cytoplasmic condensation. Cell membrane blebbing. The disintegration of chromosomal DNA. Nucleus and cytoplasm fragmentation. Formation of apoptotic bodies.	Chromatin clumping. Cellular and organelle swelling. Increased membrane permeability with eventual cell membrane rupture.
Inflammatory response	No inflammatory response.	Upregulation and release of pro-inflammatory factors.
Energy consumption	Uses ATP.	Energy independent.
Mechanism	Genetic caspase system; activation of initiator caspases that activate effector caspases.	Extracellular ion entry due to loss of cell membrane integrity Lysosomal membrane disruption
Causes	Stress response signals activating the intrinsic pathway. External ligands binding to cell-surface death receptors activating the extrinsic pathway.	Noxious stimuli from outside the cell: hypoxia, pH imbalance, radiation, heat, chemicals etc.

Compiled from Alberts et al., 2017; D'Arcy, 2019; Fink & Cookson, 2005; Kerr et al., 1972; Khalid & Azimpouran, 2021; Wyllie et al., 1980.

2.3.2 ASC in vitro characterisation

The *in vitro* characteristics of ASCs currently lack consensus, with most research focusing on the broad minimal criteria described in communications by the ISCT and IFATS (16,17).

2.3.2.1 ISCT and IFATS guidelines

The defining criteria published for ASCs by the ISCT and IFATS in a joint position statement (16,17) are the following:

- adherence to plastic
- a specific surface antigen expression profile (immunophenotype)
- trilineage differentiation potential

Besides plastic adherence and trilineage differentiation potential (ability to differentiate osteoblasts, adipocytes, and chondroblasts *in vitro*), ASC immunophenotype requirements have been further defined. Bourin and colleagues suggested the following specific surface antigen expression profile for further identifying ASCs in culture:

- ≥ 80% CD13, 29, 44, 73, 90, and 105 expression;
- ≤ 2% expression of CD31, 45, and 235a;
- Low expression of CD3, 10, 11b, 26, 34, 36, 49d, 49e, 49f, 106, and PODXL.

2.3.3 Adipogenesis

2.3.3.1 Adipose tissue and adipocytes

Adipose tissue consists of various cell types, including immune cells, pericytes, endothelial cells, blood cells, fibroblasts, and most abundantly, adipocytes and adipocyte precursors, surrounded by connective tissue (17,89). Adipose tissue, which can be classified into white adipose tissue (WAT), brown adipose tissue (BAT), and beige adipose tissue, is a dynamic organ that plays an essential physiological role in the body. WAT makes up the majority of adipose tissue in adults and is primarily responsible for energy homeostasis and storage through the uptake and release of fatty acids to and from the bloodstream. Triglycerides in intracellular lipid droplets in adipocytes may be used through lipolysis for thermogenesis or energy production during fasting (89). Adipose tissue also responds to insulin signalling to take up and store fatty acids and glucose in adipocytes after a meal, inhibiting lipolysis. Furthermore, adipose tissue releases regulatory peptides (called adipokines) and lipids (lipokines) that have local (paracrine) effects on neighbouring cells and systemic (endocrine) functions on cells in organs such as the brain, liver, skeletal muscle, and pancreas. Leptin and adiponectin are two examples of adipokines. Leptin functions in appetite suppression and energy expenditure and adiponectin has insulin sensitising and anti-inflammatory properties (89–92). BAT functions in heat production from stored triglycerides through oxidation using mitochondria (that contain uncoupling protein 1 (UCP1)) present in brown adipocytes in a process called non-shivering thermogenesis (89,92). Beige adipose tissue has a mixture of WAT and BAT properties and functions in thermogenesis.

The morphology of adipocytes can be used to identify them as they typically contain lipid droplets surrounded by cytoplasm. Preadipocytes undergo gene expression and subsequent morphological changes during differentiation. The accumulation of lipid droplets results in mature adipocyte morphology and late-stage adipogenic gene expression profile. Mature adipocyte morphology is characterised by a single large lipid droplet surrounded by a thin layer of cytoplasm. The mature adipocyte releases adipokines (cytokines specifically released by adipocytes) that are immunomodulatory, and function in insulin response, lipid metabolism and the vascular system (93–96).

2.3.3.2 Adipogenic differentiation and the transcriptional cascade

Adipogenesis is a complex process where fibroblast-like multipotent ASCs commit to the adipogenic lineage through a multistep, sequential interplay of genetic, chemical, and hormonal events to form mature adipocytes, and may be used to study obesity and obesity-related diseases (97,98). Adipogenesis has two distinct phases: the commitment/determination and the terminal/differentiation phase, summarised in Figure 2.3 (90,91,97).

In vivo adipogenesis is mediated by autocrine (affecting the cell it is secreted by), paracrine and other secreted signals, but *in vitro* adipogenesis can be induced by adding selected supplements and factors to the ASC growth medium.

The exact composition of adipogenic cocktails varies across publications, but the most widely used additions are insulin, dexamethasone (Dex), 3-isobutyl-1-methylxanthine (IBMX), and indomethacin (99–103). The induction time, cell lines, and induction medium composition used vary as well. Table 2.3 summarises the different adipogenic cocktail additions and the role they play in adipogenic differentiation and the adipogenic gene pathway.

Table 2.3:Adipogenic cocktail additions and their function in adipogenesis and the adipogenic gene pathway

Addition	Function
Insulin	Influences the stable expression of early C/EBP transcription factors of adipogenesis. Increases and accelerates lipid accumulation and the percentage of differentiating cells.
Dexamethasone (Dex)	A glucocorticoid that induces the expression of the C/EBP family of transcription factors as well as PPARγ. Reduces the expression of the adipogenic differentiation inhibitor, Pref-1.
3-Isobutyl-1-methylxanthine (IBMX)	A nonselective phosphodiesterase inhibitor that increases intracellular cAMP resulting in PPARγ expression through C/EBPβ activation and subsequent adipogenic differentiation.
Indomethacin	Upregulates C/EBPβ expression. Binds directly to PPARγ receptors, thereby directly upregulating PPARγ expression and increasing adipogenic differentiation and marker expression.

Compiled from MacDougald et al., 1995; Sakoda et al., 2000; Scott et al., 2011; Styner et al., 2010; Vater et al., 2011; Zhao et al., 2019

ASCs respond to the induction signal during the commitment phase after adding an adipogenic induction cocktail *in vitro* to undergo adipogenic differentiation. The commitment of ASCs to preadipocytes occurs at the genetic level where the bone morphogenic protein (BMP) and Wnt families are key mediators, with no visual morphological changes. The exposure of preadipocytes to the induction cocktail (usually containing high levels of insulin, dexamethasone, and a cyclic AMP (cAMP) elevator) triggers synchronous re-entry of growth-arrested preadipocytes into the cell cycle to undergo mitotic clonal expansion (MCE). MCE is the start of the adipogenic gene expression cascade and is therefore crucial, with preadipocytes undergoing about two cycles of cell division during MCE. Expression of the transcription factor CCAAT/enhancer-binding protein beta (C/EBPβ) is initiated at the start of induction but

is only activated through phosphorylation during MCE. Activation of C/EBPβ ushers preadipocytes into the differentiation phase of adipogenesis. Activated C/EBPβ induces expression of CCAAT/enhancer-binding protein alpha (C/EBPα), another transcription factor of the same CCAAT/enhancer-binding protein family, and PPARγ, the master regulator of adipogenesis. PPARγ and C/EBPα are transactivated through their respective C/EBP regulatory elements which maintains their expression throughout adipogenesis. PPARγ and C/EBPα function together to induce the expression of adipogenic genes that produce the accumulated intracellular lipid adipocyte morphology seen in mature adipocytes (Figure 2.3).

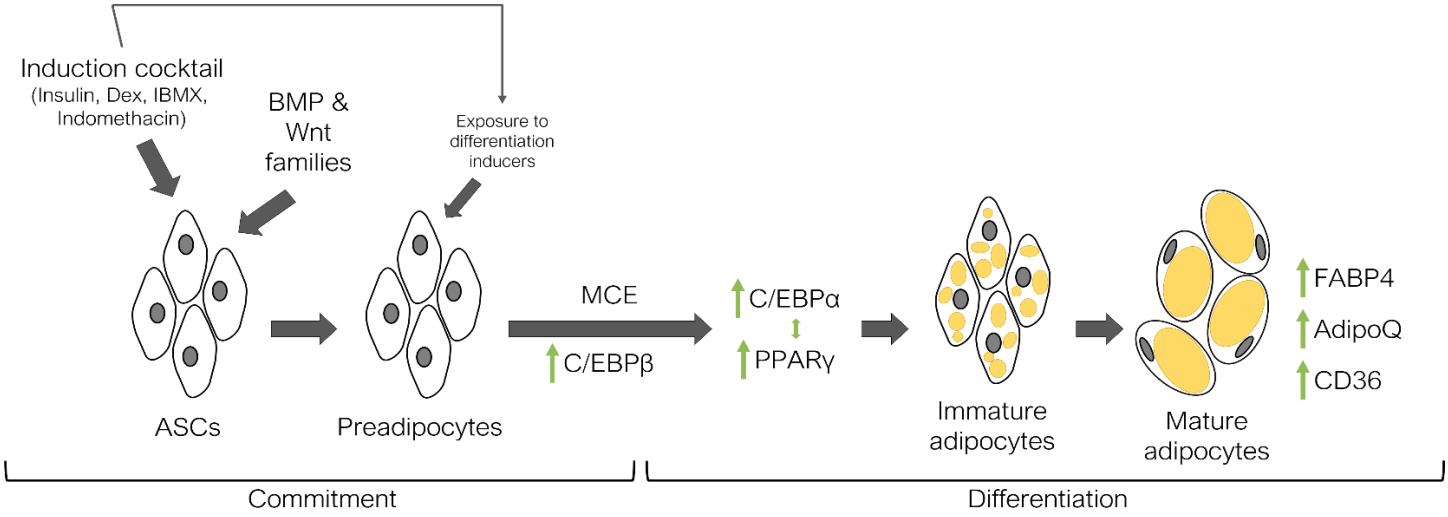

Figure 2.3: Graphical summary of the multistep adipogenesis process.
An induction cocktail induces the genetic changes for ASCs to commit to the adipogenic pathway and become preadipocytes. MCE and activation of C/EBPβ initiate the adipogenic gene expression cascade with the induction of C/EBPα and PPARγ, which result in differentiation and development of the adipocyte morphology and expression of adipogenic genes. Figure made by candidate, compiled from [89,90,103–112,92,113,114,93,94,98–102].Three examples of downstream adipogenic genes expressed in mature adipocytes are fatty acid-binding protein 4 (FABP4), adiponectin (AdipoQ), and cluster of differentiation 36 (CD36). Adipogenic genes and their functions are summarised in Table 2.4.

Table 2.4: Adipogenic genes and their function.

Gene	Abbreviation	Function
CCAAT/enhancer-binding protein beta	C/EBPβ	Expressed early in adipogenesis and initiates the adipogenic gene expression cascade (as a basic leucine zipper domain transcription factor) by inducing C/EBPα and PPARγ expression. Plays a role in MCE and the regulation of genes involved in inflammation and immune response.
CCAAT/enhancer-binding protein alpha	C/EBPα	Basic leucine zipper domain transcription factor induced by C/EBPβ. Cross talks with PPARγ during adipogenesis. Plays a role in the upregulation and activation of downstream adipogenic genes along with PPARγ.
Peroxisome proliferator activated receptor gamma	PPARγ	Transcription factor that is part of a nuclear receptor superfamily and the master regulator of adipogenesis. Induced by C/EBPβ expression. Crosstalks with C/EBPα in adipogenesis for robust adipogenic gene expression. Functions in lipogenesis, regulation of insulin sensitivity, and adipocyte survival as well.
Fatty acid-binding protein 4	FABP4	An adipokine that functions as a lipid chaperone in the transport and intracellular storage of fatty acids, associated with intracellular lipid accumulation and increased insulin secretion in obesogenic conditions. Late adipogenic marker.

Adiponectin	AdipoQ	An adipokine secreted by mature adipocytes. Increasing insulin sensitivity is the primary function of AdipoQ, but it also has classic anti-inflammatory and anti-fibrotic functions.
Cluster of differentiation 36	CD36	CD36 marker is indicative of high adipogenic capacity *in vivo* and in ASCs. Functions in high-affinity lipid uptake in immature adipocytes and contributes to lipid accumulation under conditions of excess fat supply.

Compiled from Ambele et al., 2016; Christiaens et al., 2012; de Sá et al., 2017; Fang & Judd, 2018; Gao et al., 2017; Kucharski & Kaczor, 2017; Lefterova et al., 2008, 2014; Mishkin et al., 1972; Nawrocki et al., 2006; Ockner et al., 1972; Pepino et al., 2014; Rosen & MacDougald, 2006; Q.-Q. Tang et al., 2004; Q. Q. Tang & Lane, 2012; L. E. Wu et al., 2014; Z. Wu et al., 1999

The adipogenic gene expression pathway was simplified for the scope of this study as, naturally, the process of commitment and differentiation during adipogenesis is complex, with many more genes being involved. The six chosen genes discussed in Table 2.4 have been well studied in the literature as well as in our research group (105,117,118).

2.4 GMP of ASCs for regenerative medicine

The production and use of ASCs for potential cell therapies must be per GMP as is required by the Food and Drug Administration (FDA). Compliance with GMP requires defining precise processes accounting for variables such as the production and storage areas, the personnel responsibilities, training, and hygiene throughout production, among others (21–23,119). The premises where potential cell therapy products will be stored and manufactured, such as a clean room, should be designed to minimise external contamination and contact with a non-sterile environment, but manufacturing should preferably be done in a closed system such as a bioreactor. Personnel should be trained to use equipment in an aseptic manner, designed to prevent contamination of cells in culture. Of particular interest for this study is compliance to GMP regarding serum additions to culture media to ensure the safety of ASCs intended as a therapeutic product. The medium used for cell culture should be composed of reagents that prevent exposure to potentially harmful substances. Isolation and expansion of ASCs in numerous research settings currently use animal-derived reagents such as FBS that do not comply with GMP. Replacing animal components with suitable human or recombinant alternatives is crucial for providing appropriately regulated cell therapy products that can be used safely.

2.5 Serum supplementation in ASC culture

Cell culture medium is traditionally supplemented with various sera as it provides the essential nutrients needed to support *in vitro* ASC growth, discussed in section 2.3 above.

2.5.1 Foetal bovine serum

Serum derived from cattle includes bovine calf serum, newborn calf serum and serum derived from a bovine foetus. The difference between these sera is the harvesting timeline as newborn calf serum is obtained within 24 hours after birth and bovine calf serum is collected from a calf within 10-30 days after birth (26). FBS is derived from a bovine fetus via caesarean section and is the best quality serum since the fetus has not been exposed to the environment and therefore has low levels of antibodies (26). FBS is considered the gold standard for cell culture supplementation, particularly in the research environment, to ensure optimal cell proliferation *in vitro* (20). The use of a bovine-derived serum during *in vitro* culture of ASCs poses multiple problems. The unknown composition of FBS poses a risk when ASCs are cultured in media supplemented with FBS as there may be components present such as antibodies or endotoxins that may impact cell growth *in vitro* (26,120). Unknown components in FBS may also pose a safety risk to laboratory personnel (19). The conditions required for cell growth in the human body are not mimicked when using xenogeneic sera, such as FBS (121). Another concern when using FBS for *ex vivo* ASC culture is transmitting zoonotic diseases (28). Lastly, the batch to batch variation, coupled with increasing ethical concerns regarding the suffering imposed on animals during the harvest of FBS, requires investigation into the use of animal component alternatives for tissue culture when ASCs are cultured for clinical applications (28).

2.5.2 Serum-free medium

Serum-free medium is an alternative to FBS for ASC culture. The absence of serum from a culture medium removes an unknown variable from the culture system resulting in a serum-free medium being a more favourable alternative (120). The benefits of a serum-free medium include controlled culture conditions due to the known chemical composition of the serum replacement, which in turn results in reduced variability of culture conditions and eliminates the potential for contamination or disease transmission (120,122). When using serum-free medium, any ethical concerns regarding the use of animal-derived serum are eliminated, and media can be modified to be cell type-specific (120). However, a serum-free medium has certain drawbacks. The variability of medium supplement requirements between cell types prohibits the development of a universal serum-free medium. Additionally, serum-free medium currently available commercially is costly, and preparation of the medium with animal serum alternatives in-house is time-consuming (120,122). It is therefore necessary to investigate the possibility of using human-derived medium supplements for use in MSC or ASC culture protocols, especially if these are to be applied and used in the clinical setting (20).

2.5.3 Human blood alternatives

Components derived from human blood, such as plasma, serum, umbilical cord blood serum, and blood platelet derivatives should be considered as animal component alternatives. Blood is a body fluid consisting of plasma, biconcave red blood cells (erythrocytes, mainly responsible for oxygen transport in the body), white blood cells (abbreviated WBCs, also called leukocytes that function in the immune system with multiple white blood cell types performing various functions) and platelets (thrombocytes)(123–125). Plasma is the non-cellular liquid portion of blood (123–125). Platelets are fragments of megakaryocytes and function in a variety of pathways in the body through the excretion of hormones, but their primary function is in the coagulation pathway at a site of injury (123–125).

Blood components derived from whole blood as human alternatives can be autologous, where the donor and recipient are the same person, or allogeneic, where the donor and recipient are different people. The various human alternatives and their production from whole blood are summarised in **Error! Reference source not found.** with i ndividual descriptions of the products in the following sections.

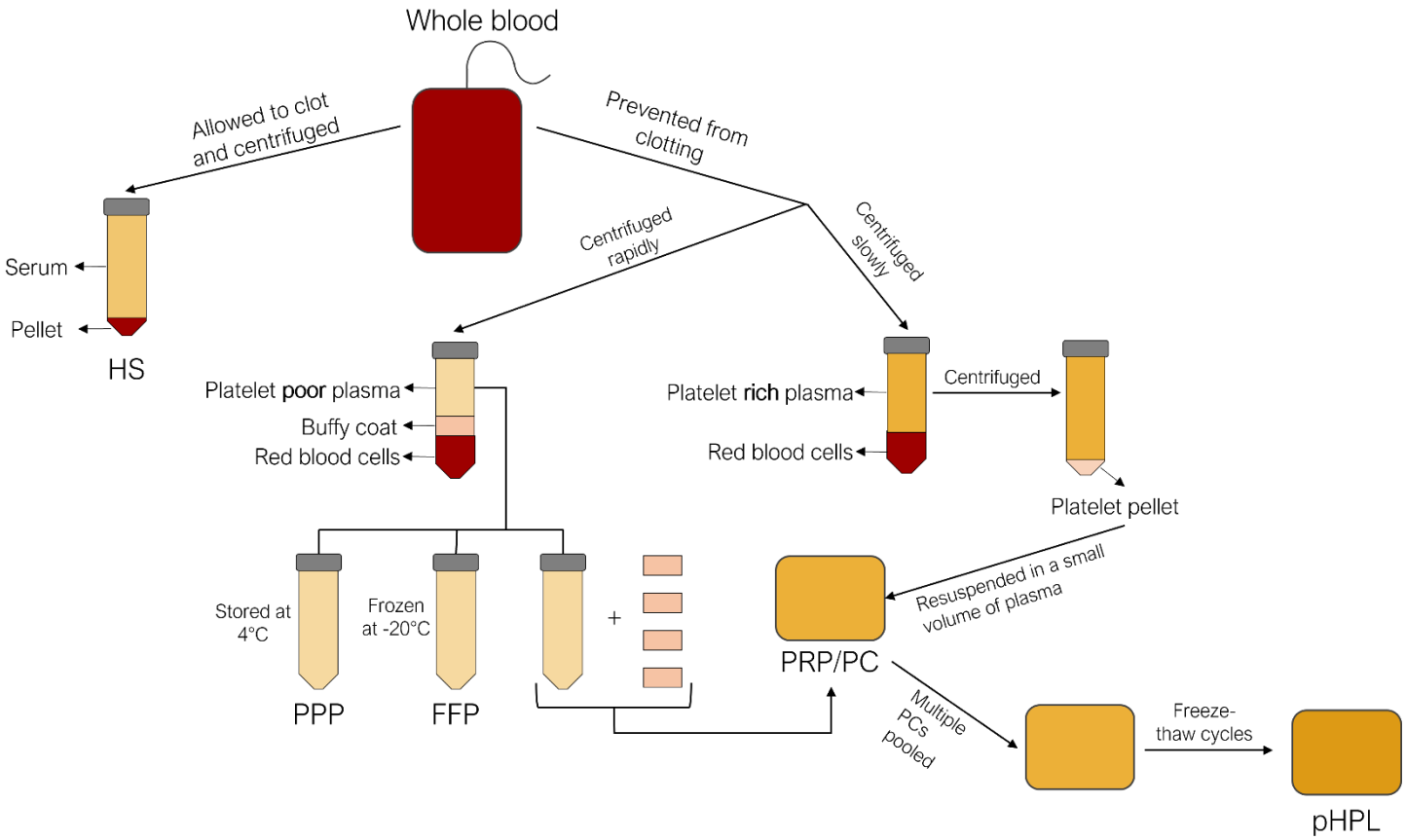

Figure 2.4: Summary of the production of different blood products from whole blood as human alternatives to FBS.
Created by candidate. compiled from 20,27,37,41,122,125–129

2.5.3.1 Human serum

HS is produced from donated whole blood and contains no platelets, red blood cells, or white blood cells. The production of HS involves the clotting of whole blood in the absence of an anticoagulant, after which the blood is centrifuged to produce a pellet that contains platelets, red blood cells and white blood cells. The supernatant produced from this step is serum (27,33). The use of both allogeneic and autologous HS for culturing is superior to FBS (25,33,131–133). Accelerated proliferation, extended lifespan, and clonogenic capacity have been observed when ASCs are cultured in HS for extended periods, suggesting that HS could be an appropriate alternative to FBS (131). No differences between FBS and HS were found in ASC differentiation potential and senescence marker expression (131).

Although HS is superior for ASC cultures, specific limitations exist regarding its use for clinical applications. There is limited availability of autologous serum and there may be significant differences between sera obtained from different donors even though autologous serum supports faster cell growth compared to FBS. Allogeneic HS may be considered instead as it can be pooled to obtain sufficient amounts for large-scale clinical application culturing. Pooled HS quality control and disease screening to ensure adequate standards are also more easily done by blood banks (33).

2.5.3.2 Platelet-rich plasma

Plasma, an alternative to serum, is the non-cellular liquid part of whole blood which may be used to suspend platelet concentrates (PCs) to obtain a plasma that is rich in platelets (31). Platelets present in the blood contain various growth factors that promote cell growth, differentiation and tissue regeneration (30). Platelet α-granules secrete growth factors such as platelet-derived growth factor (PDGF), fibroblast growth factor (FGF), transforming growth factor-β (TGFβ), vascular endothelial growth factor (VEGF) and epidermal growth factor (EGF) (30). Plasma itself does not contain large amounts of growth factors; however, platelets present in platelet-rich plasma (PRP) can be activated using various methods. Platelet activation through the use of thrombin or a freeze-thaw cycle, for instance, results in the release of the growth factors listed previously into plasma from activated platelets (31).

In short, PRP is produced by centrifuging whole blood. The supernatant (plasma) containing platelets is collected and centrifuged again to obtain a platelet pellet. The platelet pellet is then resuspended in a smaller volume of plasma (128). Alternatively, PRP can be obtained by combining buffy coats and plasma into a unit of PRP (130). Lastly, platelet-rich plasma can be collected via apheresis, whereafter clotting is prevented in the samples by the addition of heparin (127). The main difference between the methods is that apheresis separates blood components in a closed system using centrifugation which is more in line with GMP. Additionally, all blood components separated from the plasma is returned to the patient

ASCs cultured in PRP maintain their morphology and phenotype, but display increased proliferation rates compared to ASCs cultured in FBS (31,134). Atashi *et al.* (2015) found that autologous non-activated PRP (nPRP) increases MSC proliferation when compared to MSCs cultured in autologous thrombin-activated PRP (tPRP). Still, both tPRP and nPRP significantly increase MSC proliferation rates compared to FBS (30). The biological variability of donors must be considered when using PRP, as must the extensive process of obtaining plasma and platelet concentrates from whole blood (30,31,134).

2.5.3.3 Platelet-poor plasma

PPP contains various growth factors, including PDGF which plays a significant role in cell growth and proliferation by inducing mitosis and inhibiting apoptosis (126). Platelets release PDGF into the blood during coagulation when platelets aggregate; in contrast, serum produced from PPP contains almost no PDGF or platelets (126). Broadly, there are two ways to separate blood components when obtaining plasma, namely centrifugation in a sterile facility, and apheresis, as mentioned in section 2.5.3.2 above. Platelets and erythrocytes are removed from the blood by both of these procedures, resulting in low levels of growth factors being released into PPP during coagulation (126). Using PPP in cell culture medium would thus require the addition of growth factors, similar to when serum-free medium is used (20,126). Different production protocols of PPP may influence the levels of growth factors present in PPP. It was found that MSC proliferation is increased when PPP is used as a supplement and compared to conventional serum (126). These results contradict the findings of a prior study in which proliferation was increased when PDGF was present, or when serum from whole blood was used instead of PPP (135). The use of PPP as a serum supplement thus needs to be investigated further.

PPP may be a better alternative to FBS as it is easier to acquire and produce. Whole blood from conventional blood donations may be used to obtain PPP by separating the platelets and erythrocytes from the plasma through centrifugation (126).

2.5.3.4 Fresh frozen plasma

FFP is obtained from whole blood by separating blood components using one of the methods discussed in 2.5.3.2 above within 5-8 hours of blood collection, and subsequently freezing the plasma after separation (123,129). FFP can be stored for 12 months at -18°C or lower and at 4°C for 6-24 hours after thawing (123). Conventionally, FFP is used in transfusion therapy to correct coagulation deficiencies, blood loss and thrombotic thrombocytopenic purpura, to name a few (136), but FFP has been used in a cell culture setting. When FFP was used for MSC proliferation the optimal concentration was 5% (v/v) FFP in low glucose DMEM. When comparing MSC proliferation in FFP supplemented medium to that of FBS supplemented medium, FFP was superior (37). Limited studies have used FFP as a culture medium addition; thus, FFP as a medium supplement in stem cell therapy applications should be investigated further.

2.5.3.5 Pooled human platelet lysate

pHPL can be produced in two ways, similar to PRP production as discussed in 2.5.3.2 above (127,130). PCs undergo freeze-thaw cycles to lyse platelets, thereby releasing growth factors, and the lysate is then centrifuged to remove cellular debris (127). The use of HPL as a growth medium supplement for ASC culturing has been proven to be efficient relative to FBS.

ASCs cultured in pHPL displayed increased proliferation compared to FBS (130) and serum-free media (127). Furthermore, no changes in immunophenotype, no abnormal chromosomes, and an increased differentiation rate were observed (127,130). There is some evidence suggesting that the technique used to obtain PRP, from which HPL is produced, may affect the immunosuppressive capabilities of MSCs, but further investigation is needed before a conclusion can be reached (127).

2.6 Rationale

The use of ASCs in cell-based therapy is attractive, but the resulting products must adhere to GMP. Replacing standard animal-derived medium supplements with clinical-grade xeno-free alternatives is essential. These changes may change the downstream ASC products and it is therefore crucial to adhere to ASC characteristics prescribed by the ISCT and IFATS. This study aimed to determine the best human alternative supplement to FBS and to investigate the effect human alternatives may have on critical ASC characteristics. The human alternative with the best proliferative potential was then investigated for retention of ASC adipogenic differentiation potential.

Chapter 3: Study overview

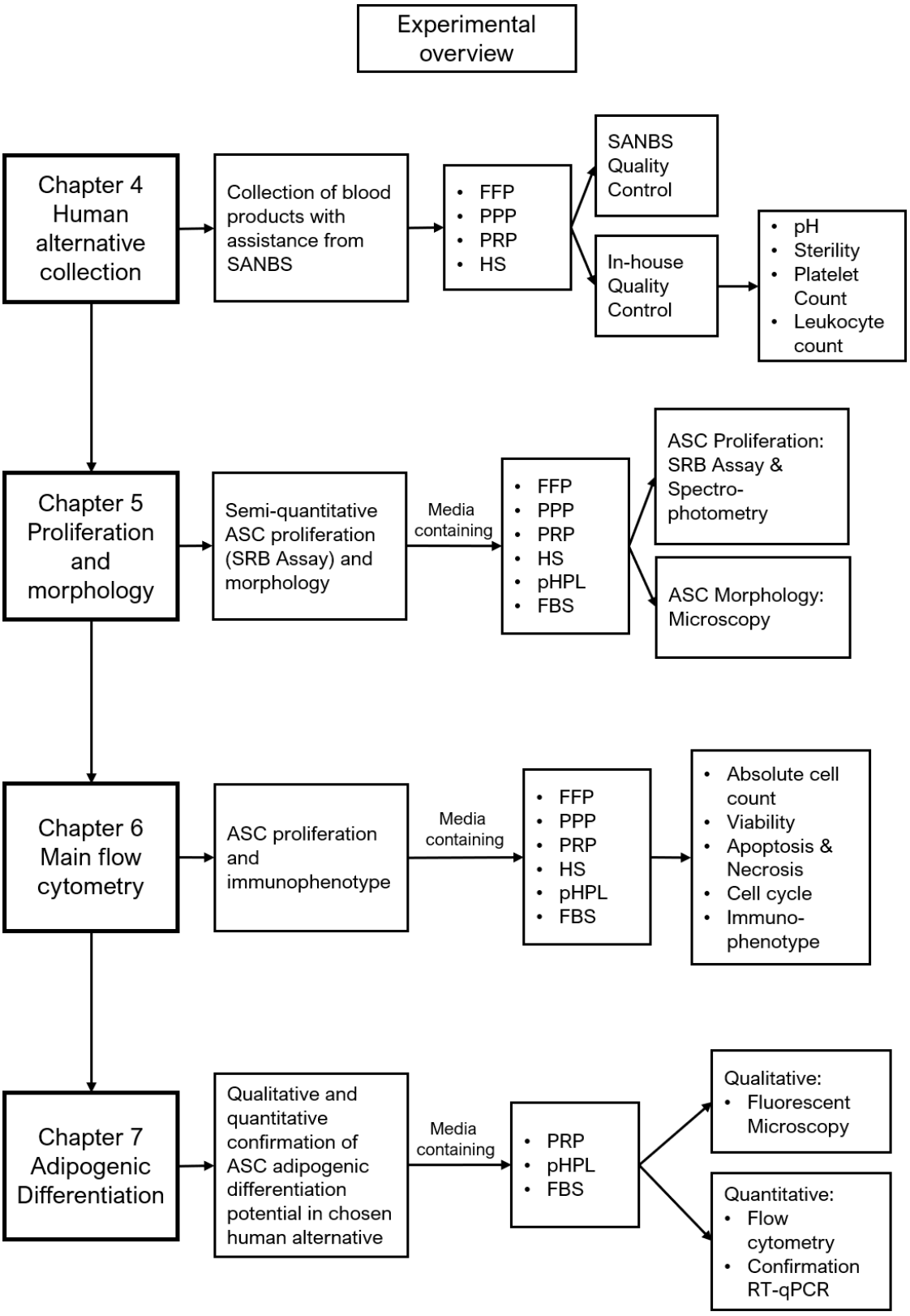

Figure 3.1: Graphical layout of the experimental overview used in this study.
Various characteristics of hASCs expanded, maintained, and differentiated in various culture media were investigated using different experimental techniques such as light microscopy, flow cytometry, spectrophotometry, fluorescent microscopy, and RT-qPCR. Created by candidate.

Chapter 4: Human alternatives production

4.1 Introduction

The previously highlighted concerns regarding the use of a xenogeneic serum supplement call for the use of a culture medium serum supplement that complies with good cell culture practise (GCCP) and GMP procedures and policies (24). Blood alternatives from humans may be a viable alternative to FBS (24,137).

Multiple human blood product medium supplements have been suggested as a replacement for FBS. These alternatives vary in composition since they are parts of whole blood (27,28,138). The different proposed alternatives are: Fresh-frozen plasma (FFP), platelet-poor plasma (PPP), human serum (HS), platelet-rich plasma (PRP), and pooled platelet lysate (pHPL).

This study set out to obtain alternative human blood product medium supplements and compare their use in the maintenance and expansion of adipose-derived mesenchymal stem/stromal cells (ASCs). We worked closely with the South African National Blood Service (SANBS) to obtain various products; consequently, this allowed us to ensure the standard of products and donor compliance. We also completed in-house quality control procedures during the receipt and processing of the products.

4.2 Materials and methods

We acquired the blood products used in this study in collaboration with SANBS who obtained the blood from healthy donors, all of whom had given informed consent. Before donation, the candidates underwent a standard SANBS blood screening (including platelet and WBC count) to qualify as donors. Only donors with typical levels for all criteria could donate. We protected the donors' privacy by keeping patient information confidential and assigning each sample a reference number, thereby ensuring donor anonymity.

We received approval for the use of the blood products in this study from the UP-Health Sciences Research Ethics Committee (reference number 424/2018) and the SANBS Ethics Committee (approval number 2013/17).

SANBS regularly produces platelet concentrates (PCs) and FFP; therefore, we purchased these products directly from the blood bank. We obtained PRP, PPP and HS in collaboration with the Specialised Therapeutics Services (STS) department within SANBS.

4.2.1 Pooled platelet lysate production

Ms Carla Dessels (UP ethics approval number 421/2013; SANBS ethics approval number 2013/17) previously manufactured pooled human platelet lysate (pHPL) using the Schallmoser & Strunk protocol with minor modifications (139).

Briefly, the PCs obtained from SANBS were frozen at -25°C for 24 hours and thawed in the original bag placed in a protective cover (SteriZip™, OriGen Biomedical, Texas, USA) in a water bath (EcoBath, Labotec, South Africa) at 37°C. Once thawed, two PCs were pooled in a sterile double pooling bag (3 L waste bag Haemonetics Corporation, Massachusetts, USA) using a sterile connection device (TCD® Sterile Tube Welder with wafers, Genesis, New Jersey, USA). A sterile tube sealer (Rapid Seal II™ SE540, Genesis, New Jersey, USA) was used to seal the pooling bags before mixing the contents thoroughly. An aliquot was taken in a small Baxter bag (PEDI-PAK® Single 75 mL Transfer Bags, Genesis, New Jersey, USA) to use for sterility testing and quality control analysis. A volume of 250 mL pooled PCs was transferred into 600 mL Baxter bags (Platelet Transfer and Storage Bags, Macopharma, Mouvaux, France) and frozen again at -25°C for 24 hours. The PCs were thawed in a 37°C water bath in a protective cover until all the ice crystals had disappeared. The contents of the bags (now pooled human platelet lysate, pHPL) were transferred into 50 mL conical tubes (Corning, NY, USA) under sterile conditions in a laminar flow cabinet. The 50 mL tubes were centrifuged at 4 000 x *g* at 4°C for 15 min, and the supernatant was transferred to new 50 mL conical tubes and stored at -25°C for future use.

4.2.2 Human serum production

The human serum blood products were purchased from SANBS in collaboration with the STS division. The STS division obtained whole blood from three healthy donors who have given informed consent at a SANBS collection site. The donors were required to donate a standard whole blood unit (approximately 200 mL) collected in a dry bag containing no anticoagulant.

After collection, the blood was suspended and allowed to clot overnight. SANBS technicians processed the samples the following day by centrifuging at 3 500 rpm for 5 min at room temperature and aspirating the supernatant (human serum) using sterile docked transfer packs. The resulting HS with a volume of roughly 200 mL was delivered to the ICMM. Upon receipt, we aliquoted each bag's contents into 15 mL conical tubes under sterile conditions in a laminar flow cabinet. A sample of each HS was taken for quality control analysis, and the remaining aliquoted HS were stored at -80°C for long-term storage and future use (140). The aliquots were not allowed to undergo more than two freeze-thaw cycles before being discarded (140).

4.2.3 Fresh frozen plasma production

Units of fresh frozen plasma (FFP) were purchased from SANBS since it is a product that they routinely manufacture. Three units of frozen FFP were obtained from SANBS. Each unit contained a volume of roughly 300 mL FFP. The units were thawed in a sterile protective cover at 37°C in a water bath (EcoBath, Labotec, South Africa). Once thawed, the units were aliquoted under sterile conditions in a laminar flow into 15 mL sterile Falcon® conical tubes and stored at -80°C for future use. A sample of each unit of FFP was taken for quality control analysis.

4.2.4 Platelet-rich plasma and platelet-poor plasma production

Platelet-rich plasma (PRP) and platelet-poor plasma (PPP) were obtained with the assistance of the STS division of SANBS. The products were collected using the Spectra Optia® Apheresis System. The plasma products were collected in the Clinical Research Unit (CRU) of the University of Pretoria (Room 2-54, Floor 2, Pathology Building, Prinshof Campus) by trained SANBS nurses from the STS division. The CRU provided beds, resuscitation equipment, and oxygen should these have been required in an emergency. Furthermore, we ensured that a doctor was always present and on standby in the CRU during the collection procedure.

PRP and PPP donors underwent standard SANBS screening to be eligible for the donations. The donors underwent additional testing to confirm calcium, magnesium, and potassium blood levels before donating due to a potential side effect of hypocalcaemia using the Spectra Optia® Apheresis System (141). Only donors with normal calcium, magnesium, and potassium blood levels could donate.

The Spectra Optia® Apheresis System's collection criteria were set to a yield of 3.5 with a platelet concentration of 1.4 x 10^6 platelets/µL (141). The criteria were decided after several pilot studies by Dr E Wolmarans (142). The PRP and PPP were collected simultaneously in blood bags containing anticoagulant, and the remaining blood components were returned to the patient. The collection volumes for PRP and PPP were set to 250 mL.

The PPP volume (roughly 250 mL) was aliquoted into 15 mL sterile Falcon® conical tubes under sterile conditions in a laminar flow. The aliquots were then stored at -80°C for future use. A sample of each PPP donation was used for quality control, and aliquots were allowed to undergo only a single freeze-thaw cycle before being discarded (28,143).

The PRP donations were placed on a benchtop after collection to allow the platelets to rest for an hour at room temperature. The entire PRP volume (roughly 250 mL) was then aliquoted into 15 mL sterile Falcon® conical tubes under sterile conditions in a laminar flow cabinet. A sample of each PRP donation was used for quality control

analysis, and the PRP aliquots were stored at -20°C. The aliquots were discarded after a single freeze-thaw cycle.

4.2.5 Quality control of blood products

Quality control of blood products is a necessary step for producing, storing, and using these products. It is crucial to ensure that the resulting cell product adheres to GCCP (24) and GMP as well as national regulations regarding their quality and safety (28).

The use of registered SANBS donors and the purchase of routinely produced blood products from SANBS ensure that the donors have completed standard SANBS screening as presented in the SANBS donor guidelines (144).

We investigated various criteria to ensure that product variability is reported and taken into consideration during data analysis. For instance, PRP is a blood product that often varies in the number of platelets present due to the various production protocols (137) and devices used when concentrating platelets using apheresis devices (28,145). The platelet counts of the different products should be above the threshold for a healthy individual (28,138,145); however, there is little consensus regarding the limits for what constitutes a platelet-rich or platelet-poor product. Some reports suggest a platelet concentration of more than 2.0×10^{11} to 3.0×10^{11} platelets/unit in platelet "rich" products and a range of less than 5×10^{4} to 2.5×10^{9} platelets/unit for platelet "poor" products (28,145–147).

We investigated whether leukocytes (white blood cells (WBCs)) were present in the various blood products since most blood products are filtered to remove WBCs. The filtration step is vital to prevent HLA alloimmunisation (124,148) that may occur when there is an immune response of recipient leukocytes against HLA antigens present on donor leukocytes (149). The result is the formation of alloantibodies by the recipient (149). In this study, HLA alloimmunization is a concern when MSCs or hASCs maintained and expanded in blood products are transplanted in a therapeutic setting. HLA alloimmunization will not occur due to an MSC reaction against leukocytes in the donor blood products, but may result from donor leukocytes being transplanted along with cultured MSCs. A common side effect of alloimmunisation is platelet refractoriness and febrile non haemolytic transfusion reactions (124,147).

Apart from this side effect, the presence of WBCs may influence cytokine composition and concentration in the culture medium leading to variability in MSC growth (28,137).

Therefore, it is essential to reduce the possibility of HLA alloimmunisation post-MSC transplantation and cytokine variability in culture medium by using leukodepleted blood products and ensuring that the WBC number is below the criteria threshold as set out by various authorities. There is lack of consensus regarding the criteria for the number of WBCs present in blood products as it varies from fewer than 1×10^6 cells/unit according to European standards to fewer than 5×10^6 cells/unit for Association for the Advancement of Blood and Biotherapies (AABB) and Canadian standards (147,150,151).

Additionally, we investigated the pH and sterility of the blood products. Lowering the risk of transmission of bloodborne diseases is necessary when considering human blood alternatives to FBS (28). It is possible to investigate the presence of microbes in the blood products by examining the pH of the blood products (a low pH is indicative of bacterial contamination (152)) and inoculating blood agar plates with the blood products to monitor for microbial growth. Table 4.1 summarises the quality control criteria.

Table 4.1: Summary of blood product criteria.

QC Parameter	Requirement	Reference
	pHPL	
Sterility	Negative	(Benjamin et al., 2019; Hoffbrand & Moss, 2011; Pavlovic et al., 2016; Schmidt et al., 2009; D. T. B. Shih & Burnouf, 2015; Simon et al., 2016; South African National Blood Service, 2014)
pH	> 6.4	
Residual WBC count	$< 5 \times 10^6$	
Platelet count	$\geq 2.4 \times 10^{11}$	
	PRP	
Sterility	Negative	(Benjamin et al., 2019; Hoffbrand & Moss, 2011; Pavlovic et al., 2016; Schmidt et al., 2009; D. T. B. Shih & Burnouf, 2015; Simon et al., 2016; South African National Blood Service, 2014)
pH	> 6.4	
Residual WBC count	$< 5 \times 10^6$	
Platelet count	$\geq 2.4 \times 10^{11}$	
	HS	
Sterility	Negative	(Hoffbrand & Moss, 2011; D. T. B. Shih & Burnouf, 2015; Simon et al., 2016; Sultan, 2010)
pH	> 6.4	
Residual WBC count	$< 5 \times 10^6$	
Platelet count	$< 2.5 \times 10^9$	
	PPP and FFP	
Sterility	Negative	(Hoffbrand & Moss, 2011; Lambrecht, Spengler, Nauwelaers, Bauerfeind, Mohr, & Muller, 2009; D. T. B. Shih & Burnouf, 2015; Simon et al., 2016; Sultan, 2010)
pH	> 6.4	
Residual WBC count	$< 5 \times 10^6$	
Platelet count	$< 2.5 \times 10^9$	

4.2.5.1 pH

The pH of the various human alternatives was assessed using a CRISON micropH 2001 pH metre (Crison Instruments, Barcelona, Spain) and recorded.

4.2.5.2 Sterility

The sterility of the various blood products was assessed by investigating the presence of aerobic and anaerobic microorganisms. A 250 µL aliquot of each blood product was spread on a 9.6 cm^2 blood agar plate (purchased from the Department of Medical Microbiology, Tshwane Academic Division, National Health Laboratory Service, South Africa) under sterile conditions in a laminar flow and incubated for seven days at 37°C/5% CO_2. Plates investigating the presence of anaerobic microorganisms were sealed with parafilm® M film (Amcor, Zurich, Switzerland) before incubation. After the 7-day incubation period, the plates were assessed for bacterial and fungal growth.

4.2.5.3 Leukocyte count

The blood products were investigated for the number of residual leukocytes present using a DNA Prep kit (Beckman Coulter, Miami, USA) by means of flow cytometry.

4.2.5.3.1 Flow cytometry for cell counts

Flow cytometry principles combine the use of fluidics and optics to evaluate single cells and particles. Cells/particles pass a light source, usually a laser, in single file suspended in fluid. The scattering of the light detected when the cells pass the laser allows the user to determine various characteristics of the cells. The use of optics also allows the user to use fluorescent dyes or fluorochromes to further investigate properties of cells or particles.

The fluidics system of a flow cytometer combines two components; sheath fluid and pressurised airlines. Sample containing cells in solution is injected by pressurised airlines into sheath fluid, which is a diluent (usually phosphate buffered saline (PBS)), into the flow chamber. The sheath fluid surrounds the sample stream which then becomes a central core in the sheath stream. This arrangement is called a coaxial flow and is achieved due to pressure differences between the sheath fluid stream and the sample stream where the sample stream pressure is always greater than that of the sheath. The coaxial flow principle of fluidics in a flow cytometer results in cells flowing past the laser beam in single file to ensure uniform illumination of cells, called hydrodynamic focusing (153).

Flow cytometry optical systems contain excitation and collection optics. The optical bench holds lasers and lenses to shape and focus the excitation laser beam, as well as a collection lens with mirrors and filters to direct and separate emitted and scattered light to appropriate optical detectors.

The excitation optics contains a laser that energises electrons with high voltage electricity. Light emission then takes place when photons are released by electrons that fall from higher orbitals in an energised state to lower orbitals. Light scattering takes place when the light is deflected around cells after the laser strikes the cell. Two types of light scatter occur, namely, forward scatter (FS) and side scatter (SS). FS is a

result of light scattering along the same axis as the laser and corresponds to the size of the particle or cell. SS is a result of refracted and reflected light collected roughly perpendicular to the laser and is equivalent to the granularity or complexity of the particle or cell (153).

The collection optics ensure the specificity of light collected by the appropriate optical detector. An optical detector's specificity for certain fluorescent dyes is achieved by long pass, short pass, or band pass filters. Band pass (BP) filters allow only light with wavelengths within a narrow range of the emission peak of a fluorescent dye to reach the detector. Long pass (LP) filters transmit wavelengths of light that have longer or equal wavelengths than a specified wavelength to the detector. In contrast, short pass (SP) filters transmit light of equal or shorter wavelengths than a specified wavelength to the detector (153).

Fluorescent dyes and fluorochromes conjugated to antibodies may be used to investigate certain properties of cells, for instance their DNA content, or proteins expressed on the cell surface. Fluorescence entails the absorbance of light at certain wavelengths by a fluorescent compound. Light energy absorbance excites electrons from a ground state to an excited state. Electrons then emit the excess absorbed energy as a photon of light to return to their ground state. This series of events is the principle behind fluorescence. Each fluorochrome has an absorbance and emission spectrum. The difference between the peaks (maxima) of the absorbance and emission spectra is called the Stoke's shift (Figure 4.1). A larger Stoke's shift indicates a larger separation between the absorption and emission spectrum of a fluorochrome. The colours and wavelengths of the absorbance and emission spectra are different, therefore optical filters can be used to distinguish between the excitation and emission wavelengths as described previously (153).

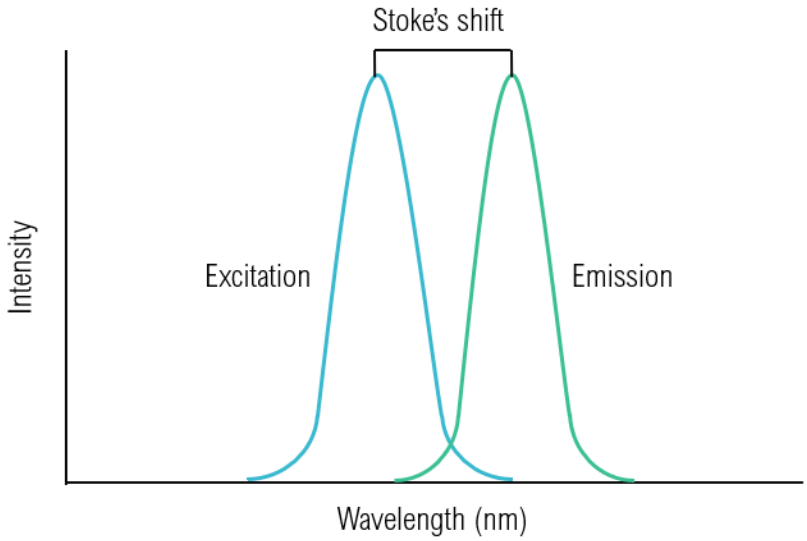

Figure 4.1: Representative excitation and emission spectra of a fluorochrome.
The difference between the peaks of the excitation (blue) and emission (green) spectra of a fluorochrome is the Stoke's shift. A higher Stoke's shift indicates a larger separation between the absorbance and emission wavelengths of a fluorochrome. Created by candidate, referenced from (153).

The use of multiple fluorochromes may result in overlap between their emission and excitation spectra, called spectral overlap. It is important to keep spectral overlap in mind when designing a multiplex panel of various fluorochromes since the emitted light by one fluorochrome may in turn spill over into the excitation spectrum of another fluorochrome and pass through its emission filter. This is a common occurrence with for instance, fluorescein isothiocyanate (FITC) and phycoerythrin (PE). The spill-over of FITC emission into the excitation spectrum of PE and subsequent detection by the PE detector can be rectified by post-acquisition colour compensation. Compensation allows for the subtraction of FITC emission from the emission recorded in the PE detection channel. This is done by recording the emission of the two fluorochromes individually and determining the percentage of their emission detected in the channel assigned to the other fluorochrome. Tools such as the Fluorescence Spectra Analyzer by BioLegend (USA) can be used to design multiplex panels to determine the spectral overlap of the various fluorochromes (154). An exported example from the tool can be found in Figure 4.2.

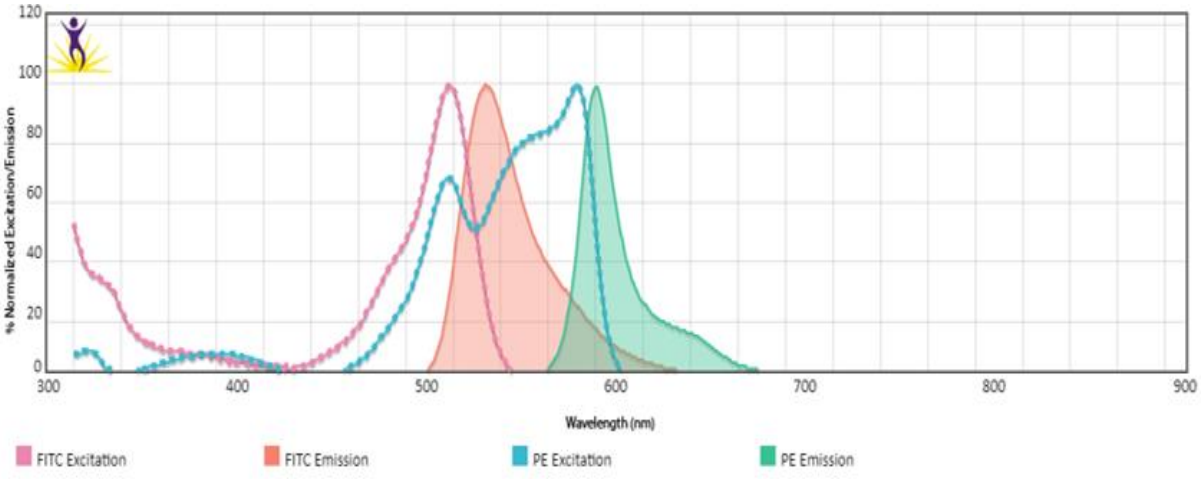

Figure 4.2: Exported image of the Fluorescence Spectra Analyzer tool showing the spectral overlap of FITC and PE.
The emission spectrum of FITC (red shaded) overlaps with the excitation spectrum of PE (blue dotted line) resulting in spectral overlap that will need to be corrected using colour compensation to ensure accurate flow cytometry results (154).

Determining the spectral overlap of fluorochromes must be done as part of the experimental set-up to ensure accurate flow cytometry data. The analysis of flow cytometric data uses gates and regions to analyse a subset or population of cells or particles of interest. A region is set around the population of interest on a graphical representation of the signals detected in the FL channels. Several regions can be set on the same graph. These regions can then be used to include or exclude (selectively gate) the specific population in the analysis of the data. For instance, using a FS vs SS plot, a region can be set around only intact cells, based on their size (FS) and complexity (SS), to exclude debris via gating in following analyses.

The Gallios™ flow cytometer (Beckman Coulter, Miami, USA) used in this study has three lasers and can detect 10 colours by using different fluorescent detector channels (FL). Table 4.2 summarises the Gallios™ laser and filter configurations.

Table 4.2: Gallios™ laser and filter configurations including frequently used laser-excited fluorochromes and the fluorescent detection channels used to detect them.

Laser	Detectors channels	Emission filter	Fluorochromes
488nm (Blue)	FL1	525/20	FITC, GFP, Annexin V
	FL2	575/20	PE, Nile Red
	FL3	620/30	PI, Flow-Count™ fluorospheres
	FL4	695/20	PE-Cy5 (Also known as PC5), 7AAD
	FL5	755 LP	PE-Cy5
638nm (Red)	FL6	660/20	PE-Cy7,
	FL7	724/20	APC, VDC Ruby
	FL8	755 LP	APC-Cy7
405nm (Violet)	FL9	450/40	BV421, DAPI
	FL10	550/40	Krome Orange (KO)

4.2.5.3.2 Leukocyte count sample preparation

Flow cytometry can be used to determine cell counts by using a sample to which a known concentration of fluorosphere beads is added. Fluorosphere beads contain fluorescent dye and are manufactured to be uniform in size and fluorescent intensity. The sample containing the beads is run through the flow cytometer and stopped after a predetermined time. The number of bead events counted can then be used to calculate the cell count by using Equation 1 and the known concentration of counting beads indicated on the product (155).

The samples were prepared for flow cytometric analysis by transferring a 100 µL aliquot into a flow tube. A 100 µL volume of LPR lysis buffer was added to the sample and briefly vortexed to lyse cells. The sample was incubated for 5 min at room temperature (RT), after which 500 µL DNA Prep stain, containing 50 µL/mg propidium iodide (PI), was added to stain DNA. Unstained controls included 500 µL PBS and no PI. The sample was then incubated for 10 min at RT in the dark. Flow-Count™ fluorospheres (100 µL) were added to the flow tube after which the sample was analysed on the Gallios flow cytometer.

4.2.5.3.3 Leukocyte count data acquisition and analysis

The flow cytometric protocol for assessing residual WBCs was previously set-up using whole blood by Dr E. Wolmarans (142). The process followed for data acquisition for this project involved firstly, the visualisation of the WBC population and Flow-Count™ by an FS Lin vs SS Log two-parameter dot plot and a SS Log vs PI [Excitation: 536 nm; Emission 620/30 BP] two-parameter dot plot. We identified the region containing nucleated cells (Figure 4.3A, Region M) and the region containing the beads (Figure 4.3A, Region L). The position of the beads was confirmed by running a sample containing only beads (Figure 4.3C). We included only intact beads from the Flow-Count™ fluorospheres using a two-parameter dot-plot with FS vs Time (gated on beads). On this dot plot, an area was used to exclude disintegrated beads (Figure 4.3B). Blood product samples were run for 5 min to obtain as many events as possible. Acquired data were analysed using Kaluza flow cytometry software (version 2.1, Beckman Coulter).

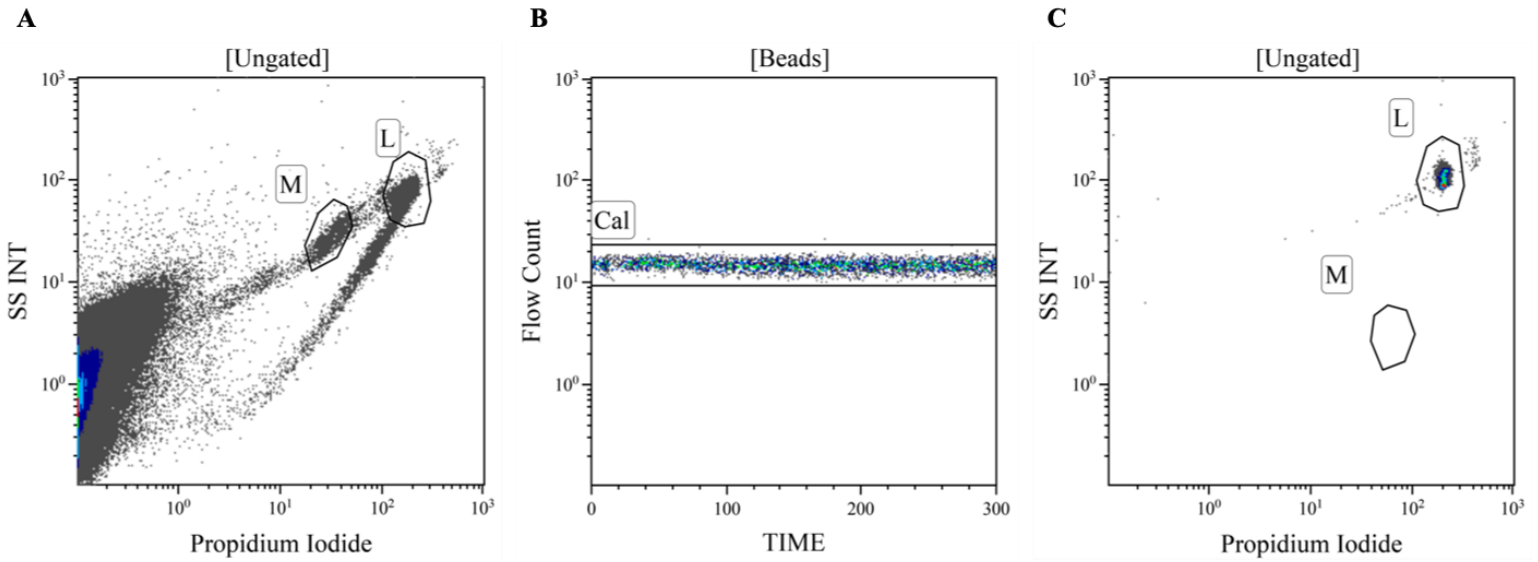

Figure 4.3: Representative plots of the gating strategy for WBC counts of the various blood products.
A: region M indicates the positively stained nucleated cell population with the Flow-Count™ fluorospheres indicated by region L. B: Disintegrated fluorosphere beads are excluded with only intact fluorospheres in the CAL region. C: a two-parameter SS vs PI plot obtained by running a sample containing only beads to confirm the beads region's position (set up by Wolmarans, 2019)

The following calculation was used to calculate the number of WBCs present in each unit of blood product:

$$\left(\frac{No.\,of\ WBCs\ counted}{No.\,of\ beads\ in\ CAL}\right) \times calibration\ factor = WBCs\ per\ \mu L\ blood\ product$$

Equation 1: Calculation of the number of WBCs present per unit of blood product

Region M (Figure 4.3A) indicated the 'number of WBCs counted', and the 'number of beads in CAL' was found in the CAL region (Figure 4.3B). The calibration factor is the number of Flow-Count™ fluorosphere beads per µL and is specified by the manufacturer. The result of this equation provides the number of WBCs per µL blood product. The total number of WBCs per unit of blood product was obtained by multiplying the number of WBCs/µL with the total volume of blood product, roughly 250 mL per unit.

4.2.5.4 Platelet count

The number of platelets in each blood product was determined to ensure that they adhered to the criteria of platelet-rich (PRP and pHPL) and platelet-poor (HS, PPP, FFP) blood products.

4.2.5.4.1 Platelet count sample preparation

Platelet counts were determined using aliquots taken from each sample. The aliquots were diluted 100 x by adding 20 µL sample to 1980 µL PBS to ensure accurate counts. We prepared flow cytometry tubes by adding 100 µL diluted sample to three tubes. We tested for the presence of two well-known platelet glycoproteins, CD42a and CD61 (156). A volume of 5 µL mouse anti-human CD42a-FITC and 5 µL mouse anti-human CD61-PE monoclonal antibodies (Beckman Coulter, Miami, USA) was added to two respective tubes. We left the third tube as an unstained control containing no antibody. The tubes were incubated for 10 min in the dark at RT. Before analysis on a Gallios™ flow cytometer, 1 mL PBS and 100 µL Flow-Count™ fluorospheres were added to each tube.

4.2.5.4.2 Platelet count data acquisition and analysis

Dr E. Wolmarans previously set up the flow cytometry protocol during the plasma product collection demo runs (142).

For data acquisition, the events recorded for the platelet counts were visualised on a two-parameter FS vs SS dot plot. The platelet population and Flow-Count™ fluorospheres were gated on this plot (Figure 4.4A). The CAL region was determined by a two-parameter FS vs Time dot plot to ensure only intact Flow-Count™ fluorospheres were included in the CAL region (Figure 4.4C). Platelets that stained positive for the antibodies were visualised on a two-parameter SS vs FL1 dot plot (Figure 4.4B). The platelets were stained with two antibodies separately, and the samples stained with CD61 PE (Excitation: 480 nm, Emission: 582/15 BP) or CD42a FITC (Excitation: 480 nm; Emission: 550 SP) were analysed separately on the flow cytometer to avoid spill-over of the emission spectra of the two fluorochromes. The region of positively stained platelets was determined by running an unstained control sample to determine the correct threshold. The samples were allowed to run for 5 min

to obtain as many events as possible. Acquired data were analysed using Kaluza flow cytometry software (version 2.1, Beckman Coulter).

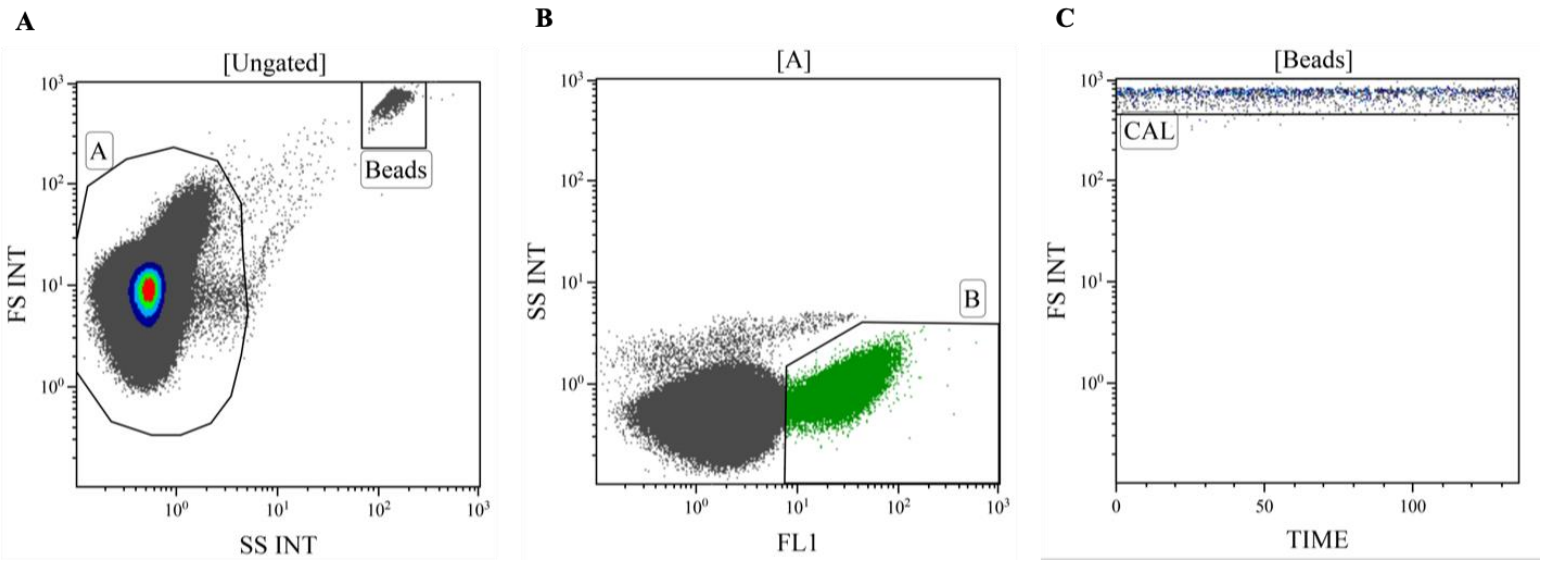

Figure 4.4: Representative dot plots illustrating the gating strategy to determine the number of platelets per unit of human alternative blood product (142).
A: Indicates the region of the platelet population (region A) and the region containing Flow-Count™ fluorospheres (Beads region) visualised on a two-parameter (SS Log vs PI log) dot plot. B: Identifies the platelets that stained positively for either CD61 PE or CD42a FITC (region B). C: Disintegrated fluorospheres were excluded and only intact fluorospheres were included in the CAL region, gated on beads.

The platelet counts were calculated using the following equation:

$$\left(\frac{No.\,of\ platelets\ counted}{No.\,of\ beads\ in\ CAL} \times Calibration\ factor\right) \times Dilution\ Factor$$

Equation 2: Calculation for the number of platelets present per unit of blood product

The 'number of platelets counted' was obtained from region B on Figure 4.4B. The 'number of beads in CAL' was obtained from the CAL region in Figure 4.4C. The Calibration factor was obtained from the Flow-Count™ product as it represents the number of fluorospheres per µL product. The dilution factor was 100, as stated previously. The calculation was done for the platelet counts of CD61 and CD42a stained samples (Figure 4.4B, region B). The final platelet count per unit of blood product was obtained using the average of the CD61 and CD42a stained counts and

multiplying this by the total volume of blood product received, which was around 250 mL.

4.3 Results

4.3.1 pH

The pH measurements (Table 4.3) indicated all units of the human alternatives obtained had a pH above 6.5, which meets the quality control criteria as outlined in Table 4.1

Table 4.3: pH measurements of all human blood products

Blood product	HS1	HS2	HS3	FFP1	FFP2	FFP3	PPP1	PPP2	PPP3	PRP1	PRP2	PRP3
pH	8.12	7.99	8.14	8.3	8.05	8	8.42	8.09	8.26	8.07	8.1	7.98

4.3.2 Sterility

Figure 4.5 illustrates blood agar plates on which 250 µL of each human blood product was spread and left to incubate for seven days at 37°C/5%CO_2. Figure 4.5A-C shows the results for microbial growth in each of the allogeneic human serum units. Figure 4.5 D-F represents the three allogeneic fresh frozen plasma units purchased from SANBS. Figure 4.5 J-L and G-I represent the three allogeneic units of PPP and PRP, respectively. Figure 4.5 M is a positive control for microbial growth. All the obtained human alternative blood products were negative for microbial growth, thus meeting the QC requirements.

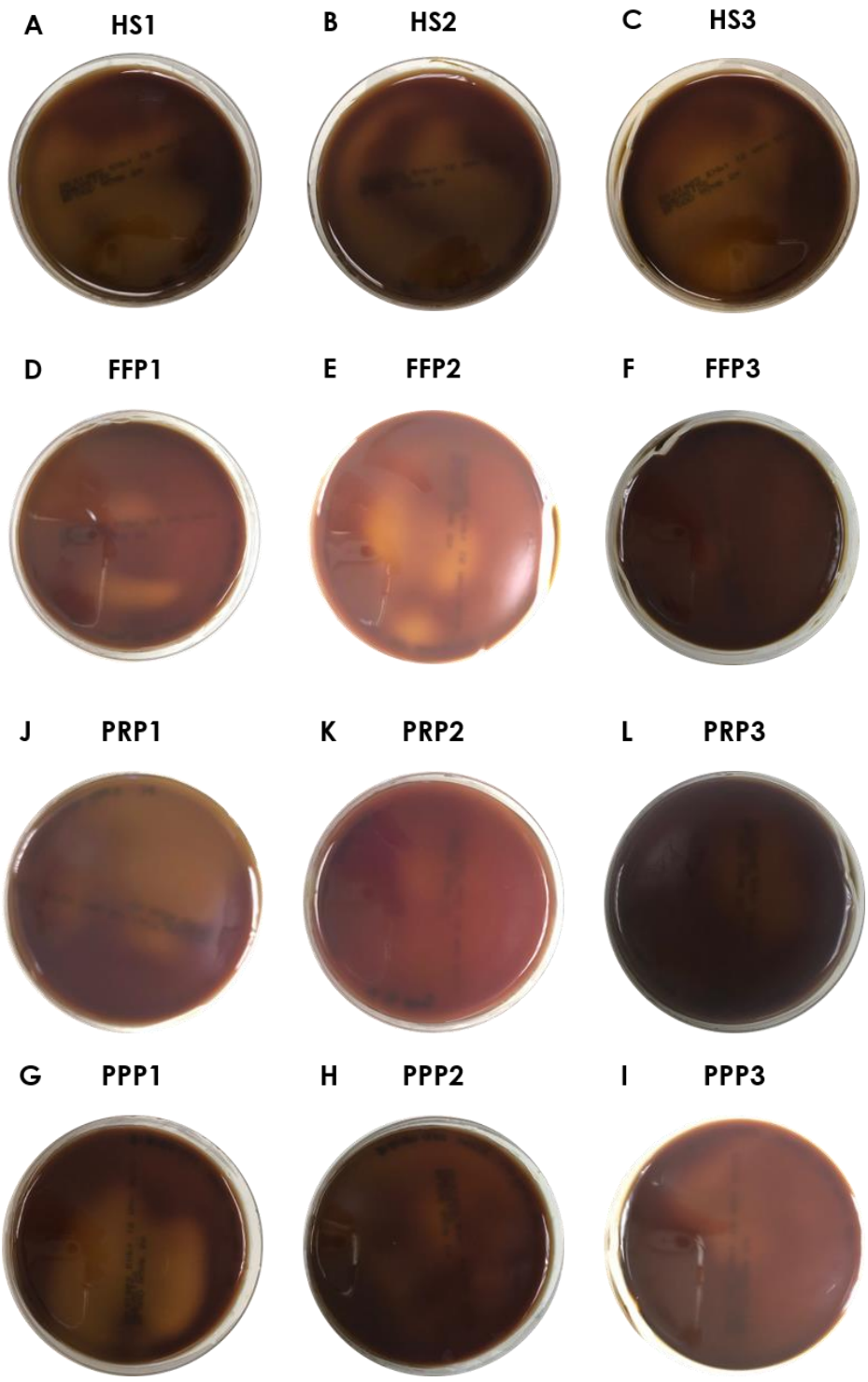
A HS1
B HS2
C HS3
D FFP1
E FFP2
F FFP3
J PRP1
K PRP2
L PRP3
G PPP1
H PPP2
I PPP3

Figure 4.5: Blood agar plates illustrating the lack of growth of microorganisms in human blood products used

A volume of 250 µL of each blood product was spread on a blood agar plate and investigated for microbial growth. A-C show the HS units, D-F represent FFP units. J-L and G-I show PPP and PRP units, respectively. M is a positive control for microbial growth. None of the blood products showed microbial growth, thus meeting the QC requirements outlined in Table 4.1 for sterility.

4.3.3 Leukocyte counts

Leukocyte counts were used to determine whether the blood products adhered to the selected composition criteria (Table 4.1). pHPL was tested previously (157); thus, we did not repeat it in this study.

The results Table 4.4 show that all blood products adhered to the selected composition criteria of less than 5×10^6 residual WBCs per unit of blood product as stated in AABB and Canadian standards (124,147).

Table 4.4: Results and calculations of WBC counts in human blood products

Blood product	No. of WBCs counted	CAL	Calibration factor	WBC/µL blood product	Total blood product volume (µl)	Total WBCs	Recommended (WBCs/unit)
Fresh frozen plasma							
FFP1	8	1942	1 014	4.18E+00	3.00E+05	1.25E+06	5.00E+06
FFP2	7	2224	1 014	3.19E+00	2.60E+05	8.30E+05	5.00E+06
FFP3	7	2117	1 014	3.35E+00	3.00E+05	1.01E+06	5.00E+06
Human serum							
HS1	3	2117	1 014	1.44E+00	1.60E+05	2.30E+05	5.00E+06
HS2	6	2167	1 014	2.81E+00	1.60E+05	4.49E+05	5.00E+06
HS3	7	2187	1 014	3.25E+00	1.39E+05	4.51E+05	5.00E+06
Platelet-poor plasma							
PPP1	6	2311	1 014	2.63E+00	2.46E+05	6.46E+05	5.00E+06
PPP2	7	2259	1 014	3.14E+00	2.58E+05	8.11E+05	5.00E+06
PPP3	9	2063	1 014	4.42E+00	2.55E+05	1.13E+06	5.00E+06
Platelet-rich plasma							
PRP1	12	1965	1 014	6.19E+00	2.25E+05	1.39E+06	5.00E+06
PRP2	24	1991	1 014	1.22E+01	2.52E+05	3.08E+06	5.00E+06
PRP3	11	1780	1 014	6.27E+00	2.50E+05	1.57E+06	5.00E+06

The total WBCs is the final number of WBCs per unit of blood product. The recommended WBCs/unit is the maximum number of WBCs recommended per unit of blood product.

4.3.4 Platelet counts

Platelet counts in the human blood products were performed to determine whether the human alternatives adhered to the previously specified composition criteria. Dessels and colleagues previously tested the pHPL (157) and thus, we did not repeat the tests.

The results in Table 4.5 show that all three allogeneic PRP samples adhered to the criteria for platelet-rich products with platelet counts above 2.5×10^{11} platelets per unit (PLTs/unit) (28,145). The platelet-poor products (FFP, HS, PPP) had platelet numbers above the criteria of 2.5×10^{9} PLTs/unit (146), however still below the threshold for platelet-rich products (above 2.5×10^{11} PLTs/unit). Therefore, we decided to record the values for the platelet-poor products and continue with the experiments, using the products as is.

Table 4.5: Results and calculations of platelet counts in human blood products

Blood product	Antibody	Counted events	CAL	Cal factor	Dilution Factor	PLTs/µL	Total volume (µL)	Total (PLTs/unit)	Mean total (PLTs/unit)	Recom-mended (PLTs/unit)
Fresh frozen plasma										
FFP1	CD61	965	1895	1014	100	5.16E+04	3.00E+05	1.55E+10	1.06E+10	< 2.50E+09
	CD42a	369	1981	1014	100	1.89E+04		5.67E+09		
FFP2	CD61	932	1981	1014	100	4.77E+04	2.60E+05	1.24E+10	1.02E+10	< 2.50E+09
	CD42a	566	1888	1014	100	3.04E+04		7.90E+09		
FFP3	CD61	1617	1786	1014	100	9.18E+04	3.00E+05	2.75E+10	1.82E+10	< 2.50E+09
	CD42a	535	1817	1014	100	2.99E+04		8.96E+09		
Human Serum										
HS1	CD61	5576	2361	1014	100	2.39E+05	1.60E+05	3.83E+10	2.12E+10	< 2.50E+09
	CD42a	473	1898	1014	100	2.53E+04		4.04E+09		
HS2	CD61	1419	1956	1014	100	7.36E+04	1.60E+05	1.18E+10	7.58E+09	< 2.50E+09
	CD42a	420	2008	1014	100	2.12E+04		3.39E+09		
HS3	CD61	2063	1993	1014	100	1.05E+05	1.39E+05	1.46E+10	1.05E+10	< 2.50E+09
	CD42a	859	1914	1014	100	4.55E+04		6.33E+09		
Platelet-poor plasma										
PPP1	CD61	424	1965	1014	100	2.19E+04	2.46E+05	5.37E+09	3.80E+09	< 2.50E+09
	CD42a	289	3227	1014	100	9.08E+03		2.23E+09		
PPP2	CD61	954	1711	1014	100	5.65E+04	2.58E+05	1.46E+10	1.22E+10	< 2.50E+09
	CD42a	674	1795	1014	100	3.81E+04		9.82E+09		
PPP3	CD61	315	1788	1014	100	1.79E+04	2.55E+05	4.56E+09	3.96E+09	< 2.50E+09
	CD42a	233	1786	1014	100	1.32E+04		3.37E+09		
Platelet-rich plasma										
PRP1	CD61	59554	1702	1014	100	3.55E+06	2.25E+05	7.98E+11	7.48E+11	> 2.50E+11
	CD42a	50 791	1661	1014	100	3.10E+06		6.98E+11		
PRP2	CD61	47443	1807	1014	100	2.66E+06	2.52E+05	6.71E+11	6.75E+11	> 2.50E+11
	CD42a	45095	1696	1014	100	2.70E+06		6.79E+11		
PRP3	CD61	56519	1752	1014	100	3.27E+06	2.50E+05	8.18E+11	8.19E+11	> 2.50E+11
	CD42a	54015	1668	1014	100	3.28E+06		8.21E+11		

The mean total (PLTs/unit) indicates the final number of platelets per unit of blood product as it is the mean of the counts obtained from staining with CD61 and CD42a. Recommended PLTs/unit is the criteria for the minimum and maximum limits for platelet numbers according to literature.

4.4 Discussion and conclusion

We completed the production and quality control of the chosen blood products and stored the products for future use—the blood products adhered to the criteria set out in Table 4.1. All the blood products had a pH > 6.5 and the negative sterility tests revealed the absence of contaminating microorganisms. The pH measurement and negative sterility results indicate no bacterial or fungal microbes present in the blood products. These results reduce the risk of bloodborne disease transmission (28,152) and adhere to GMP and GCCP (24).

All the blood products used contained less than 5×10^6 leukocytes. The leukocyte count is an important quality control step to ensure that WBCs do not significantly alter the cytokine composition of the culture medium in a manner that introduces variability in the growth or other characteristics of the MSCs we plan to expand and maintain in these media (28,137). An accurate count of leukocytes present in the blood products as part of the description of the products used is important for reproducibility in clinical products to ensure that all quality criteria can be maintained and compared (148). Furthermore, this is a critical quality control step to introduce, should hASCs intended for clinical use be expanded and maintained in culture media containing human blood products. One wants to avoid potential side effects after hASC transfusion such as HLA alloimmunisation, as discussed previously.

The platelet counts for PRP were well above the threshold of 2.5×10^{11} platelets/unit; however, there were more than the recommended 2.5×10^9 platelets/unit in the platelet-poor products. A reason for this may be the collection protocol of the apheresis machine that we used. Another possibility may be that we can improve the counting protocol for specificity and sensitivity since it is not a commercially standardised kit that was used. One can consider using a more diverse panel of antibodies specific to platelet surface markers to obtain a more accurate representation of the number of platelets present in the blood products (156). It is important to note that since the blood products we obtained we acquired in collaboration with SANBS, the products underwent the SANBS quality controls and adhered to the standards set out by the blood bank before being made available to us (158). As mentioned previously, there is little consensus regarding the threshold for

the number of platelets in platelet-poor products with wide-ranging recommendations for platelet counts in these blood products (28,145,146,151). Furthermore, increased platelet number in the platelet-poor products was still well below the threshold for platelet-rich products; consequently, these products cannot be considered platelet-rich, and we deemed them to be platelet-poor for the purpose of this study. Higher platelet numbers in platelet-poor-products could result in faster proliferation. Future studies should include investigation into standardisation of platelet numbers in products to be used in a therapeutic setting as well as the collection procedures and protocols to ensure a consistent product of high quality.

All the blood products were investigated for the discussed quality control criteria and found to adhere satisfactorily to the requirements.

Chapter 5: Proliferation and morphology

5.1 Introduction

The proliferation and morphology of hASCs expanded in the various human alternatives and FBS were compared. The morphology and proliferation of the hASCs were examined at different time points (days two, four, and six, based on work previously completed in the ICMM by Ms Carla Dessels (157)) using light microscopy and the sulforhodamine B (SRB) assay, respectively.

FBS was used as a control (19). as well as pHPL which has been studied extensively in our laboratory (157), and was therefore included as a control.

From previous studies, changes in hASC size and proliferation rate were expected when comparing human alternatives to the current standard, FBS. Deviation from the widely accepted fibroblast-like spindle-shaped morphology of MSCs was not expected (159). A higher proliferation rate for hASCs maintained in the platelet-rich human alternatives was expected, due to the higher levels of growth factors present in the human alternatives (148,160). Higher proliferation rates of hASCs are beneficial in the clinical setting as this reduces the time required in culture to obtain sufficient cell numbers for cell transplantation and patient treatment.

5.2 Materials and methods

5.2.1 α-MEM vs DMEM pilot study

Before comparing the different human alternatives, a pilot study was undertaken to compare hASC proliferation in Minimum Essential Medium Eagle – Alpha Modification (α-MEM) versus Dulbecco's Modified Eagles Medium (DMEM) as basal culture medium.

The pilot study was done to determine whether there was variability in morphology, proliferation, and viability of cells maintained in DMEM versus the α-MEM used in previous studies in our group (157). This comparison was necessary since the research group switched from α-MEM to DMEM as a basal culture medium after completion of the previously mentioned study. Since pHPL was previously extensively

studied in our group (157), it was chosen as the control human alternative supplement for the pilot study experiments that followed, and the two basal media were supplemented with 10% (v/v) pHPL. DMEM supplemented with 10% (v/v) FBS was also used as a control (19). The comparison was performed with three hASC biological replicates, which were maintained in the various media for six days.

5.2.1.1 Media preparation, thawing, and maintenance

5.2.1.1.1 Media preparation

Three different media were prepared: α-MEM (GIBCO, Invitrogen™, USA) supplemented with 10% (v/v) pHPL, DMEM (GIBCO, Invitrogen™, USA) supplemented with 10% (v/v) pHPL, and DMEM supplemented with 10% (v/v) FBS (GIBCO, Invitrogen™, USA) as the control. Complete growth medium (CGM) referred to in this study typically consists of: a supplement (FBS or human alternative(s)), basal culture medium, penicillin-streptomycin (p/s, GIBCO, Life technologies™, USA), and heparin (Biochrom, Merck Millipore, Germany), if needed. Table 5.1 shows the composition of the three different media.

Table 5.1: Medium composition for the initial study comparing α-MEM and DMEM as basal culture medium.

Medium	Supplement	Penicillin-Streptomycin	Heparin
α-MEM	10% (v/v) pHPL	2% (v/v)	2 U/mL
DMEM	10% (v/v) pHPL	2% (v/v)	2 U/mL
DMEM	10% (v/v) FBS	2% (v/v)	N/A

Heparin (2 U/mL medium) was added to CGM to prevent medium coagulation. Medium coagulation can occur as a result of clotting factors released by platelets present in the human alternatives which in turn results in a culture medium that is jelly-like (19).

5.2.1.1.2 Thawing and maintenance of hASCs

Three cryopreserved hASC cultures (A070415, A260515, A280616; P2) previously isolated according to the *Coleman* method (161) in the ICMM laboratory from abdominal lipoaspirate after obtaining informed consent (Appendix B), and expanded in CGM containing FBS and frozen in freezing medium (90% (v/v) FBS CGM and 10% (v/v) dimethyl sulfoxide (DMSO)) were used in experiments. Cultures removed from liquid nitrogen were thawed by pipetting 2 mL pre-warmed FBS CGM into the cryovial and pipetting up and down until the frozen cell suspension had thawed. The cells were transferred into a 15 mL sterile conical centrifuge tube and centrifuged at 300 × *g* for 5 min at room temperature (RT). The supernatant was discarded, and the cells were resuspended in pre-warmed PBS containing 2% p/s (unless stated otherwise). The cells were centrifuged again for 5 min at 300 × *g*. The supernatant was discarded, and the cells suspended in PBS once again. This step was repeated for a third time to ensure that all traces of DMSO and FBS were removed from the samples. It has been shown that cells previously expanded in FBS show no priming effect in terms of morphology, differentiation potential, proliferation, or chromosome stability before being exposed to human alternatives (130,157).

Cells resuspended in PBS were seeded in 4 mL CGM in 25 cm^2 tissue culture flasks (NUNC™, Denmark) at a density of 5000 cells/cm^2. The cells were incubated at 37°C, 5% CO_2 with medium replacement on day three.

Medium replacement was done by carefully aspirating the CGM from the respective tissue culture flasks and replacing it with 4 mL of the corresponding pre-warmed CGM. Care was taken not to accidentally aspirate hASCs.

Figure 5.1 represents the experimental layout.

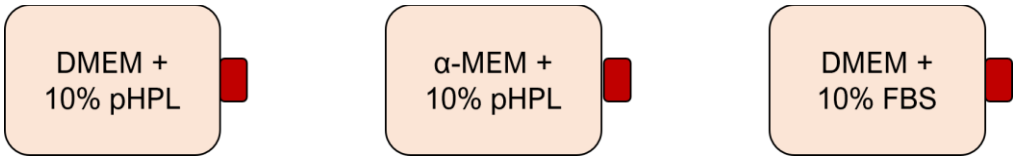

Figure 5.1: Pilot study experimental layout for comparing α-MEM and DMEM as basal culture medium.

5.2.1.2 hASCs were seeded into 25 cm^2 tissue culture flasks at 5000 cells/cm^2 Dissociation of cells

On day six, the cells were dissociated from the tissue culture flasks by removing the culture medium and gently washing with 2 mL pre-warmed PBS. TrypLE™ (2 mL, GIBCO, Life Technologies™, New York, USA) was added to the flasks and incubated for 10 min at 37°C, 5% CO_2 to allow the cells to detach. TrypLE™ is a gentle, highly pure, recombinant dissociation enzyme that is animal component free (162) which is important for GMP for cells intended for clinical use. To inactivate TrypLE™, it was diluted by adding 2 mL of the corresponding medium to each flask. The entire volume in each flask was transferred to a separate 15 mL centrifuge tube. Each flask was washed with 1 mL PBS which was also transferred to the centrifuge tube. The cells were centrifuged for 5 min at 300 × *g* at RT, the supernatant aspirated, and the cells resuspended in 1 mL PBS. Cell counts and viability (discussed in section 5.2.1.3 below) were determined to assess whether there was a significant difference in the proliferation and viability of hASCs expanded in DMEM compared to α-MEM.

5.2.1.3 Flow cytometry for cell count and viability

The cell count and viability of hASCs maintained in DMEM vs α-MEM (DMEM 10% FBS as control) were assessed to ensure that DMEM as the basal culture medium in future studies will be comparable to previous studies completed in α-MEM.

All flow cytometry data was analysed using the Kaluza analysis (version 2.1) software.

The cell counts and cell viability were determined separately using separate flow tubes.

5.2.1.3.1 Cell count

The experiment was terminated after six days, and the cell count and viability determined. The results are displayed in Figure 5.6. All summary statistics and error bars presented on graphed data are expressed as mean cell count/percentage viability ± SEM. Significant differences were determined using the non-parametric Kruskal-Wallis test (163). Post-hoc analysis was done using Dunn's multiple comparisons test with Bonferroni correction to determine significance between groups and to correct for multiple sampling (164).

The cell counts for each medium were done by using separate flow tubes for each medium and adding 100 µL cell suspension, 100 µL Flow-Count™ fluorospheres counting beads (Beckman Coulter, Miami, USA), and 1 mL PBS to each tube. The 1 mL PBS was added to the tube to ensure that the probe does not run out of sample and to account for dead volume at the bottom of the flowtube where the probe does not reach. The cells were counted on a Gallios flow cytometer (Beckman Coulter, USA). Data was acquired for 2 min.

Figure 5.2 represents the gating strategy followed to determine hASC number. Regions were set around populations of interest. Gates were used to include or exclude populations in regions in the data analysis. An ungated forward-scatter (FS) vs side-scatter (SS) two-parameter dot plot was used to visualise cells. We excluded debris by setting a region around intact cells (Figure 5.2A, region 'ASCs'). The Flow-Count™ fluorospheres were visualised on a two-parameter FS vs fluorescence detector (FL) 3 dot-plot (Figure 5.2B, region 'BEADS'). Intact Flow-Count™ fluorospheres were visualised on a second two-parameter dot plot using FS vs Time

(gated on ‘BEADS’). A region was set to exclude disintegrated Flow-Count™ fluorospheres (‘CAL’ region, Figure 5.2C). A Boolean gating strategy (Exclude Beads = NOT ‘BEADS’) was used to exclude beads from the hASC population counted in Figure 5.2D, region ‘ASCs’ (FS vs SS). Smaller hASCs and Flow-Count™ fluorospheres are similar sizes, leading to an overestimation of the hASC count if fluorospheres are not excluded.

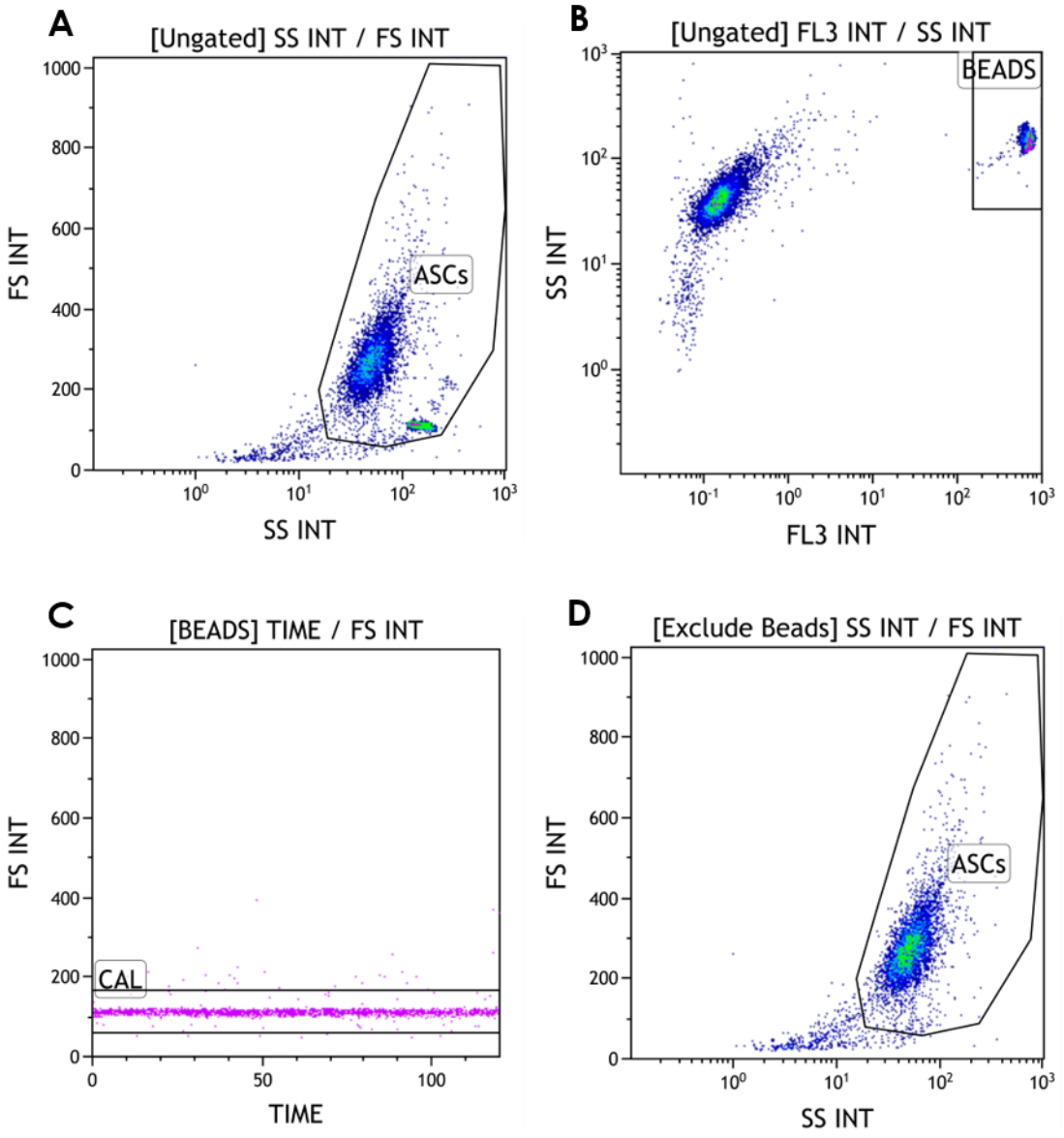

Figure 5.2: Representative images showing the gating strategy for hASC counting on the Gallios flow cytometer
A: Region ‘ASCs’ around cells excluded debris. B: Flow-Count™ fluorospheres were visualised on a two-parameter FS vs FL 3 dot-plot. C: broken Flow-Count™ fluorospheres were excluded using region ‘CAL’. D: Counted ASCs were determined using region ‘ASCs’ and excluding beads from the count using a Boolean gating strategy (Exclude Beads = Not BEADS).

We calculated cells per µL using Equation 3:

$$Cells\ per\ \mu L = \left(\frac{No.of\ events\ in\ ASC\ region}{No.of\ events\ in\ CAL\ region}\right) \times Calibration\ Factor$$

Equation 3: hASC count

The number of events in the ASC region was obtained from Figure 5.2D, region 'ASCs'; it is the number of hASCs in the ASC region. The number of intact Flow-Count™ fluorospheres in the 'CAL' region in Figure 5.2C was used as the number of events in the CAL region. The calibration factor is specified on the Flow-Count™ fluorospheres product. It is the number of fluorospheres per µL, the known concentration of beads.

5.2.1.3.2 Cell viability

7-Amino-actinomycin D (7AAD) was used to determine hASC viability. 7AAD is a DNA intercalating dye that is excluded from viable cells. 7AAD cannot permeate cell membranes; therefore, cells will only stain positive for 7AAD if their membrane integrity is compromised. 7AAD positive cells are therefore considered non-viable.

Viability of hASCs was determined by adding 5 µL 7AAD (488 nm excitation, 647 nm emission, FL4 channel) and 100 µL cell suspension to a flow tube followed by a 10 min incubation in the dark at RT. PBS (1 mL) was added to the flow tube before being analysed on the Gallios flow cytometer. An unstained control was included to set the gates and was handled in precisely the same manner as the stained sample.

The cell population was visualised on an ungated two-parameter (FS lin vs SS log) dot plot. In Figure 5.3A, the gated 'ASCs' region represents the cell population that excludes cell debris and any debris in the culture medium. Viable cells were visualised on a plot gated on 'ASCs' (to include only cells) representing the cells detected in the FL4 channel (Figure 5.3B, region B).

The unstained control was used in this instance to set the gate for region B, as this would indicate the cells that stained negatively for 7AAD; therefore, region B represents viable cells.

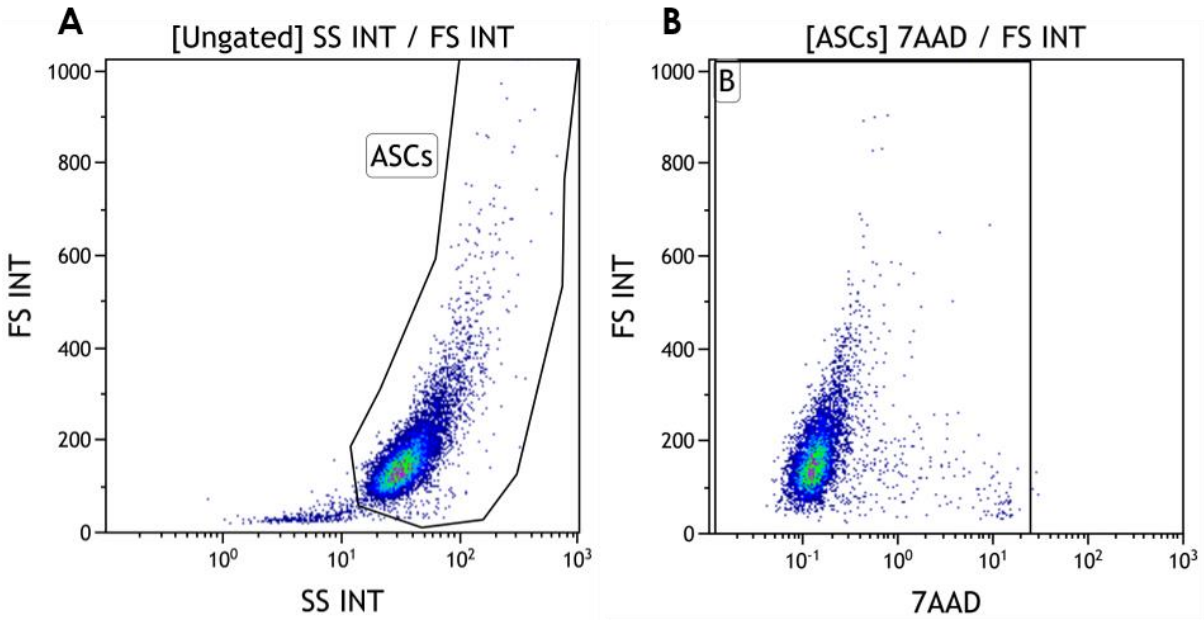

Figure 5.3: Gating strategy to determine viable hASCs.
A: two-parameter (FS vs SS) dot plot to visualise hASCs. The 'ASCs' region represents the hASCs and is used to exclude debris. B: The cell population in the FL4 (7AAD emission) channel is visualised by gated on the ASC population to exclude debris). Region B in B was set using an unstained control and represents viable hASCs.

5.2.1.4 Pilot study hASC morphology

We assessed the morphology of hASCs expanded and maintained in the various media using a Zeiss AxioVert A1 microscope. Representative images were taken after six days in culture at 5x magnification using a Zeiss Axiocam Ic5.5 digital camera. AxioVision software (Version 4.8.2) was used to take images that were enhanced for contrast and brightness but were not manipulated.

5.2.2 Main morphology and proliferation study

5.2.2.1 Media preparation

Complete growth media containing the various human alternatives as supplements were prepared. As mentioned previously, complete growth medium refers to the basal medium (DMEM) to which the various supplements have been added. In total, 14 different media (Table 5.2) were prepared by adding 10% (v/v) of each different human alternative to a base of DMEM supplemented with 2% (v/v) p/s. For PPP, FFP, HS, and PRP, three independent media were made since we received three allogeneic donations of each of these blood products. Preservative-free heparin (2 U/mL medium) was added to media containing pHPL, PRP, PPP, and FFP to prevent coagulation due to platelets releasing clotting factors in the medium (19). The human alternative supplements are expected to have donor-dependent and preparation-dependent variation in terms of their composition. Therefore, for the purpose of this study, a fixed 10% (v/v) serum supplement concentration was chosen to ensure continuity between FBS and the human alternatives.

As mentioned previously (section 5.1), FBS and pHPL CGM were considered to be controls. FBS was included as it is the current standard and pHPL as it has been studied extensively in our laboratory (157). It is important to note that the work with pHPL done previously used α-MEM as the basal growth medium. We did, however, complete a pilot study discussed in section 5.2.1 and showed that there was no significant difference between the two media when supplemented with pHPL (section 5.3.1).

Each of the human alternatives was filtered through a 70 µm cell strainer (BD Biosciences, Bedford, MA, USA) to remove debris before addition to the DMEM. Additionally, the human alternative complete growth media were filtered through a 0.22 µm filter before storage at 4°C.

Three cryopreserved hASC cultures (A071016, A100317, and A150817 at P2-3) were used for the SRB assay. The cultures were thawed and expanded in the various media in 75 cm^2 tissue culture flasks, as discussed in section 5.2.1.1.

Table 5.2: Summary of various media prepared

Medium	Serum/Plasma 10% (v/v)	p/s 2% (v/v)	Heparin (2 U/mL)	DMEM	Total
FBS	4.5 mL	900 µL	N/A	39.6 mL	45 mL
pHPL	4.5 mL	900 µL	18 µL	39.42 mL	45 mL
HS 1	4.5 mL	900 µL	N/A	39.6 mL	45 mL
HS 2	4.5 mL	900 µL	N/A	39.6 mL	45 mL
HS 3	4.5 mL	900 µL	N/A	39.6 mL	45 mL
FFP 1	4.5 mL	900 µL	18 µL	39.42 mL	45 mL
FFP 2	4.5 mL	900 µL	18 µL	39.42 mL	45 mL
FFP 3	4.5 mL	900 µL	18 µL	39.42 mL	45 mL
PPP 1	4.5 mL	900 µL	18 µL	39.42 mL	45 mL
PPP 2	4.5 mL	900 µL	18 µL	39.42 mL	45 mL
PPP 3	4.5 mL	900 µL	18 µL	39.42 mL	45 mL
PRP 1	4.5 mL	900 µL	18 µL	39.42 mL	45 mL
PRP 2	4.5 mL	900 µL	18 µL	39.42 mL	45 mL
PRP 3	4.5 mL	900 µL	18 µL	39.42 mL	45 mL

DMEM supplemented with 10% (v/v) FBS and pHPL respectively were used as controls. DMEM supplemented with 10% (v/v) serum/plasma was made using the separate allogeneic donations of HS, FFP, PPP, and PRP. Other additions to the media (heparin and p/s) are also listed. Volumes were adjusted according to total volumes needed throughout different studies.

5.2.2.2 Microscopy to determine hASC morphology in human alternatives

We assessed the morphology of hASCs expanded and maintained in culture media supplemented with the various human alternatives using a Zeiss AxioVert A1 microscope. Representative images were taken after six days in culture (at days two, four, and six)

at 5x magnification using a Zeiss Axiocam Ic5.5 digital camera. AxioVision software (Version 4.8.2) was used to take images that were enhanced for contrast and brightness but were not manipulated.

5.2.2.3 SRB assay to determine hASC proliferation in human alternatives

The SRB assay can be used to semi-quantitatively measure cell mass utilising the level of protein staining observed. Sulforhodamine B is a bright pink aminoxanthene dye that binds stoichiometrically to amino acid residues under mildly acidic conditions and can be solubilised and extracted under mild basic conditions (165–167). This colourimetric assay has been used in cytotoxicity screenings where cell mass can be determined from the amount of dye extracted (166,167). This property can be used to determine cell proliferation since higher cell numbers will contain more protein which will result in darker stained samples and a higher optical density (OD) value when analysed on a spectrophotometer. In short, faster hASC proliferation in media containing the various serum supplements will result in higher cell numbers containing higher protein levels, resulting in more dye binding and being extracted during the assay. The reverse will be observed if slower proliferation occurs.

We decided to use the SRB assay as an initial proliferation comparison assay since it is inexpensive and requires simple equipment. It also allows for high sample throughput experimental layouts. Results from the SRB assay were used to identify an appropriate time point for future investigations.

5.2.2.3.1 SRB sample preparation

The SRB assay was performed on cells seeded (at 5000 cells/cm^2) and expanded in 6-well tissue culture plates (NUNC™, Denmark) in the various media. Figure 5.4 is a graphic representation of the experimental layout. We adapted the protocol from multiple publications (166–168). Briefly, cells were fixed by adding 500 µL cold 50% (v/v) Trichloroacetic acid (TCA) to each well without removing the CGM and incubated at 4°C for 1 h after which the plates were washed four times with 2 mL distilled water and left to air dry at RT. Cells were stained by adding 1 mL (50% of the cell culture medium volume in the well) of a 0.4% (w/v dissolved in 1% (v/v) acetic acid) SRB solution to each well and incubated at RT for 30-60 min. The plates were rinsed four times with 2 mL 1% (v/v) acetic acid to remove any unbound dye and left to air dry at RT until completely dry. Dye solubilisation was achieved by adding 2 mL 10 mM tris

base solution (pH 10.5) to each well. The plates were shaken for 5 - 10 min on an orbital shaker. Samples were diluted (4% (v/v) dilution, (discussed in section 5.2.2.3.2)) in 200 µL total per well in a 96-well plate and read on a PowerWave™ spectrophotometer at 565 nm (the wavelength that is optimal to measure the absorbance of SRB dye). A reference wavelength of 690 nm was used to account for background absorbance in the multi-well plates and any other variation not due to the analyte. A blank measurement that contained only distilled water was also included. The SRB assay was performed on days 2, 4 and 6 after cells were seeded.

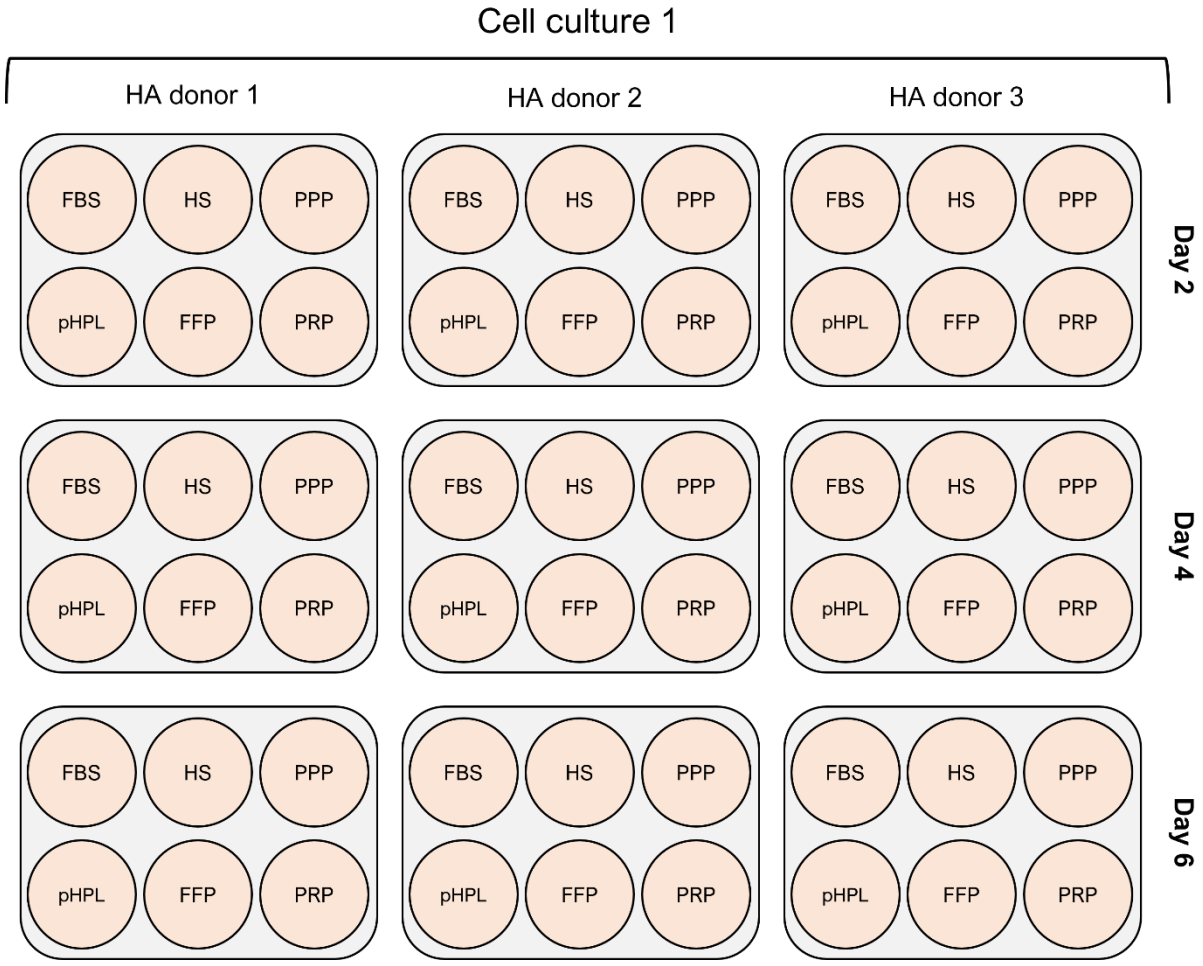

Figure 5.4: SRB cell culture experimental layout.
hASCs were seeded in 6-well plates for the various time points and human alternative supplement donors. The depicted configuration was repeated for three different hASC cultures. For pHPL and FBS n=3 with three technical replicates. For FFP, PPP, HS, and PRP n=9. Figure created by candidate.

5.2.2.3.2 SRB limit of linearity determination

A limit of linearity titration experiment was done to ensure the SRB assay's accuracy since SRB dye has a limit of linearity for detection at an OD ~2 (165–167). The limit of linearity is the linear range where the absorbance (or OD value) accurately reflects the concentration of the analyte actually present (169). On a graph of ODs plotted against a range of concentrations, the limit of linearity can be identified as the OD value where the graph starts to deviate from linearity (169,170). It is important to ensure that the OD of samples measured falls within the linearity range to ensure the results accurately reflect the true concentration of SRB present in the samples.

A serial dilution in a total volume of 200 µL per well was used in a 96-well plate using various concentrations of the darkest stained sample diluted in distilled water. The concentrations included 100%, 50%, 25%, 15%, 7%, 4%, 3%, 2%, 1% and 0% which contained only distilled water. The readings were taken at the same wavelengths described previously, in triplicate, on a PowerWave™ spectrophotometer, and graphed. The concentration where the graph started to plateau was used for diluting future samples to ensure that the OD values accurately reflect the amount of SRB dye present in the sample. As mentioned, the amount of dye will be used as an indication of cell proliferation in the various human alternatives.

5.3 Results

5.3.1 α-MEM vs DMEM pilot study

The purpose of the pilot study comparing α-MEM to DMEM was to ensure that results obtained in our study can be compared to work done by Ms Carla Dessels in α-MEM (157). Results are presented for n=3 experiments.

5.3.1.1 Pilot study morphology

The morphology of the cells (representative images from culture A280616 at P3) grown in pHPL (Figure 5.5 A-B) was more spindle-shaped and smaller than cells grown in FBS, similar to the findings from previous studies by Ms Carla Dessels (157). This morphology was observed regardless of the basal culture medium used (α-MEM or DMEM). The cells in pHPL were 100% confluent by day six in culture, whereas the cells in the FBS control were only 50-60% confluent by day six (Figure 5.5C).

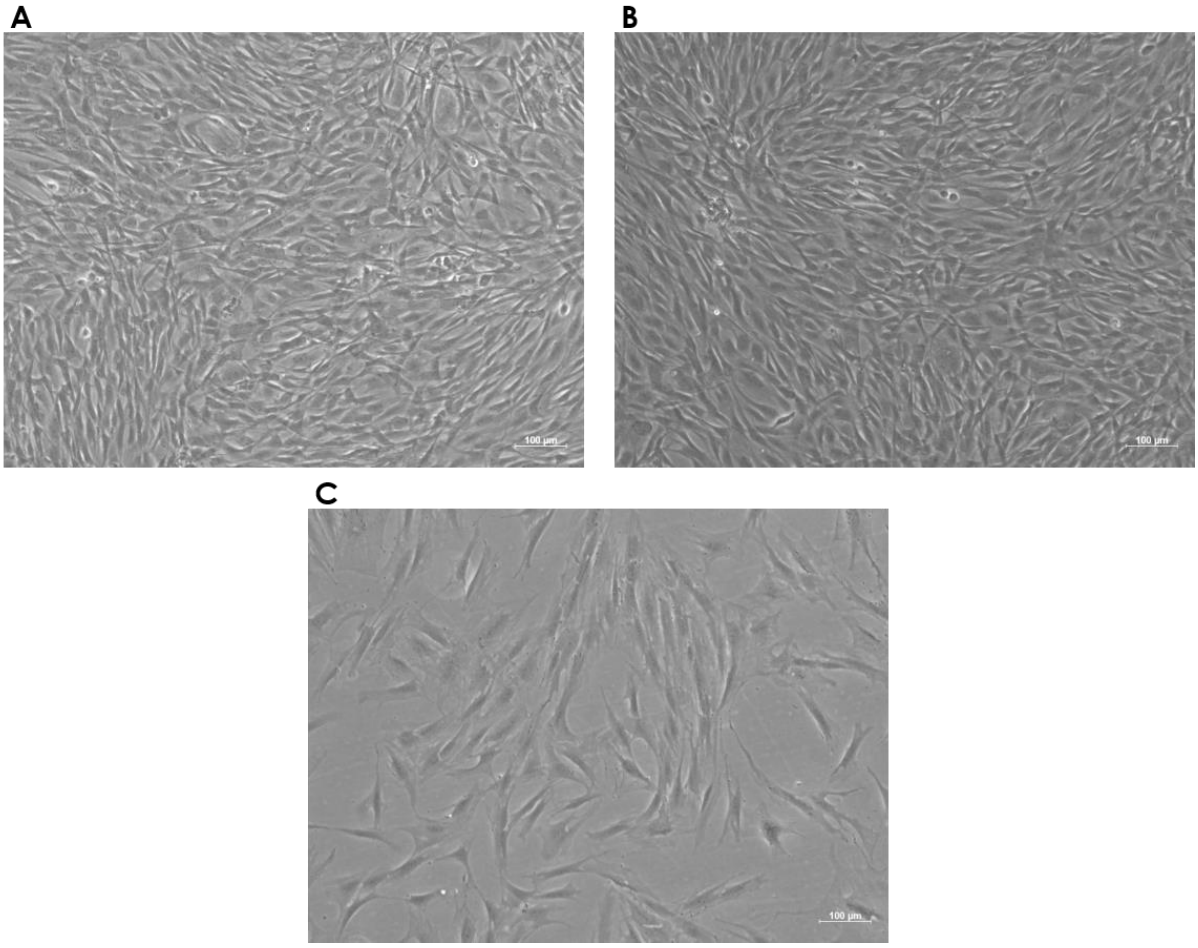

Figure 5.5: Representative light microscopy images of hASC morphology in various media at day six.
A represents the morphology of hASCs (A280615 P3) in α-MEM supplemented with 10% (v/v) pHPL. The morphology of hASCs in DMEM 10% (v/v) pHPL is shown in B. The control (10% (v/v) FBS in DMEM) is shown in C. Images were taken at 5x magnification. Scalebar = 100 µm. n = 3 for all medium supplements.

5.3.1.2 Pilot study cell count and viability

The significance level was set at $\alpha = 0.05$, and a p-value of < 0.05 was considered significant. Statistical analysis and graphical representation of the data were performed using R (version 4.0.3) and RStudio (version 1.4.1103).

A significant increase in cell number after six days in culture was observed for hASCs maintained in 10% (v/v) pHPL, regardless of the basal medium used (Figure 5.6A). The mean number of cells in α-MEM supplemented with 10% pHPL was 1 877 474 ± 315 537 after six days. DMEM supplemented with 10% pHPL yielded a mean of 1 830 035 ± 530 843 cells after six days. DMEM with 10% FBS resulted in a cell count of 288 897 ± 29 602 at day six. There is little difference when comparing the proliferation rates of hASCs maintained in 10% pHPL DMEM and 10% pHPL α-MEM after six days.

The viability of hASCs maintained in all three media was above 95%, depicted by the red line in Figure 5.6B. The average viability for hASCs in 10% FBS was 96.30% ± 0.21. For 10% pHPL supplemented α-MEM and DMEM, the average viabilities were 98.88% ± 0.25 and 99.21% ± 0.27 respectively.

The results show no difference in pHPL-supplemented α-MEM- or DMEM-expanded hASCs in terms of morphology, proliferation, or viability. We used DMEM supplemented with 10% pHPL as a human alternative control for the rest of the study.

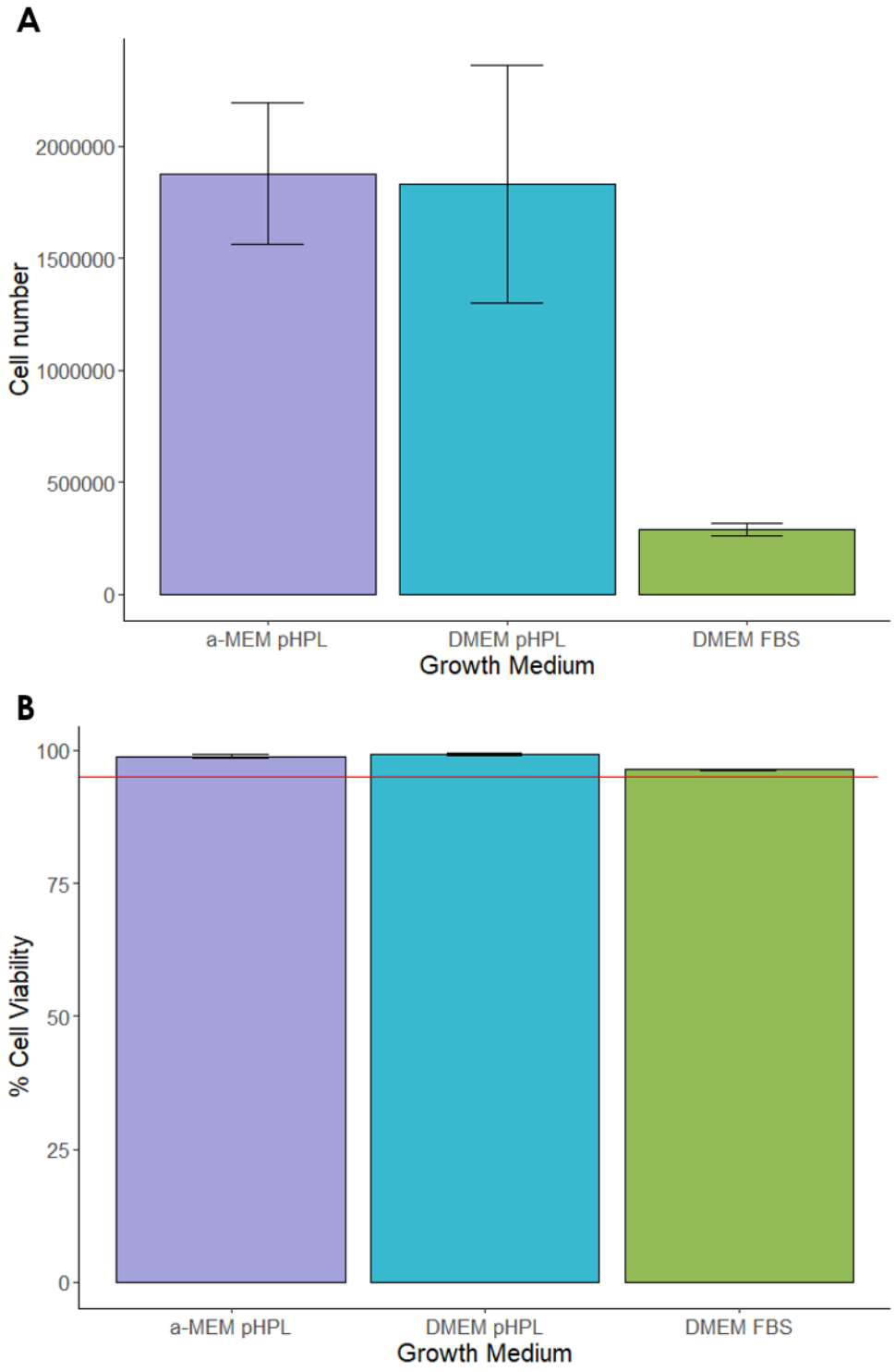

Figure 5.6: Cell count and viability of cells grown by flow cytometry in various media after six days. The number of cells grown in 10% (v/v) pHPL in α-MEM and DMEM and 10% (v/v) FBS in DMEM as control is shown in A with statistically significant higher cell numbers in both pHPL supplemented media compared to FBS. B represents the percentage of viable cells under the same experimental conditions with the red line indicating 95% viability. Error bars represent mean ± SEM and n=3 for all media.

5.3.2 Main morphology and proliferation study

The SRB assay is an inexpensive, semi-quantitative approach for comparing the proliferation of hASCs maintained in medium supplemented with the various human alternatives. Three hASC cultures were used for this experiment. For the two control media, (FBS and pHPL) n=3 experiments with three technical replicates per experiment. For the human alternatives (PPP, PRP, FFP, and HS) n=9: three allogeneic blood product donations were combined with three separate hASC cultures demonstrated in Figure 5.4. For the purpose of this study, results of the three allogeneic donations of each human alternative were combined (to achieve n=9) for statistical robustness and because this study aims to compare human alternatives to FBS, not the biological donors of blood products to each other.

5.3.2.1 hASC morphology in human alternatives

Figure 5.7 displays light microscopy images of one hASC culture (A071016 at P2) representing hASCs maintained in the various supplemented media on day six. The morphology of hASCs was spindle-shaped in all the media. Cells in PRP and pHPL (Figure 5.7E and F) were noticeably smaller than cells grown in the other media when comparing to the scale bar. hASCs in FFP- and PPP-supplemented media (Figure 5.7B & C) were similar in shape and size to hASCs in FBS-supplemented medium (Figure 5.7A). In HS-supplemented medium (Figure 5.7D), hASCs were smaller than in FBS-supplemented medium but larger than in PRP-and pHPL-supplemented media. The images also illustrate the differences in the proliferation of hASCs grown in the various culture media after six days as there are visibly more cells present in some media than other. This is, however, not a quantitative measure for proliferation in the various media, but supports results in 5.3.2.2 and 6.3.126.

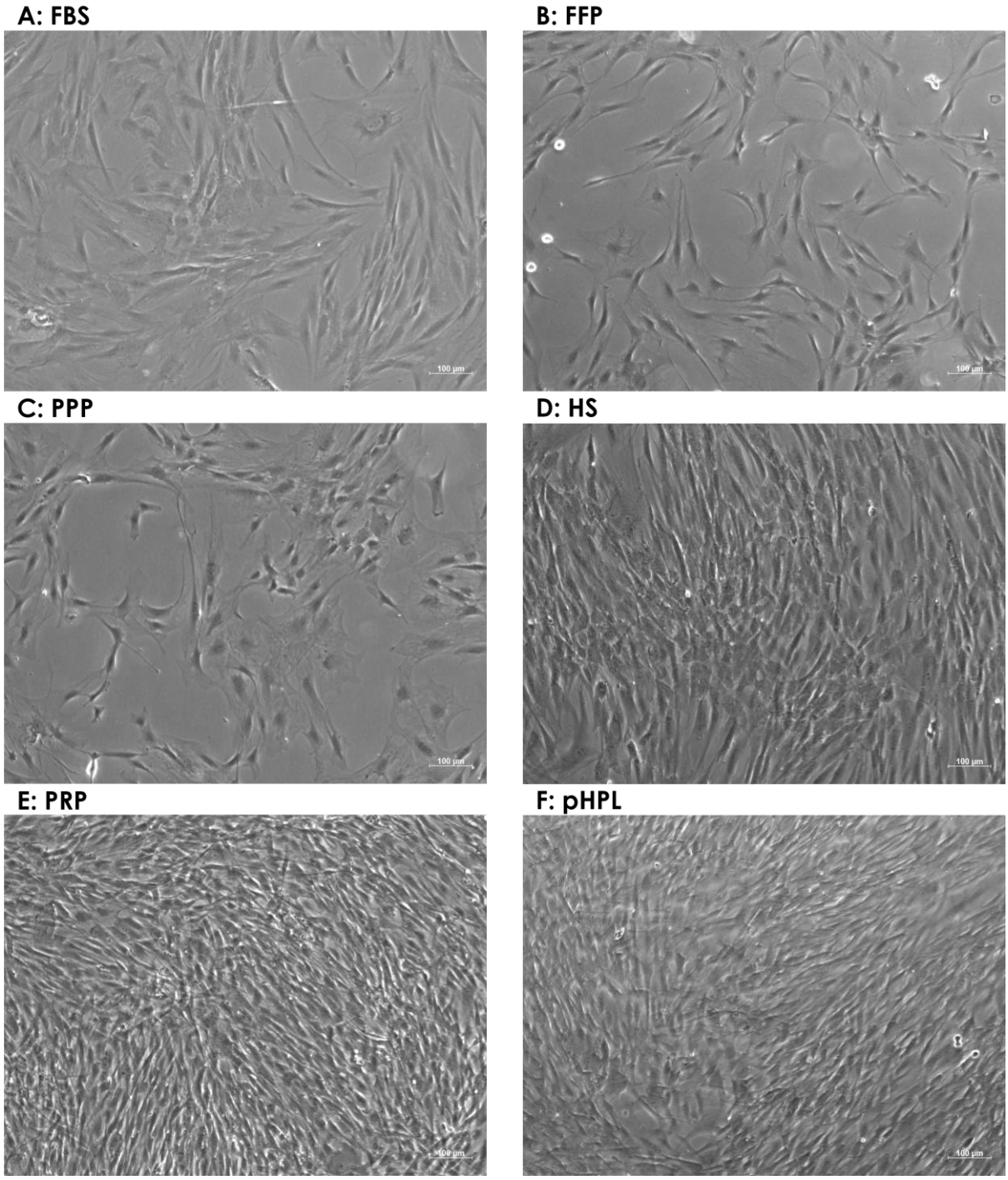

Figure 5.7: Representative light microscopy images displaying the differences in morphology and proliferation rate of hASCs maintained in various supplemented media after six days.
A-F represent hASCs maintained in FBS-, FFP-, PPP-, HS-, PRP-, pHPL-supplemented media respectively. For FBS and pHPL n=3 with three technical replicates, for PPP, PRP, FFP, and HS, n=9. (Scalebar = 100 µm, 5x magnification)

5.3.2.2 hASC proliferation in human alternatives

To determine if proliferation was significantly different between human alternatives and FBS, mean ODs on days 2, 4, and 6 were subjected to statistical analysis using the Kruskal-Wallis test and the Dunn's post-hoc multiple comparisons test with Bonferroni correction to correct for multiple sampling. Results of allogeneic human alternative donations were combined for the purpose of this study to ensure statistical robustness and because the aim of this study is to compare human alternatives to FBS. All summary statistics and error bars presented on graphed data are expressed as mean OD ± SEM. The significance level was set at $\alpha = 0.05$, and a p-value of < 0.05 was considered significant. Statistical analysis and graphical representation of the data were performed using R (version 4.0.3) and RStudio (version 1.4.1103).

The SRB assay's accuracy was ensured by doing a titration experiment to determine the assay's linear dynamic range where the OD values accurately reflect the concentrations of SRB present in the sample. The OD values were normalised to a blank of distilled water. Figure 5.8 shows the results obtained from the titration experiment. The OD graph of the readings starts to plateau at concentrations lower than 15% (Figure 5.8A). When looking at the concentrations of 0-15% (Figure 5.8B), the graph starts to plateau at a concentration of 4%. The 4% dilution equates to 8 µL SRB stained sample in 192 µL distilled water per well in a 96-well plate. All samples were diluted to this concentration for future OD measurements to ensure accurate measurements.

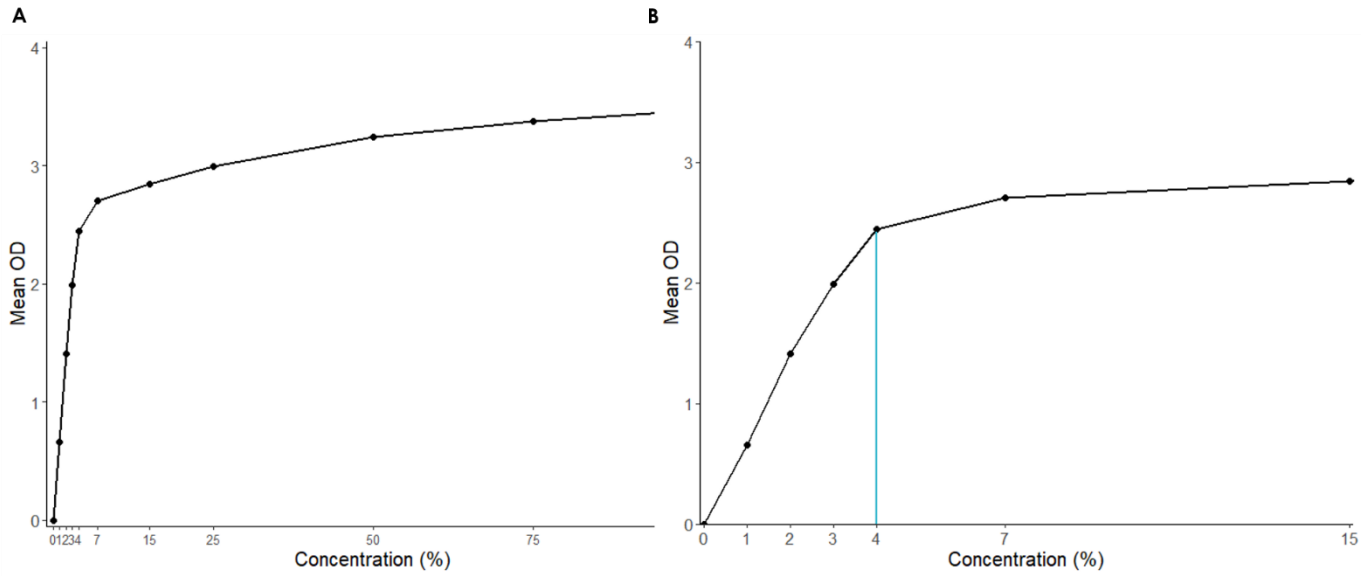

Figure 5.8: Line graphs displaying the concentration dilution series and resulting OD values of the SRB assay sample to determine the linear limit of detection of the assay.
A displays the plateau in OD values between 0-15% concentration indicating that samples more concentrated than 15% do not accurately reflect the amount of protein present. B, a closer look at the OD values between 0-15% concentration, shows the plateau is reached at 4% concentration (indicated by the blue line). This indicates the concentration at which the amount of SRB dye accurately reflects the amount of protein in the sample. OD values of three technical replicates plotted and normalised by subtracting the OD values of a blank of distilled water.

The SRB assay was used to compare the proliferation rate of hASCs maintained in the various supplemented media. After measuring the absorbance of the extracted SRB dye, OD values were plotted against time points. The dye intensity is an indication of the cell proliferation on days two, four, and six in culture.

The proliferation rate trends of hASCs in the various supplemented media are represented by the ODs displayed in Figure 5.9A. Figure 5.9B represents the same OD values as a bar graph and illustrates the results as mean OD ± SEM and statistical significance.

Results show increased OD over the six-day culture period for all the media, indicating that the hASCs proliferated in all media. The OD for FBS-supplemented media had the smallest increase across the time points, indicating that the cells proliferated at the slowest rate in FBS-supplemented medium compared to the human alternative-supplemented media.

At day two there was a statistically significant ($\alpha \leq 0.05$) increase in proliferation for all media (FFP, PPP, HS, pHPL, PRP) compared to FBS (OD = 0.02 ± 0.002). HS (0.23 ± 0.06), pHPL (0.38 ± 0.11), and PRP (0.62 ± 0.20) showed a significant increase in proliferation compared to FBS (0.03 ± 0.004) on day four as well. At day six, HS (0.22 ± 0.03), PRP (0.38 ± 0.07), and pHPL (0.45 ± 0.08) again showed significantly higher proliferation than FBS (0.04 ± 0.01). PRP and pHPL also had significantly higher OD values when compared to FFP (0.14 ± 0.01) on day six.

The results indicate that the proliferation rate for hASCs was the highest in PRP-supplemented medium, followed by pHPL-, and HS-supplemented media. FBS-supplementation resulted in the lowest proliferation rate.

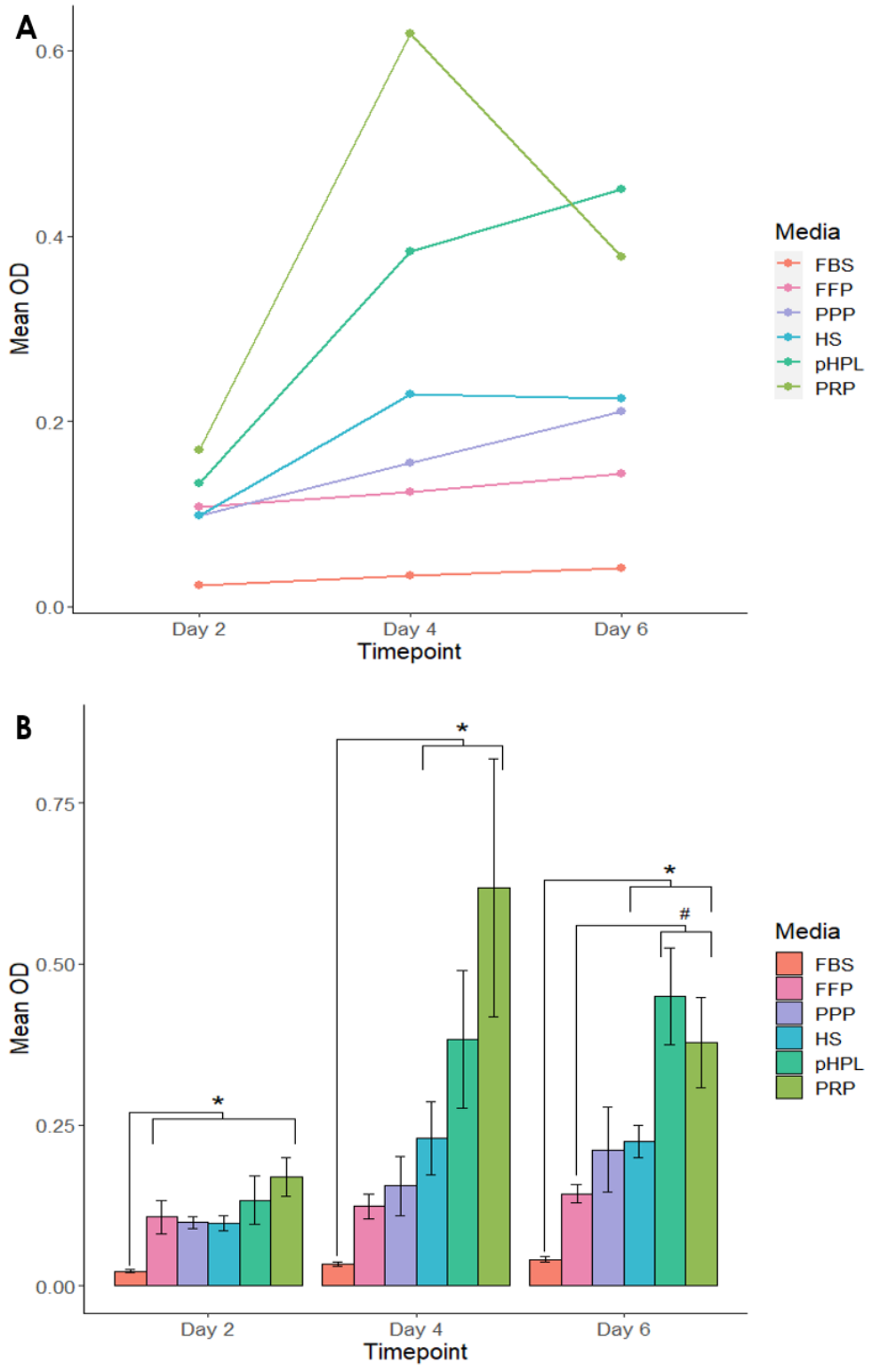

Figure 5.9: Graphs representing the mean OD values measured at various time points in the various supplemented media.

A demonstrates a line graph indicating the mean optical density (OD) value trends of hASCs in the different media. B represents a bar graph of the same mean OD values but includes SEM and statistical significance. On day two, all human alternatives proliferated significantly (indicated by * at day two) ($\alpha \leq 0.05$) more than FBS. Three human alternatives (HS, pHPL, and PRP) showed a significant increase in proliferation compared to FBS on days four and six (indicated by * at day four and six). PRP and pHPL also had significantly higher OD values than FFP on day six (indicated by # at day six). OD values were

normalised by subtracting OD values of a blank of distilled water. For FBS and pHPL n = 3 with three technical replicates, for FFP, PPP, PRP, and HS n = 9.

5.4 Discussion and conclusion

The initial study to compare DMEM and α-MEM as basal culture media did not show any significant differences in hASC morphology, viability, or cell count, similar to results previously reported (Czapla et al., 2019). Although cell number for hASCs in DMEM was slightly lower than in α-MEM, both were higher than in FBS, similar to previous reports by Czapla et al. (2019). We concluded that we could use DMEM as a basal culture medium for this study, and would still be able to compare it to previous work done using α-MEM supplemented with pHPL (157).

hASC proliferation and morphology in human alternative-supplemented media (FFP, PPP, PRP, HS, pHPL) yielded noticeable differences compared to FBS.

The confluence differences visible on day six micrographs and the semi-quantified results from the optical density values obtained from the SRB assay indicate that all the human alternatives displayed higher hASC proliferation than FBS with PRP, pHPL, and HS, showing significantly faster proliferation across all timepoints over six days. PRP, pHPL, and HS also proliferated the fastest, with PRP displaying the fastest proliferation and pHPL and HS showing the second and third highest proliferation. From previous studies (Choi et al., 2013; Czapla et al., 2019; Felthaus et al., 2017; Riis et al., 2016; Witzeneder et al., 2013), the higher proliferation of the human alternatives were expected. The spike in PRP growth on day four and subsequent decrease on day six could be due to over-confluence resulting in contact inhibition reducing proliferation, combined with hASC detachment from the tissue culture plate (175). It is important to keep in mind that these conclusions are drawn from a semi-quantifiable assay and a more precise investigation into the cell numbers is discussed in 6.2.1.

An explanation for the increase in hASC proliferation in human alternatives may be the presence of platelets releasing growth factors. Platelets release growth factors such as platelet-derived growth factor (PDGF), transforming growth factor-β (TGF-β), and vascular endothelial growth factor (VEGF), to name a few (38,160). These α-granule-derived growth factors increase cell proliferation (160,171). All human alternatives underwent a minimum of a single freeze-thaw cycle, as explained in the human alternative preparation chapter, which has been proven to function as a platelet

activation step to release growth factors (28,38). Future studies should investigate relationships between the proliferation of hASCs, the platelet numbers in blood products, and subsequently the composition of growth factors present to further understand the faster hASC proliferation seen in human alternative supplemented media.

The morphology of hASCs in all culture media maintained the traditional spindle shape expected from previous studies (25,30,34,171,176). However, hASCs in HS, PRP, and pHPL were smaller than in FBS, PPP, and FFP as can be seen when comparing size to the scalebar on the micrographs. The smaller size for pHPL and PRP was expected, as noted in previous studies (127,171,176). On the contrary, Riis and colleagues, 2016 (174) reported that hASCs in α-MEM supplemented with pHPL were larger than hASCs in FBS, and the authors attributed this to the fact that α-MEM was the basal medium, as other studies had reported the opposite for hASCs in DMEM with pHPL. From the pilot study, the results showed no noticeable difference in size between hASCs in α-MEM vs DMEM supplemented with pHPL, and in both media, the hASCs were smaller than in FBS. These results contradict Riis et al. 2016 (174) but confirm findings by Czapla et al. 2019 (171).

The differences in size between human alternatives and FBS could be explained by the differences in proliferation (Oikonomopoulos et al., 2015). The faster proliferation in human alternatives may have an impact on cell size since smaller cell size increases the efficiency of cell metabolism in terms of diffusion rates and cell surface area relative to volume (79). In HS, hASCs were slightly smaller than in FBS but larger than hASCs maintained in PRP and pHPL. Patrikoski et al. reported a wide spindle-shaped, cuboidal morphology for hASCs in HS (25). The current study's results, however, showed hASCs that were wider but with morphology similar to that of hASCs maintained in PRP and pHPL. The smaller cell size in HS could result from the slightly higher platelet number in HS, as discussed in the previous chapter.

Future studies should include a more in-depth analysis of the cell sizes mentioned using image analysis software or flow cytometry for a quantified conclusion to cell size. The study should also aim to compare the cell sizes using micrographs where hASCs in the various media are at similar confluency, roughly 50-60%.

From these results, any of the five human alternatives are suitable replacements for FBS as no noticeable changes in morphology were observed, and human alternatives result in a high proliferation rate. Since hASC numbers are higher than in FBS, it is possible to obtain clinically relevant cell numbers faster, making human alternatives the better choice in terms of hASC time required in culture. Studies of the immunophenotype and differentiation capacity of hASCs in the human alternatives will have to be considered before a definitive conclusion can be reached as to which human alternative is best suited to replace FBS, if any. Future research prospects also include investigating donor-related variability of the various human alternatives to determine a suitable autologous product for personalised regenerative medicine instead of a global standard option. The pooling of blood products from multiple donors for a medium supplement, as in the case of pHPL, may reduce the inherent biological variability (171) but excludes the possibility of an autologous therapeutic product.

Chapter 6: Main flow cytometry study

6.1 Introduction

In Chapter 5, the SRB assay was done as a preliminary estimation of the proliferation of hASCs in the various human alternatives compared to FBS. For a more complete quantitation of proliferation, the absolute count, cell cycle stages, and cell death and viability were evaluated by flow cytometry. The immunophenotype of the hASCs was also confirmed using flow cytometry. These parameters were measured for hASCs cultured for four days in the different media. The culture time was selected based on previous work in the SRB assay and visual cues indicating that hASCs have begun to proliferate without being overconfluent, which would risk contact inhibition (78).

The immunophenotype of hASCs in the various human alternatives was compared to FBS to ensure that culture and maintenance in the human alternatives do not alter the hASC immunophenotype from recommended guidelines. The hASCs must adhere to the required expressed immunophenotype to be classified as MSCs from adipose tissue (16,17).

After the immunophenotype was confirmed, an absolute cell count was done. The absolute count yielded a better representation of the increase or decrease in hASC cell number in the various media than the SRB assay, which examined proliferation in a broader context since it measures cellular protein content (167).

Cell proliferation was also evaluated by measuring the increasing DNA content of cells progressing through the cell cycle before nuclear replication (mitosis). Mitosis is the process whereby the replicated genome of a cell is segregated and split into two daughter cells. The cell cycle consists of four stages (G_1, S, M, G_2) and senescence (G_0, resting phase) where no proliferation occurs. Cells at rest (in G_0) enter the cell cycle at G_1, the first gap phase, after which genome duplication occurs in the S phase (S indicative of DNA synthesis). Cells then advance to the G_2 phase, another gap phase, where the integrity of the duplicated genome is scrutinised before progressing to the M (mitosis) phase, where nuclear and cytoplasmic division occurs. After mitosis, the two daughter cells can either re-enter the cell cycle to keep proliferating or enter G_0 (78,80,177,178). Should the cell cycle be arrested during the G_2 phase due to lack of

DNA integrity, programmed cell death (apoptosis) may be initiated if DNA repair is not feasible (78). Control of the cell cycle is vital as dysregulation may result in uncontrolled proliferation, which can be associated with high levels of cell death and potential tumour formation (81). Ultimately, cell proliferation is a delicate balance between an increase in cell number – through cell growth and progression through the cell cycle – and cell death.

Cell viability and death were investigated to ensure that the culture and maintenance of hASCs in human alternatives do not negatively impact cell proliferation and viability. Changes in the cell environment, for instance, a change in culture medium composition as in this study, can increase cell death (81,84) through internal or external mechanisms. Multiple processes for cell death are possible, including apoptosis and necrosis. Apoptosis and necrosis are often intertwined but can function separately and are distinct in their origins (84,179). Apoptosis is an ordered, programmed cell death resulting from internal signalling pathways. Apoptotic cells undergo morphological changes with an intact plasma membrane that includes cellular and nuclear shrinkage, chromatin cleavage, the formation of apoptotic bodies, and exposure of molecules on the cell exterior, such as phosphatidylserine (PS). In contrast, necrosis is considered accidental cell death due to external environmental disturbances and is characterised by rupture of the plasma membrane and subsequent leakage of cellular contents (84,87,179). Apoptosis is not necessarily guaranteed cell death and can be reversed, whereas necrosis is seen after cell death has already occurred, and cells cannot recover (84).

Investigation and understanding of hASC proliferation and death in human alternatives is essential for reaching therapeutic hASC cell numbers as efficiently as possible.

6.2 Materials and Methods

Three cryopreserved hASC cultures (P2-4) were thawed, seeded, and cultured for four days in the different media described in Chapter 5 (section 5.2.1.1). On day four, cells were dissociated as previously described (section 5.2.1.2), pelleted by centrifugation, and resuspended in 500 µL of the various media. The cell suspension was then used for absolute cell count, immunophenotyping, cell cycle analysis, and cell viability using flow cytometry. All flow cytometry data were analysed using Kaluza analysis (v2.1) software.

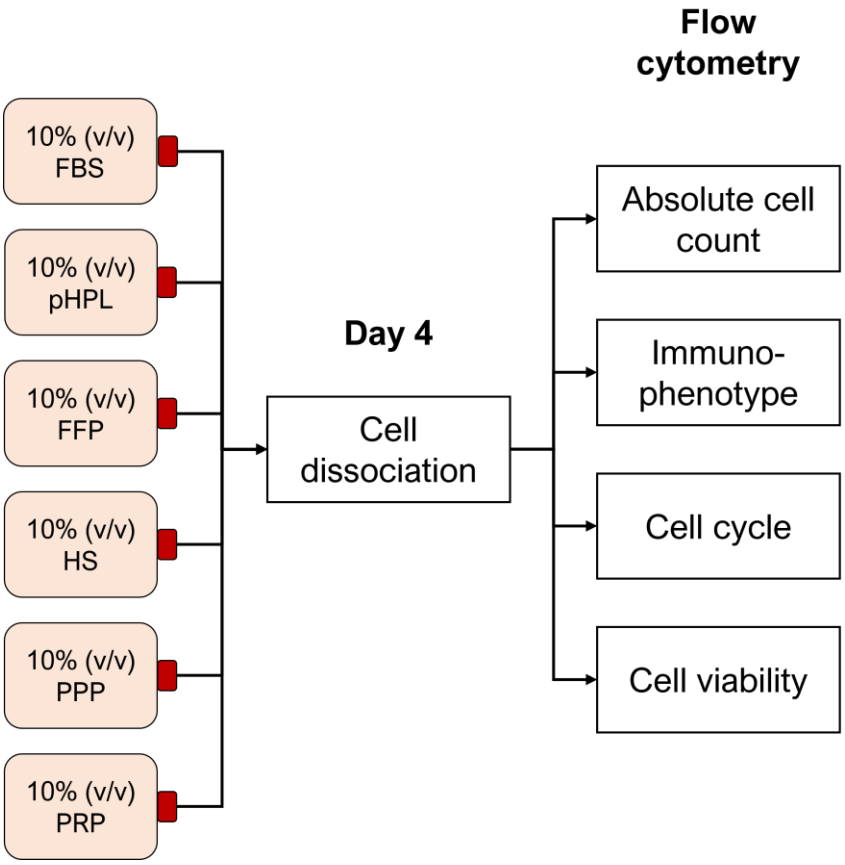

Figure 6.1: Experimental layout of the flow cytometry experiments.
hASCs were seeded in the various media (10% v/v) in 25 cm^2 tissue culture flasks and dissociated after four days. hASC cell count, cell viability, cell cycle stages, and immunophenotype in the various media were investigated and compared.

6.2.1 Absolute cell count

Cell counting by flow cytometry allows a good approximation of the number of cells present in the various media and a better indication of their proliferation than the SRB assay done in Chapter 5. A total of 125 000 hASCs were seeded per 25 cm^2 flask. The absolute cell number was determined using a fluorescent DNA stain called Vybrant® DyeCycle™ Ruby (VDC Ruby, Invitrogen/Molecular Probes®, Life Technologies, Eugene, USA). VDC Ruby is a stain that fluoresces upon binding to double-stranded DNA and can permeate the membranes of live cells (180). VDC Ruby can thus be used to discern between nucleated cells and debris or platelet remnants from the human alternatives in the culture medium. Its use ensures that only nucleated cells are included in the cell count.

6.2.1.1 Absolute cell count sample preparation

Dissociated hASCs resuspended in the various media were prepared for flow cytometry by adding 50 µL of the different cell suspensions and 0.5 µL VDC Ruby to separate flow tubes. The flow tubes were incubated for 5 min at RT in the dark to allow the dye to cross cell membranes and stain the DNA. Flow-Count™ fluorospheres (50 µL) were added to the flow tube along with 500 µL PBS. The PBS was added to ensure sufficient sample volume and account for dead volume at the bottom of the flow tube. The samples were analysed on the Gallios flow cytometer.

6.2.1.2 Absolute cell count data analysis

The nucleated ASC population in Figure 6.2B ('Nucleated ASCs_2') was identified by first visualising the ASCs on a two-parameter SS vs VDC Ruby (FL7; excitation: 488nm; emission 725/20 BP) dot plot. The cells that stained positive for VDC ruby were identified and included in the 'Nucleated ASCs' region (Figure 6.2A). The final nucleated ASC population was determined using a two-parameter FS vs SS dot plot gated on the 'Nucleated ASCs' area (Figure 6.2B). The 'Nucleated ASCs_2' region (Figure 6.2B) was drawn around the nucleated cells to exclude any debris, and the number of events in this region was used as the final nucleated cell count. The gating strategy described in 5.2.1.3.1 was used to identify the Flow-Count™ fluorosphere population shown in Figure 6.2C and D. The concentration of hASCs (cells per

microlitre) was calculated using equation 3 in section 5.2.1.3.1. The total number of hASCs was determined by multiplying the hASC concentration by the total resuspension volume for each medium.

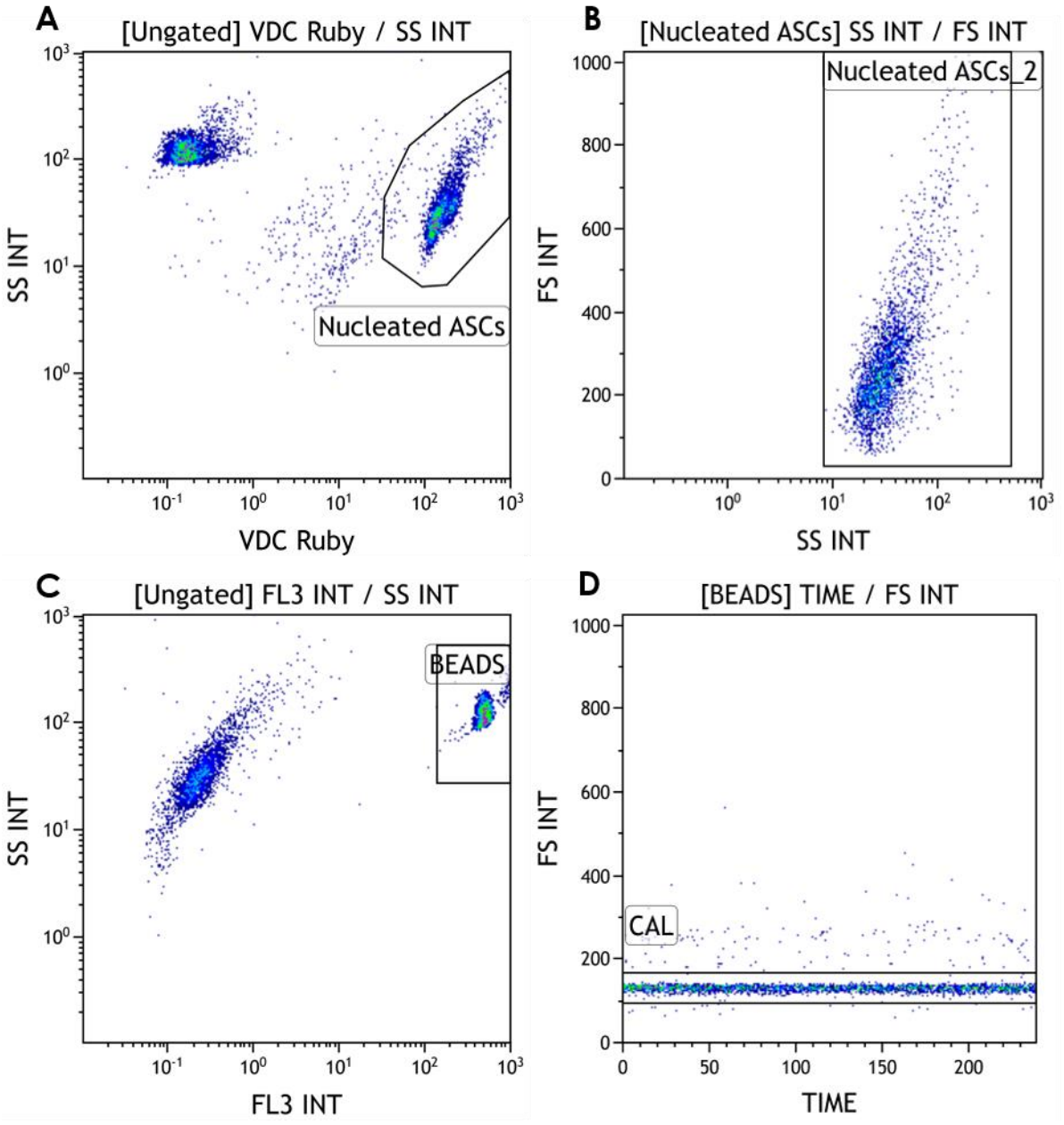

Figure 6.2: Representative plots of the gating strategy used for absolute cell counting.
A: 'Nucleated ASCs' area shows the cell population positive for VDC Ruby. B: 'Nucleated ASCs_2' region displays the cell population obtained after gating on 'Nucleated ASCs' in A. C and D were used to determine the Flow-Count™ fluorosphere population as described in section 5.2.1.3.1 above.

6.2.2 Immunophenotypic characterisation

Immunophenotyping is used to assess the specific antigen expression profile on cell surfaces by flow cytometry (16) to determine whether the hASCs cultured in the various human alternative-supplemented media adhere to the prescribed immunophenotype (16,17). A seven-colour flow cytometric panel was used to characterise hASCs according to the following well-described criteria: $CD90^+$, $CD44^+$, $CD73^+$, $CD105^+$, $CD36^+$, $CD45^-$, and $CD34^+$ (16,17,181).

6.2.2.1 Immunophenotype sample preparation

Dissociated hASCs resuspended in the various media were analysed for their external immunophenotype. Immunophenotype flow tubes were prepared for each medium by adding 100 µL cell suspension to two separate flow tubes. The first tube was used as an unstained sample to which no antibodies were added. To the second tube, 5 µL of each of the monoclonal antibodies (Beckman Coulter, USA) in the panel in Table 6.1 was added. The tubes were incubated at RT for 20 min in the dark before washing by adding 500 µL PBS (2% p/s), centrifuging for 5 min at 300 x g, and removing the supernatant. The wash was performed to remove unbound antibody, preventing non-specific staining that may result in increased background staining and poor resolution of positive and negative populations. The cells in each tube were resuspended in 500 µl PBS (2% p/s) before analysing on the Gallios™ flow cytometer.

Table 6.1: Seven-colour monoclonal antibody (Beckman Coulter, USA) panel for hASC flow cytometric immunophenotyping.

Monoclonal antibody	Fluorochrome	Excitation	Emission	Detection channel
CD 90	FITC	480 nm	550 SP	FL1
CD 44	APC Cy7	633 nm	725/20 BP	FL8
CD 105	PE	480 nm	582/15 BP	FL2
CD 73	BV421	405 nm	450/50 BP	FL9
CD 45	KO	405 nm	550/40 BP	FL10
CD 36	APC	633 nm	660 BP	FL6
CD 34	PC5 (PE-Cy5)	480 nm	675/20 BP	FL5

6.2.2.2 Immunophenotype data analysis

A sequential gating strategy was used to determine the cell surface co-expression profile of hASCs expanded in the various media.

An FS vs SS log two-parameter dot plot was used to visualise the hASC population. Debris was excluded by drawing a region around intact hASCs (Figure 6.3A, region A). Subsequent two-parameter plots with quadrants were used to determine the hASC co-expression profile as this allowed for the analysis of two cell surface markers at the same time. Figure 6.3B displays the bivariant CD44 vs CD90 dot plot gated on region A using intact hASCs after excluding cell debris (region A, Figure 6.3A). The hASC population positive for both markers was identified and was used to gate the subsequent plot. Figure 6.3C represents intact hASCs that have $CD90^+$ and $CD44^+$ expression visualised on a bivariant CD73 vs CD105 plot. The hASCs positive for both markers were identified. Figure 6.3D was gated on the previously identified hASC population and visualised on a bivariant CD45 vs CD36 plot. As previously, the hASC population of interest (positive for CD36 and negative for CD45) was identified. Consequently, Figure 6.3E represents intact hASCs that display $CD90^+$, $CD44^+$, $CD73^+$, $CD105^+$, $CD36^+$, $CD45^-$ cell surface marker expression on a bivariant CD90 vs CD34 plot. The final hASCs population that adheres to the prescribed cell surface-marker expression profile can be seen in Figure 6.3E in the $CD90^+$, $CD34^+$ quadrant.

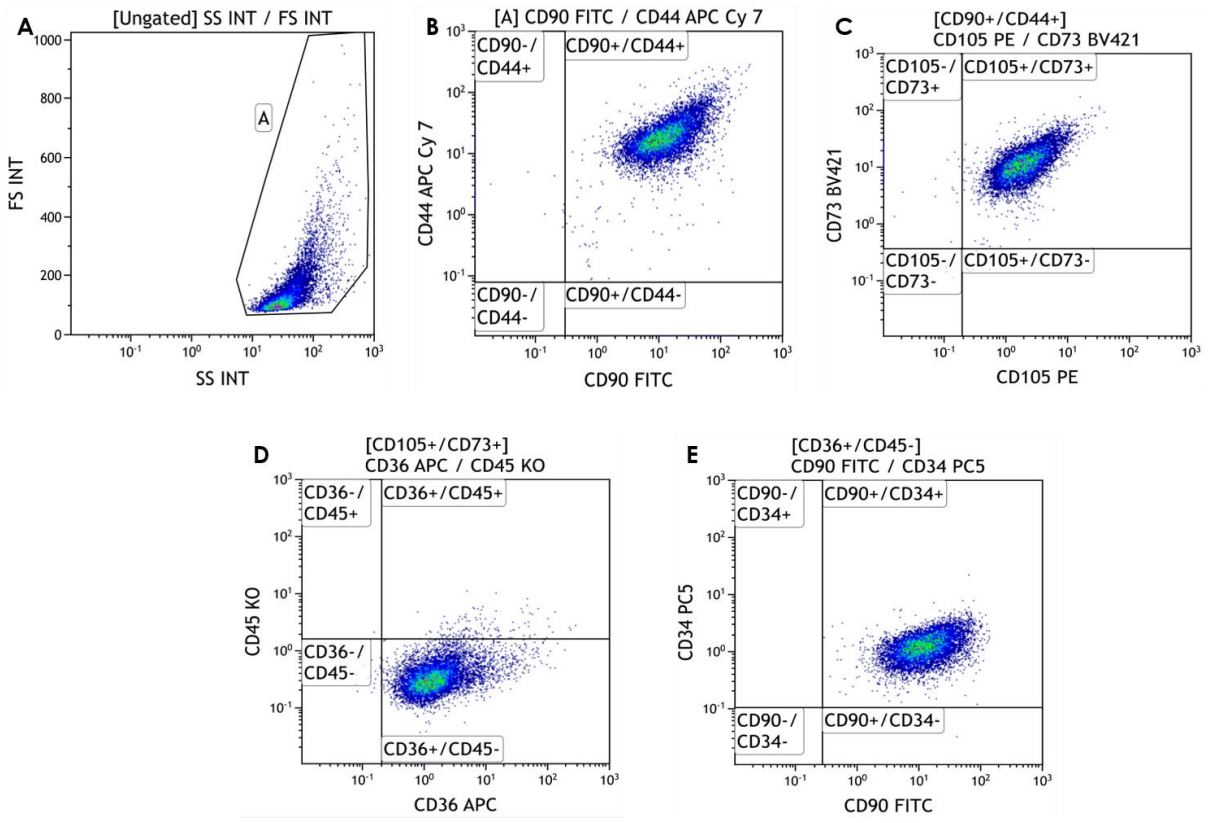

Figure 6.3: Representative images of the gating strategy followed to determine hASC immunophenotype.

A represents a two-parameter FS vs SS dot plot with region A gating out cell debris. B-E are bivariant dot plots divided into quadrants and gated on the populations identified in the previous plots that adhere to the immunophenotype co-expression described as the minimum requirements for MSCs. The sequential gating strategy was used to identify the hASCs in the final population visualised in E that has the co-expression immunophenotype $CD90^{+}$, $CD44^{+}$,$CD73^{+}$,$CD105^{+}$,$CD36^{+}$,$CD45^{-}$,$CD34^{+}$.

6.2.3 Cell cycle analysis

Cells in the various phases of the cell cycle can be assessed by using a fluorescent DNA binding dye. During the different stages of the cell cycle, cells have different amounts of DNA. During the G_0/G_1 phases, cells will only contain a single complement of DNA (2n). During the S phase, when DNA replication occurs, cells will have a varying amount of DNA since the genome is in the process of being duplicated. After the S phase, cells will contain twice the amount of DNA (4n) since the genome has been copied, but cytokinesis has not yet occurred (80). The changes in DNA content during the cell cycle phases (G_0/G_1, S, and G_2/M) were assessed using 4', 6-diamidino-2-phenylindole (DAPI, Invitrogen™, USA) staining. DAPI is a DNA fluorescent stain that preferentially binds to AT-rich regions in the minor groove of dsDNA molecules resulting in a roughly twenty-fold increase in DAPI fluorescence after binding (182,183).

6.2.3.1 Cell cycle analysis sample preparation

After dissociation, a 100 µL aliquot of hASCs in suspension in the various media was added to separate 15 mL centrifuge tubes and washed with 500 µL PBS by centrifuging for 5 min at 300 × *g.* The supernatant was removed, and the cell membranes were permeabilised by adding 100 µL DNA-Prep LPR buffer (DNA Prep Reagent Kit, Beckman Coulter, USA) to each tube and incubating on ice for 5 min. A 100 µL volume of DAPI wash buffer (PBS with 2% (v/v) p/s and 5% (v/v) FBS) was then added. The tubes were then centrifuged for 5 min at 300 × *g* and the supernatant discarded. The resulting cell pellet was resuspended in 1 mL DAPI staining buffer (3 µM) made up of 100 mM Tris (pH 7.4), 150 mM NaCl, 1 mM $CaCl_2$, and 0.5 mM $MgCl_2$, and incubated in the dark for 15 min.

6.2.3.2 Cell cycle analysis data analysis

Cell cycle flow cytometry data was analysed using Kaluza Analysis software v2.1. The hASCs were visualised on an ungated FS vs SS dot plot and a region drawn around the cell population to exclude debris present in the samples (Figure 6.4A, 'ASCs'). Doublets were excluded by visualising the hASC population identified in Figure 6.4A on a two-parameter FL9-area vs FL9-Height (DAPI, Excitation 358nm, Emission 450/50

BP) dot plot gated on the 'ASCs' region. The exclusion of doublets is crucial since it may skew the percentage of cells identified in the G_2/M phase. A doublet in the G_0/G_1 phase will have the same amount of DNA present (2n) as a single cell in G_2/M. The cell cycle was assessed by visualising the single, DAPI stained, nucleated cells on a single parameter histogram Count vs FL9 plot gated on the single-cell region identified in Figure 6.4B, 'Single ASCs' region. At least 20 000 events were acquired. If the number of events could not be reached, data was obtained until the flow tube was empty.

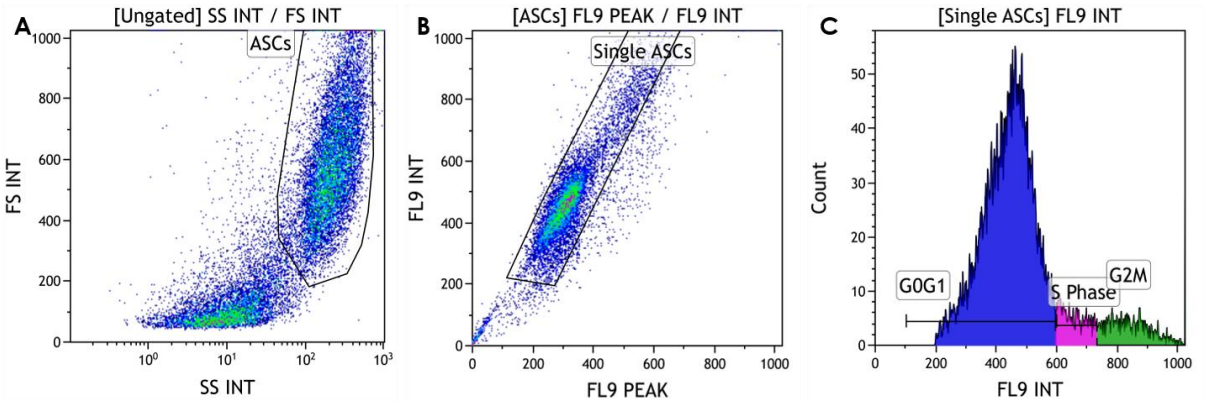

Figure 6.4: Representative plots of the cell cycle analysis gating strategy.
A was used to identify the hASC population and exclude debris ('ASCs' region). Doublets were excluded to ensure accurate results by visualising the hASCs on an FL9-Area vs FL9-Height dot plot and identifying single hASCs in B, region 'Single ASCs'. The cell cycle of single hASCs was assessed on a Count vs FL9 (DAPI) histogram plot (C).

6.2.4 Cell viability assay

The viability and stage of apoptosis/necrosis of the cells grown in the different human alternatives were investigated using Annexin V, which detects apoptosis, and propidium iodide (PI), which detects necrosis.

Annexin V is a phospholipid-binding protein that binds with high affinity to phosphatidylserine (PS). PS translocates to the exterior of the intact plasma membrane of apoptotic cells (153,184). Conjugation of a fluorophore to Annexin V allows Annexin V bound to PS on the exterior of the plasma membrane to be detected by flow cytometry (153,184).

A necrotic state can be determined by examining the integrity of the plasma membrane using PI. PI is an inexpensive nuclear stain that is excluded from viable cells since PI staining is dependent on the loss of integrity of the plasma membrane. The loss of membrane integrity of late apoptotic and necrotic cells allows PI to pass through the membrane and intercalate into DNA, resulting in red fluorescence (153,184). Early apoptotic cells will exclude PI due to the plasma membrane still being intact.

A co-stain of Annexin V-FITC and PI (Annexin V-FITC kit, Beckman Coulter, Miami, USA) can be used to assess apoptotic, necrotic, and viable (live) cells. Cell populations positive for Annexin V but negative for PI were considered apoptotic but still viable since apoptosis has begun. However, the plasma membrane is still intact and therefore, the cell can still recover. Populations positive for both Annexin V and PI were considered to be in late-stage apoptosis. The plasma membrane has started losing its integrity; therefore, positive staining for only PI was interpreted as necrotic, non-viable cells.

6.2.4.1 Cell viability sample preparation

Dissociated hASCs in the various media were prepared for viability analysis according to the Annexin V-FITC kit (Beckman Coulter, Miami, USA) instructions. Separate flow tubes were prepared by adding 100 µL cell suspension, 100 µL 1× binding buffer, 1 µL Annexin V, and 5 µL PI to each flow tube. The tubes were incubated on ice in the dark for 15 min to allow binding of Annexin V and PI, after which 400 µL 1× Binding buffer was added. A positive control for cell death was prepared by incubating 100 µL cell

suspension with 3% (v/v) formaldehyde in PBS for 30 min. A minimum of 10 000 events were acquired for data analysis.

6.2.4.2 Cell viability flow cytometry data analysis

An ungated two-parameter FS vs SS Log dot plot was used to identify single cells and exclude debris. The 'ASCs' region was drawn around this population, as in Figure 6.5A. Two parameter Annexin V (FL1 Excitation 480nm, Emission 550 SP) vs PI (FL3, Excitation; 488nm, Emission; 620/30 BP) dot plots were gated on the hASC population identified previously and assessed for sub-populations (Figure 6.5B). Cells in the lower left quadrant are negative for both Annexin V and PI and are considered healthy and viable.

A positive control for cell death was included, along with a negative unstained control to verify protocol settings. A minimum of 10 000 events were acquired and included in the data analysis.

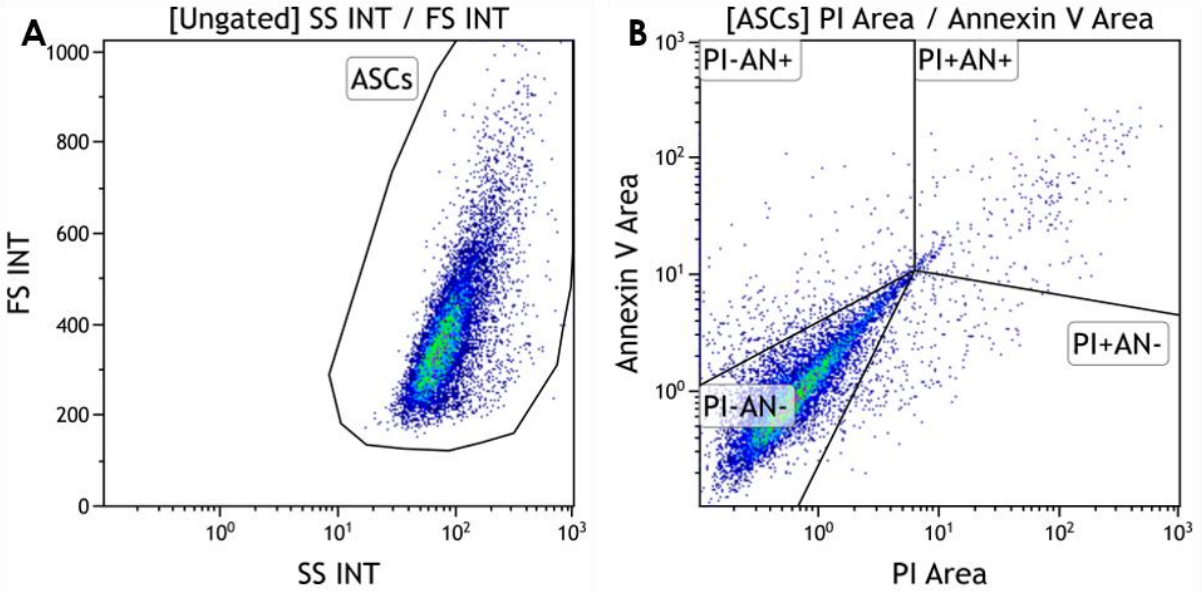

Figure 6.5: Representative plots of the gating strategy followed for the viability of hASCs maintained in the various media.
Single cells were included in the analysis, and debris was excluded by drawing a region around the hASC population ('ASCs' in A). The identified population was investigated for subpopulations positive or negative for annexin V and PI, gated on 'ASCs' in B.

6.3 Results

The results are shown as mean ± standard error after four days in culture. For pHPL and FBS, the controls, n=3. For the human alternatives, FFP, PPP, HS, and PRP; n=9 since three hASC cultures were combined with three allogeneic human alternative donors for statistical robustness.

All flow cytometry data were analysed using Kaluza analysis (v2.1) software.

The results from the various experiments were subject to statistical analysis using the Kruskal-Wallis test to test for significant variance between groups. Dunn's posthoc multiple comparisons test was also done to determine between which groups the variance is with Bonferroni correction in order to correct for multiple sampling. All summary statistics and error bars presented on graphed data are expressed as the mean percentage/count ± SEM. The significance level was set at $\alpha = 0.05$, and $p < 0.05$ was considered significant. Statistical analysis and graphical representation of the data were performed using R (version 4.0.3) and RStudio (version 1.4.1103).

6.3.1 Absolute cell count

After four days in culture, the absolute number of hASCs was determined to obtain a more precise indication of hASC proliferation in the various human alternatives.

125 000 hASCs were seeded per 25 cm^2 flask (the red line in Figure 6.6). In all the media, the cell number increased. PRP was the human alternative with the highest cell number (3 442 418 ± 360 034), which was significantly higher ($p < 0.05$) than PPP (1 158 181 ± 160 550), FFP (1 376 530 ± 201 227), and FBS (688 409 ± 74 588) after four days. pHPL had the second-highest cell number (2 555 773 ± 623 765), followed by HS (1 883 997 ± 246 639). PRP cells showed a five-fold increase compared to FBS and a 1.35-fold increase compared to pHPL.

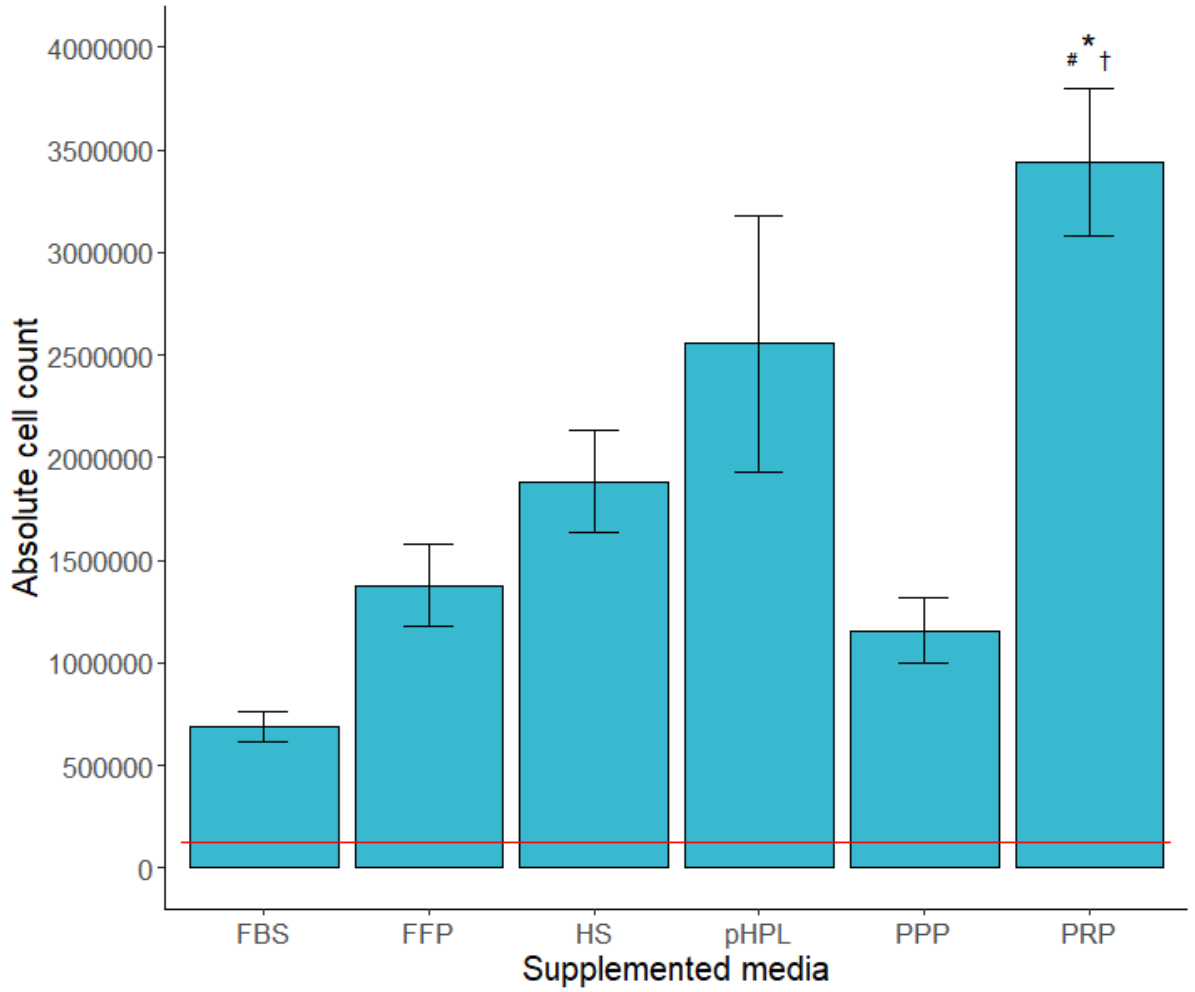

Figure 6.6: Absolute count using flow cytometry of hASCs expanded in the various media after four days.
The red line indicates 125 000 cells seeded at day zero of the experiment. hASCs in all media proliferated as all day four cell counts were higher than the initial 125 000 cells. Significance ($p < 0.05$)

for PRP vs FFP*, PRP vs PPP#, and PRP vs FBS† is indicated by the three symbols. For FBS and pHPL n = 3 with three technical replicates, for PPP, PRP, FFP, and HS n = 9.

6.3.2 Immunophenotype

The immunophenotype of hASCs in the supplemented media adhered to published criteria (16,17). In all supplemented media more than 90% of hASCs expressed the immunophenotype: $CD73^+$, $CD105^+$, $CD44^+$, $CD90^+$, $CD45^-$, $CD34^+$, CD36+ (Figure 6.7). The hASCs showed a mean of 93.04 ± 0.45% cells being $CD73^+$, $CD105^+$, $CD44^+$, $CD90^+$, $CD45^-$, $CD34^+$, $CD36^+$ regardless of the culture media supplement.

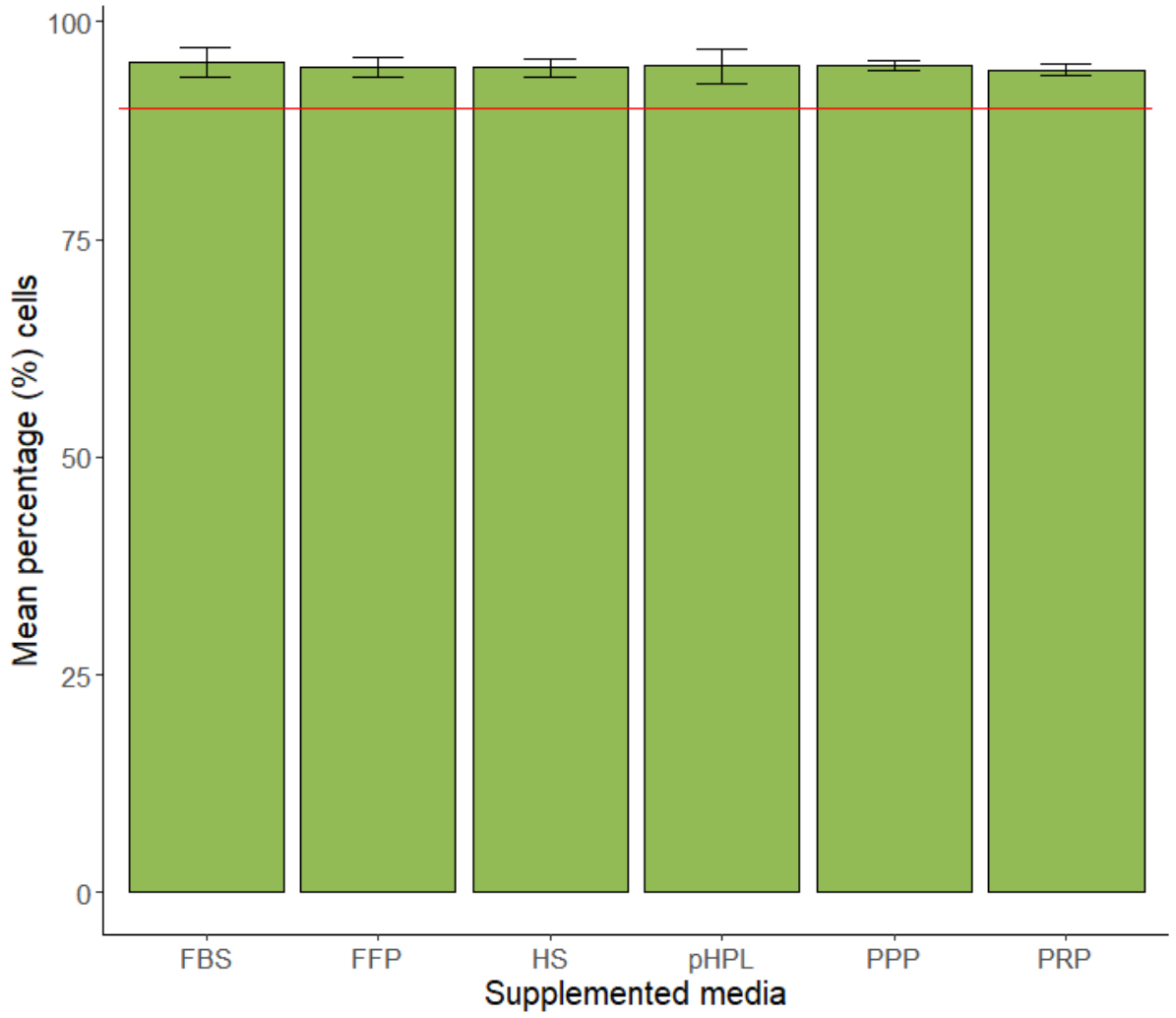

Figure 6.7: The mean percentage of hASCs displaying CD73+, CD105+, CD44+, CD90+, CD45-, CD34+, CD36+ co-expression in the various culture media after four days obtained by flow cytometry.
The red line indicates 90%. The 7-colour phenotype panel was done to determine the adherence of hASCs to the published guidelines in the various media with more than 90% of hASCs adhering to these criteria in all media. For FBS and pHPL n = 3 with three technical replicates and for FFP, PPP, PRP, and HS n = 9.

6.3.3 Cell cycle

The cell cycle analysis results (Figure 6.8) revealed that the highest percentage of cells were in the G_0/G_1 phase across all media. In FBS, significantly more ($p < 0.05$) hASCs were in G_0/G_1 phase (92.57 ± 1.46%) compared to PRP (82.27 ± 1.32) and pHPL (80.55 ± 2.00).

Variable percentages of hASCs in the media were in S-phase, with the lowest percentage in S-phase in FBS (2.65 ± 0.85%). In contrast, the largest percentage of hASCs in the S-phase was observed in pHPL (12.57 ± 2.35%) and PRP (11.75 ± 0.88%). The percentage of cells in the S-phase in PRP was significantly higher ($p < 0.05$) than in FBS (2.65 ± 0.85%) and HS (5.73 ± 1.31%).

No significant differences were found with regard to hASCs in the G_2/M phase between the various media, with an average of 5.90 ± 0.32% of hASCs in the G_2/M phase across all supplemented media.

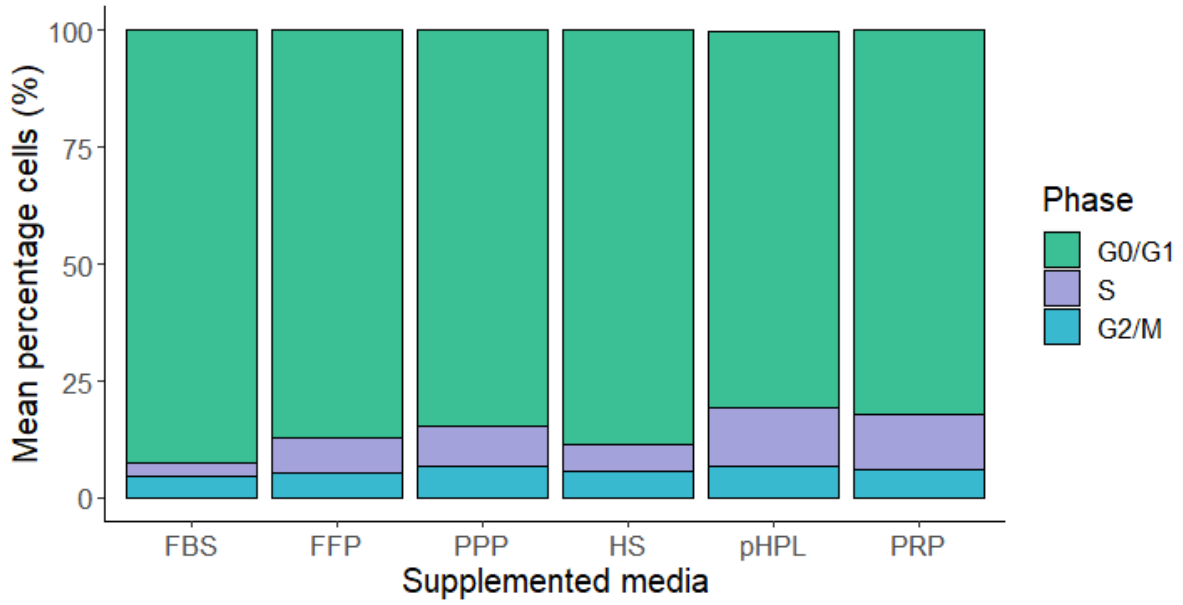

Figure 6.8: Mean percentage of hASCs in different cell cycle phases in the various media after four days obtained by flow cytometry.
Significantly more hASCs were in the G_0/G_1 phase in FBS vs PRP and pHPL. PRP showed significantly more hASCs in the S-phase compared to FBS and HS. No other statistically significant differences were seen regarding the cell cycle analysis. For FBS and pHPL n = 3 with three technical replicates and n = 9 for FFP, PPP, PRP, and HS.

6.3.4 Cell viability

More than 85% of hASCs were viable (Annexin V^-/PI^-, Figure 6.9). No significant differences (at $p < 0.05$ since analysis showed $p > 0.05$) in viability were found between the various media. FFP medium had the highest percentage of viable cells (96.00 ± 0.62%), closely followed by PRP (95.71 ± 0.48%). PPP showed the lowest percentage viability (87.05 ± 4.18%).

No significant differences were found between the various media for hASCs in early apoptosis (Annexin V^+/PI^-). Cells in late apoptosis (Annexin V^+/PI^+) also showed no significant differences between the various media. A significantly higher percentage of cells in FBS* (4.96 ± 1.54%) and HS# (2.69 ± 0.46%) were necrotic (Annexin V^-/PI^+) compared to FFP (0.96 ± .11). No significant differences was seen between other groups for necrotic cells.

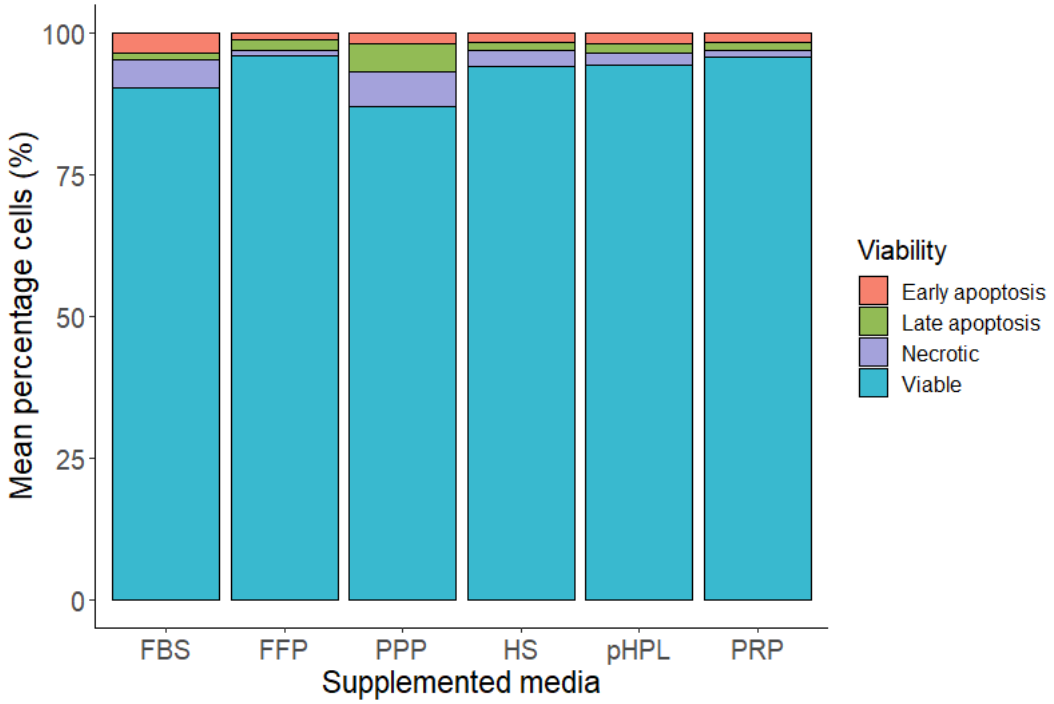

Figure 6.9: Mean percentage of hASCs that are apoptotic (early or late), necrotic, or viable across the various media after four days obtained by flow cytometry.
FFP showed statistically significantly less hASCs were necrotic compared to hASCs in FBS and HS. There were no statistically significant differences between any other groups. For FFP, PPP, PRP, and HS n = 9 and n =3 with three technical replicates for FBS and pHPL.

6.4 Discussion and Conclusion

The absolute cell count confirms the proliferation trend seen in Chapter 5 with the SRB assay. After four days in culture, all the human alternatives displayed better hASC proliferation than FBS, also seen in the SRB assay and previous literature (171,172). PRP produced the highest cell number, which was higher than FBS in accordance with previous work (41,173,185) as well as pHPL. Comparing the control media, pHPL consistently displayed greater proliferation than FBS (as seen in Cowper et al., 2019; Oikonomopoulos et al., 2015; Riis et al., 2016). The higher proliferation seen previously for HS compared to FBS (chapter 5 and Choi et al., 2013; Patrikoski et al., 2013; Witzeneder et al., 2013) was observed in the absolute count as well. The similarity in cell number between PPP and FBS has also been reported (173,185). FFP is, in essence, PPP that has been frozen as described previously in section 2.5.3, and the similar cell counts for hASCs expanded in FFP vs PPP vs FBS is therefore also expected.

The cell cycle analysis indicates that most cells in all the media supplements are in the G_0/G_1 phase. FBS has significantly more cells in the G_0/G_1 phase than PRP and pHPL, confirming the findings of D'Esposito et al. (2015). It is expected that most of the cells in the various media will be in G_0/G_1 as cells spend the most time in the G_1 phase before passing the restriction point to commit to cell division and cell cycle progression if external conditions are favourable (80).

The higher percentage of cells in S-phase in PRP and pHPL can be interpreted as more cells actively dividing in these media and points towards faster progression through the cell cycle (188). These results again confirm the higher proliferation rates of hASCs in PRP and pHPL seen in the SRB assay and the absolute cell count. Furthermore, higher levels of cells in the S-phase in PRP and pHPL align with previous work from Laner-Plamberger et al. (2019), where mitotic checkpoint transcription factors were upregulated in hASCs cultured in pHPL-supplemented media. The authors attributed this upregulation to platelet specific growth factors resulting from the high levels of platelets present in pHPL. PRP medium likely has the same cytokine and growth factor composition as pHPL medium due to the similar level of platelets in

PRP that undergo a single freeze-thaw cycle (described in Chapter 4), but this will have to be confirmed in future studies.

The percentage of cells in the G_2/M phase is similar across all media. In combination with results from the G_0/G_1 and S-phase percentages, this suggests that the cells in human alternative media have started dividing but have not yet progressed to the final steps of mitosis (78,80). Previous literature confirms the lower levels of cells in the G_1 phase without affecting the level of cells in the G_2/M phase in PRP and pHPL media compared to FBS medium (187,189). The similarities in percentages of cells in HS in the S- and G_2/M phase has also previously been reported, although the authors used 15% HS (190). Previous studies rarely included cell cycle analysis for hASCs cultured in FFP and PPP. Future studies may involve studying cell cycle progression across multiple time points in culture.

The cell viability results indicate that more than 85% of the cells are viable across all media. According to Bourin et al. (2013), >90% of ASCs should be viable. In PPP, only 87.05 ± 4.18% cells were viable. Aside from PPP, all the culture media adhered to this criterion. Overall, hASCs maintained in PRP and FFP had the highest viability. The difference in viability seen in hASCs maintained in FFP compared to PPP is noteworthy as FFP is, in essence, PPP that is frozen directly after separation with subtle differences (136,191). One would thus expect the results for FFP and PPP to be similar. Across all media, low percentages of cells (less than 6%) are apoptotic or necrotic, indicating no significant intrinsic cell death pathway progression or external factors contributing to cell death (84,179). The highest percentage of hASCs that were apoptotic or necrotic was seen in PPP. A balance between hASC progression through the cell cycle and cell death needed for overall proliferation is seen in all the culture media supplements (80). Aside from PPP, all the human alternatives showed higher levels of viable cells than FBS, making them better choices for therapeutic hASCs. A possible explanation of the low viability of PPP may result from false-positive events due to PI staining cytoplasmic RNA. Prospects to investigate possible false-positive PI events across all media include following a protocol by Rieger and colleagues. (192) that suggests the addition of an RNAse A digestion step for a more accurate view across all supplements.

The immunophenotype of the hASCs showed no differences when human alternatives were compared to FBS. In all media, hASC surface antigen co-expression adhered to the pre-determined guidelines set out by ISCT and IFATS (16,17). Investigating the hASC immunophenotype is crucial to determine whether the human alternatives alter this vital MSC characteristic. No deviations in immunophenotype expression indicate the human alternatives do not impact on MSC immunophenotype. Furthermore, the lack of variation seen in the immunophenotypic expression of hASCs maintained in the various human alternatives compared to FBS is confirmed by previous studies (25,33,157,160,186,190,193).

This study is to the author's knowledge the first to compare the proliferation and immunophenotype of all five of the chosen human alternatives head-to-head. Most previous studies have compared MSCs maintained in hPL, PRP, HS, or a combination of the five human alternatives to FBS *in vitro* (34,171–173,185). The results in this study show that in terms of high proliferation rates to reduce time in culture before a transplant and hASC viability, the best human alternatives for autologous therapies are HS and PRP. Therapeutic hASCs expanded in pHPL is also an option if allogeneic products are acceptable.

Chapter 7: Adipogenesis

7.1 Introduction

In this study, RT-qPCR, flow cytometry and fluorescent microscopy were applied to confirm the retention of the adipogenic potential of hASCs in the various culture media as a critical MSC characteristic (16,17). Adipogenesis is the process whereby preadipocytes differentiate into adipocytes containing intracellular lipid droplets with mature adipocyte morphology consisting of a single large (unilocular) intracellular lipid droplet with the nucleus displaced toward the periphery (97).

There are various ways in which the presence of an internal lipid droplet may be determined during adipogenic differentiation. A qualitative approach is fluorescent microscopy with the appropriate dyes, allowing visual confirmation of cell morphology and the presence of lipid droplets. The use of fluorescence microscopy enables one to combine the visualisation and magnification of a sample with fluorescence excitation and emission using a filter cube (194). The emission signal and location are captured with a camera. As described in chapter 4, the principles of fluorescence should be kept in mind when staining with multiple fluorescent compounds during fluorescent microscopy. The emission spectra of the markers should not overlap as this may lead to inaccurate results. The visualisation of the intracellular lipid droplets using fluorescence microscopy is advantageous; however, it is a qualitative technique and may also be subjective. The limited field of vision may impact the accuracy of the results at a given moment which may lead to an under-or over-estimation of the actual number of cells that accumulated lipid droplets during adipogenesis.

Additionally, fluorescent compounds may lose fluorescence when specimens are viewed under the microscope. According to recommended guidelines by Bourin et al., 2013, a quantitative evaluation of adipogenic potential should be included. As a result, flow cytometry and reverse transcription quantitative real-time polymerase chain reaction (RT-qPCR) were also included in this study.

Flow cytometry with the appropriate fluorescent dyes allows a more quantitative estimation of adipogenesis as individual cells are investigated. As described in chapter 4, cells pass a laser in a single file, after which emitted light is captured (153). The

advantage of including flow cytometry is that hASCs that contain lipid droplets as a result of lipid accumulation can be quantified by determining the percentage of hASCs that contain lipid droplets. Adipogenic gene expression drives the adipocyte phenotype in hASCs thus, using RT-qPCR for gene expression analysis serves as a quantifiable technique (117,195). The expression of CCAAT/enhancer-binding protein alpha and beta (C/EBPα and C/EBPβ), peroxisome proliferator-activated receptor gamma (PPARγ), fatty-acid binding protein 4 (FABP4), adiponectin (AdipoQ), and cluster of differentiation 36 (CD36) was analysed. C/EBPα and C/EBPβ both function as transcription factors that activate the expression of PPARγ, the master regulator of adipogenesis (91,93,196). FABP4 is a lipid chaperone protein involved in the accumulation of intracellular lipids forming lipid droplets (93). AdipoQ is expressed by adipose tissue and functions as an insulin sensitising factor which increases the percentage of cells differentiating into adipocytes (93,106). Lastly, CD36 plays a role in lipid uptake, and its expression is associated with an increase in adipogenesis (95,113).

7.2 Materials and Methods

Cells can be induced to undergo adipogenesis by adding a chemical cocktail containing 3-Isobutyl-methylxanthine (IBMX), indomethacin, dexamethasone, and insulin to CGM. IBMX and dexamethasone are added as they are known to activate C/EBPβ expression. Insulin is used to induce proliferation and differentiation of preadipocytes (99). Indomethacin is added as it up-regulates PPARγ (100).

The evaluation of hASC adipogenic potential retention in the various media was done by staining accumulated intracellular lipid droplets with Nile Red (9-diethylamino-5H-benzo[a]phenoxazine-5-one). Nile Red (NR) is a hydrophobic fluorescent dye that binds preferentially to cytoplasmic lipids and does not require cell fixation. It has been used in flow cytometry and fluorescent microscopy to determine the cytoplasmic lipid content of cells (117,157,195,197,198). The nuclei of differentiating hASCs were visualised using DAPI and VDC Ruby for fluorescent microscopy and flow cytometry, respectively. The inclusion of nuclear staining was done to ensure that cells containing a cytoplasmic lipid droplet(s) were investigated and not free-floating lipids or lipid droplets. Sterile Pasteur pipettes were used during staining to avoid dislodging lipid droplets from adipocytes and care was taken to work slowly and cautiously.

After differentiation, expression of six adipogenesis-specific genes was analysed via RT-qPCR using SYBR Green I. SYBR Green I is a non-specific DNA intercalating dye that fluoresces upon binding to the minor groove of dsDNA and was used in conjunction with gene-specific primers to determine the expression of the adipogenic genes.

The abovementioned experiments were performed on day 0 and day 14 for induced (I) and non-induced (NI) samples. Initially, day 21 was also included as a time point, but was removed due to incomplete data and a concern that the results may be unreliable due to fungal contamination in the cell culture facility. Since the accumulation of lipid droplets was detectable 14 days post-induction, and the objective was to determine whether hASCs retained adipogenic potential with different serum supplements, adipogenesis was assayed on day 14. Additionally, day 14 as a timepoint reduced the time in culture, which reduced the risk of fungal contamination.

7.2.1 Adipogenic differentiation of hASCs

Three different cryopreserved hASC cultures were thawed as described previously (chapter 4) and expanded in CGM containing 2% (v/v) p/s, and 0.5 µg/mL fungizone anti-fungal (amphotericin B, Gibco, Carlsbad, California, USA) and 5% (v/v) PRP, or pHPL, or 10% (v/v) FBS. PRP and pHPL were chosen as the human alternatives to investigate in this study as they showed the fastest proliferation which also includes one option for both an autologous and an allogeneic therapeutic approach. The anti-fungal agent amphotericin B was added due to repeated fungal contamination in cell cultures in the facility where the differentiation experiments were performed. Samples in culture that were contaminated were terminated. The facility was cleaned thoroughly and decontaminated by fumigation. The anti-fungal agent was included in all CGM for hASC expansion and differentiation. hASCs were expanded and differentiated in 10% (v/v) FBS (standard concentration) and expanded in 5% (v/v) in PRP and pHPL and differentiated in 2.5% (v/v) PRP and pHPL. The lower concentration of PRP and pHPL in the CGM compared to FBS was decided on from previous work done by Ms Carla Dessels (157) and others that compared concentrations of serum additions to media (173) and found that 2.5%-5% (v/v) pHPL/PRP show similar proliferation to the standard 10% (v/v) FBS. The lower concentrations reduced the usage of reagents, eliminating the need for blood product recollection throughout this study to ensure as much continuity with the previous work performed by Ms Carla Dessels at the ICMM as possible.

At 80-90% confluence, cells were dissociated as described previously in chapter 4. Cells were seeded at a density of 5000 cells/cm^2 according to the experimental layout in Figure 7.1. Following seeding, cells were maintained in CGM (2.5% PRP, 2.5% pHPL, or 10% FBS) until 50-60% confluence and induced to undergo adipogenic differentiation at 50-60% confluence in accordance with work previously done by Ms Carla Dessels. Differentiation induction was performed on hASCs at P3-5. As indicated in Figure 7.1, two 75 cm^2 cell culture flasks and three wells on each 6-well plate were induced.

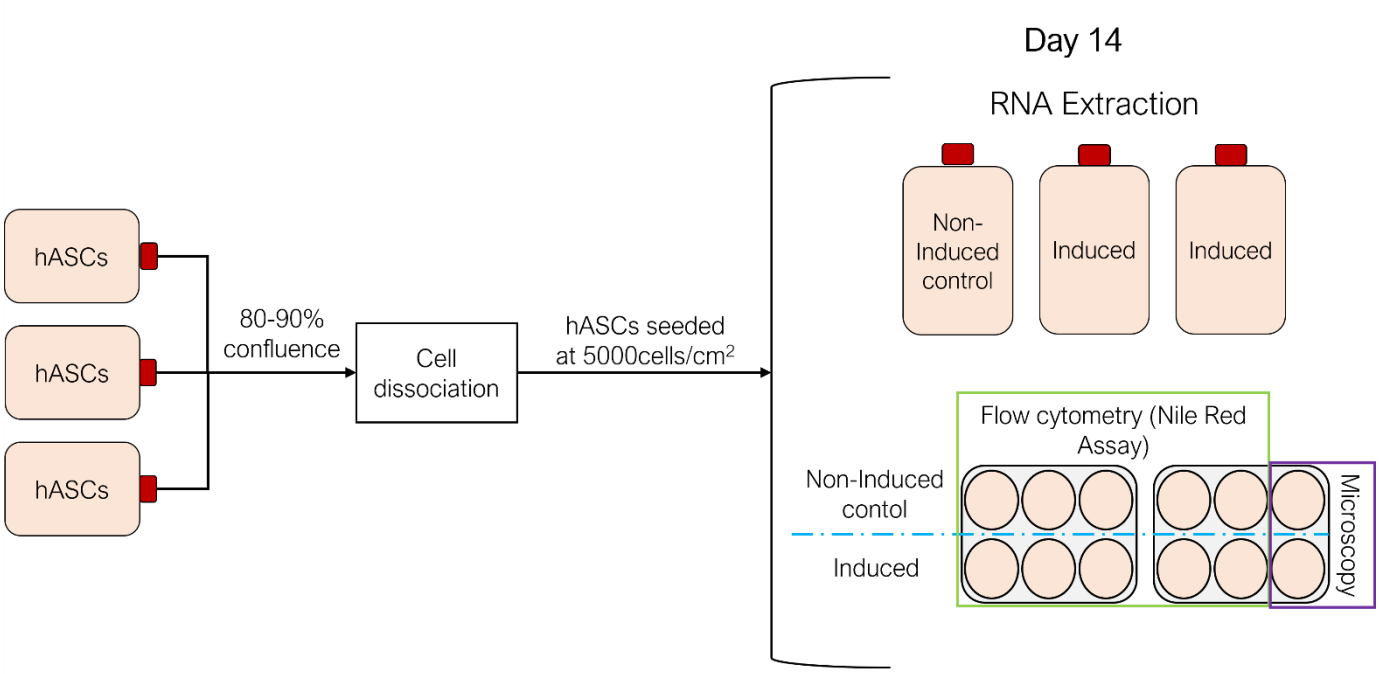

Figure 7.1 Adipogenic differentiation experimental layout

Adipogenic induction media were prepared by adding final concentrations of the following to CGM: 0.5 mM IBMX (Sigma-Aldrich, Merck, Missouri, USA), 200 µM indomethacin (Sigma-Aldrich, Merck, Missouri, USA), 10 µg/mL insulin (human recombinant Zinc, GIBCO by Life Technologies™, Grand Island, NY, USA), 1 µM dexamethasone (Sigma-Aldrich, Merck, Missouri, USA). Serum supplements were added to the media at the indicated concentrations.

Non-induced cells were maintained in CGM (2.5% PRP, 2.5% pHPL, 10% FBS) concurrently to serve as a control. Adipogenic differentiation was assessed on day 0 and 14 using flow cytometry, fluorescence microscopy, and RT-qPCR.

Kruskal-Wallis testing was used to evaluate variance between groups, followed by Dunn's post-hoc multiple comparisons test with Bonferroni correction to identify variant groups and correct for multiple sampling, respectively. Summary statistics and error bars presented on graphed data are expressed as the mean percentage ± SEM. The significance level was set at $\alpha = 0.05$, and $p < 0.05$ was considered significant. Statistical analysis and graphical representation of the data were performed using R (version 4.0.3) and RStudio (version 1.4.1103).

7.2.2 Adipogenesis evaluation by fluorescence microscopy

The accumulation of lipid droplets was visualised using fluorescent microscopy. Cells for fluorescence microscopy were differentiated in 6-well plates, as indicated in Figure 7.1. Induced and non-induced cells were stained simultaneously with NR and DAPI, a fluorescent dye that binds to DNA, by adding 5µL DAPI stock solution [2.5 µg/mL final concentration] to the well containing 2 mL medium and incubating in the dark overnight at 37°C/5% CO_2. The following day, lipid droplets were stained using NR (50 ng/mL final concentration, Sigma-Aldrich, Merck, Missouri, USA). The wells were incubated in the dark for 20 min at 37°C/5% CO_2. The culture medium was removed, and the wells were washed with PBS three times to remove unbound dye. A volume of 2 mL PBS was added to the wells before imaging on an AxioVert A1 inverted fluorescence microscope (Carl Zeiss, Gottingen, Germany) using an AxioCam Cm1 camera (Carl Zeiss, Gottingen, Germany). Induced and non-induced cells were visualised, and representative images of each well were captured at 10x magnification. The representative images were captured using ZEN 2.3 blue edition software (Carl Zeiss, Gottingen, Germany) and were enhanced only by adjusting brightness and contrast using ZEN 3.3 blue edition software. The images were captured using two fluorescence channels overlayed for the final image showing nucleated cells and intracellular lipid droplets in Figure 7.2C. The first image was captured using the DAPI Filter Set (filter set 1, excitation BP 359 – 371 nm; emission LP 397 nm) to visualise nuclei (Figure 7.2A). The second image (Figure 7.2B) was used to visualise staining with NR indicating lipid formation using filter Set 9 (excitation BP 450 – 490 nm; emission LP 515 nm).

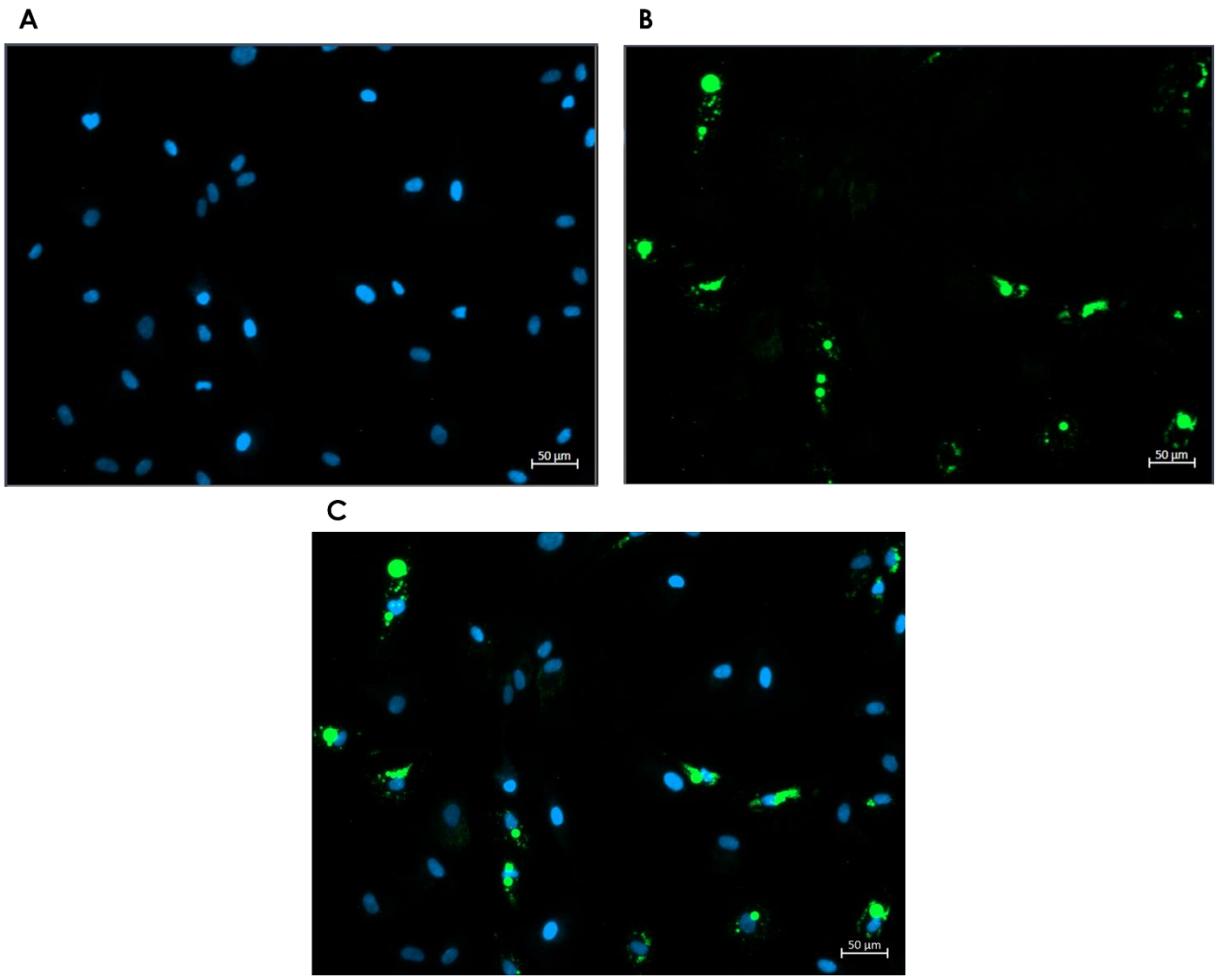

Figure 7.2 Fluorescence microscopy imaging overlay for DAPI and Nile Red.
A: Images captured using the DAPI filter set to visualise hASC nuclei. B: Lipid droplet visualisation using the NR filter set. C: Overlay of the two preceding images to visualise nucleated cells that accumulated lipid droplets. Scale bar: 50 µM

7.2.3 Adipogenesis evaluation by flow cytometry

Staining with NR and VDC Ruby were used to analyse the percentage of hASCs that accumulated lipid droplets after 14 days of adipogenesis using flow cytometry.

7.2.3.1 Adipogenesis flow cytometry sample preparation

Cells were dissociated from 6-well plates by removing medium, adding 500 µL TrypLE™to each well and incubating at 37°C for 15 - 50 min until they were entirely dissociated. The TrypLE™was neutralised by dilution; an equal volume of the respective CGMs was added to wells containing TrypLE™after visual confirmation that the cells had been dislodged. The cells were transferred to separate 15 mL centrifuge tubes using sterile Pasteur pipettes and topped up to 8 mL using the respective CGM. A 1 mL aliquot of cell suspension was added to a flow cytometry tube. Nile Red (20 ng/mL final concentration) and VDC Ruby (2.5 µM final concentration) were added, and the tubes were incubated in the dark at RT for 20 min before analysis on a Gallios or CytoFLEX flow cytometer. Ideally, all samples should be analysed using the same equipment; however, one PRP biological replicate and all FBS replicates were analysed on a CytoFlex flow cytometer (Beckman Coulter, Brea, California, United States). Technical problems with the department's Gallios flow cytometer and its subsequent replacement by the research group necessitated a change in the instrument. Sample preparation was the same regardless of the flow cytometer used. These steps were repeated for each CGM supplement (PRP1, PRP2, PRP3, pHPL, FBS) on day 0 and day 14. Care was taken to avoid a jarring physical impact to the cells to ensure that lipid droplets did not dislodge from cells. All data were analysed using Kaluza Flow Cytometry Analysis Software (v2.1) with the gating strategy described in 7.2.3.2.

7.2.3.2 Adipogenesis flow cytometry data acquisition and analysis

The nucleated cell population was identified using a one-parameter ungated histogram plot for the VDC Ruby channel (FL7 Gallios, FL8 Cytoflex; excitation: 488nm; emission 725/20 BP, Figure 7.3A, 'Nucleated cells' region). The nucleated cell population was visualised on a two-parameter FS vs SS dot plot gated on the 'Nucleated cells' region, and debris was excluded by drawing a region around the nucleated hASCs (Figure 7.3B, 'Nucleated hASCs' region). Lastly, the percentage of NR^+ cells were visualised on a two-parameter FS vs Nile Red (FL2 Gallios and Cytoflex, excitation 488nm; emission 575/30 BP) dot plot, gated on 'Nucleated hASCs' (Figure 7.3C, 'NR+ Cells' region).

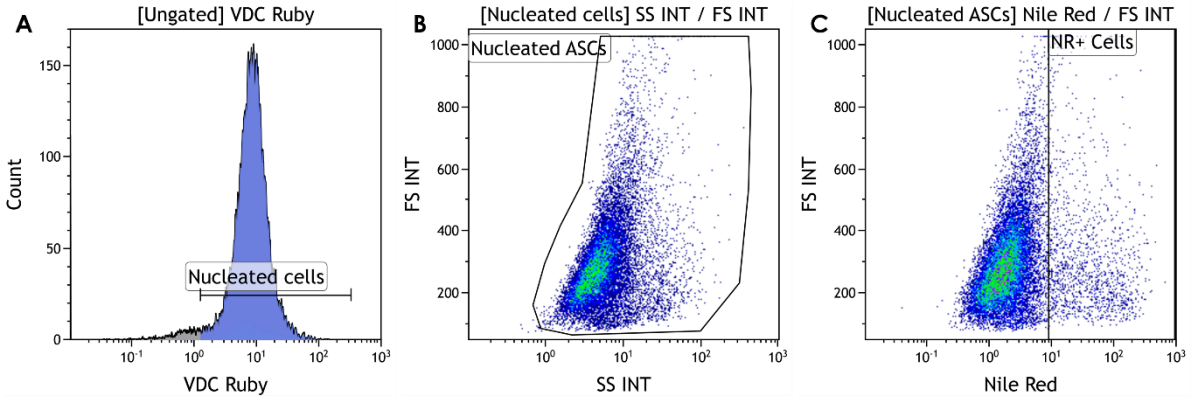

Figure 7.3 Representative images of gating strategy for flow cytometry Nile Red assay.
A: The nucleated hASC population containing VDC Ruby was identified. B: Gated on the nucleated hASC population, debris was excluded by drawing a region around the hASC population. C: The percentage NR^+ hASCs was determined.

7.2.4 Adipogenesis gene expression confirmation

RT-qPCR is a technique that combines reverse transcription, PCR amplification, and fluorescence detection of the amplified product in real time. Complementary DNA (cDNA) is synthesised through reverse transcription from extracted RNA as a template. The cDNA is then used in a PCR amplification reaction with SYBR Green I to monitor amplification. SYBR Green I is a fluorescent dye that has low fluorescence when unbound, and increased fluorescence when bound to dsDNA. The fluorescence will exponentially increase as amplification occurs since more dsDNA will be available for SYBR Green I binding. The point at which the fluorescent signal surpasses the background fluorescence of unbound SYBR Green I is called the threshold cycle (C_T) or quantification cycle (C_q). Higher initial target template amounts will require fewer cycles to pass the threshold. Eventually, a plateau phase will be reached due to the depletion of dNTPs and primers available for amplification (199–201).

There are two ways to quantify gene expression using RT-qPCR: absolute and relative quantification. Absolute quantification requires a known initial copy number of the target gene and subsequently generates standard curves using a set of standards at different concentrations. The obtained C_q value of the sample of interest is then compared to the standard curves. Relative quantification forgoes the use of standards and instead calculates the expression of the sample of interest relative to a reference gene, calibrator, and untreated or time 0 control. This study used relative quantification to report differences in gene expression between treated (induced) and untreated (non-induced control) samples using the comparative C_T mathematical method (also known as the delta delta C_T ($\Delta\Delta C_T$) method) in Equation 4, which was subsequently used to calculate the relative fold increase in gene expression of target genes relative to the reference genes and non-induced controls.

Equation 4: The comparative C_T method:

Step 1: Calculate the difference between the target and reference gene for the treated (induced) group ($\Delta C_{T\ INDUCED}$):

Equation 4.1

$$\Delta C_{T\ INDUCED} = C_T \text{ target gene} - C_T \text{ reference gene}$$

Step 2: Calculate the difference between the target and reference gene for the untreated (non-induced) group ($\Delta C_{T\ NON\text{-}INDUCED}$):

Equation 4.2

$$\Delta C_{T\ NON\text{-}INDUCED} = C_T \text{ target gene} - C_T \text{ reference gene}$$

Step 3: Calculate the difference between the two groups ($\Delta\Delta C_T$)

Equation 4.3

$$\Delta\Delta C_T = \Delta C_{T\ INDUCED} - \Delta C_{T\ NON\text{-}INDUCED}$$

As described in section 7.1 , six adipogenic genes were investigated. The genes selected were AdipoQ, C/EBPα, C/EBPβ, FABP4, PPARγ/PPARG, and CD36. Three reference genes were used in this study: tyrosine 3-monooxygenase/tryptophan 5-monooxygenase activation protein, zeta (YWHAZ), peptidylprolyl isomerase A (PPIA), and TATA-binding protein (TBP). Target genes are normalised to reference genes when doing RT-qPCR gene expression analysis so it is important to choose reference genes that are expressed stably under the experimental conditions and at levels similar to the target genes (202,203). The reference genes were chosen based on previous work in our group by Dr Chrisna Durandt, Ms Carla Dessels, Ms Carina da Silva, and previously published literature that concluded these genes are suitable as reference genes for this study purpose (118,202,203).

7.2.4.1 RNA extraction

RNA was extracted for each hASC culture in each medium at Day 0 and Day 14 (induced and non-induced) (Figure 7.1). Cells were dislodged from 75 cm^2 flasks as described in chapter 5. The dissociated cells were washed with PBS three times by resuspending the cells in 1 mL/flask and centrifuging for 5 min at 300 x g. This wash

step is essential to remove the phenol red present in the culture medium that may interfere with RNA extraction.

Total RNA was extracted using the RNeasy mini kit (Qiagen, Hilden, Germany) according to the manufacturer's instructions. In short, dissociated cells resuspended in PBS were centrifuged for 5 minutes at 300 x g. The supernatant was discarded, and the pellet was resuspended in 350 µL RLT buffer to lyse the cells. The cell suspension was homogenised by vortexing for approximately 1 min, after which 350 µL 70% (v/v) ethanol was added and the homogenate vortexed again to provide optimal binding conditions. The resulting 700 µL lysate was added to an RNeasy spin column placed in a 2 mL collection tube supplied with the kit and centrifuged for 15 sec at 8000 x *g* to allow total RNA to bind to the column membrane. The flow-through was discarded, and 700 µL buffer RW1 was added to the column, which was centrifuged for 15 sec at 8000 x *g* to remove contaminants. Once again, the flow-through was discarded and the wash step repeated by adding 500 µL buffer RPE to the column and centrifuging for 15 seconds at 8000 x *g*. The previous step was repeated, but with a centrifugation step of 2 min at 8000 x *g*. The collection tube and flow-through were discarded, and the column was placed in a new 2 mL collection tube and centrifuged for 1 min at maximum speed. The column was placed in a 1.5 mL Eppendorf® tube, and 40 µL RNase free water was added to the column. The column was centrifuged for 1 min at 8000 x g to elute the RNA. The eluted RNA product was placed back into the column and centrifuged again for 1 min at 8000 x *g* to increase the RNA concentration. The RNA concentration and quality were assessed on a Nanodrop ND 1000 spectrophotometer (Thermo Fisher Scientific, Waltham, MA, USA) and recorded for each extraction.

7.2.4.2 cDNA synthesis

The SensiFast™ cDNA synthesis kit (Bioline, London, England) was used to synthesise cDNA, according to the manufacturer's instructions. The total reaction volume was 20 µL which was made up of 4 µL 5× TransAmp Buffer, 1 µL reverse transcriptase enzyme, 1 µg of RNA and nuclease-free water to make up the final reaction volume. A no reverse transcriptase control (NoRT) reaction was also included. The NoRT reaction contained the same reagents, but the reverse transcriptase enzyme was replaced with

nuclease-free water (Table 7.1). The reactions were transferred to a thermal cycler with the following program: priming for 10 min at 25°C, followed by reverse transcription at 42°C for 15 min, and finally reverse transcriptase inactivation at 85°C for 5 min.

Table 7.1: Reaction Conditions for reverse transcription

Reagent	cDNA synthesis (µL)	NoRT control (µL)
5× TransAmp Buffer	4	4
Reverse Transcriptase	1	0
RNA (1 µg total)	Variable	Variable
Nuclease free H_20	Variable	Variable
Total volume	20	20

7.2.4.3 Reverse transcription-quantitative Polymerase Chain Reaction (RT-qPCR)

The RT-qPCR reaction was performed on a LightCycler 480 II instrument (Roche, Basel, Switzerland) with the following program: denaturation at 95°C for 5 min, followed by 45 amplification cycles at 95°C for 30 sec, 62°C for 30 sec, and 72°C for 30 sec. The amplification cycles were followed by a melt curve at 95°C for 30 sec, 40°C for 30 sec, and ramped at 0.11°C per second.

Each reaction consisted of LightCycler® 480 SYBR Green I Master Mix (Roche, Basel, Switzerland), 400 nM of each primer (IDT, Coralville, USA, sequences in Table 7.3) and a total of 40 ng cDNA template (from 20 ng/µL stocks) to a final reaction volume of 10 µL (Table 7.2).

Table 7.2: Reaction conditions for RT-qPCR

Reagent	Stock solution	Quantity 1 × reaction	Volume (µL) 1 × Reaction
Nuclease free H_20	-	-	2.2
SYBR Green Master Mix	2 ×	1 ×	5
Forward primer	10 µM	400 nM	0.4
Reverse primer	10 µM	400 nM	0.4
cDNA template (20 ng/µL)	-	-	2
Total volume	-	-	10

Table 7.3 Primer sequences (5'-3') for genes of interest and reference genes

Gene		Forward primer	Reverse primer
Target genes			
Adiponectin	AdipoQ	GCCTGTTTCTGACCAATC	CCACTCTCCTATTTCTGATAAC
CCAAT/Enhancer-binding protein alpha	C/EBPα	GTCTCTGCTAAACCACCA	AAAGGAAAGGGAGTCTCAG
CCAAT/Enhancer-binding protein beta	C/EBPβ	TCCAAACCAACCGCACAT	AGAGGGAGAAGCAGAGAGTTTA
Fatty-acid binding protein 4	FABP4	ATCAACCACCATAAAGAGAAA	AACTTCAGTCCAGGTCAA
Peroxisome proliferator-activated receptor gamma	PPARγ	CGTGGATCTCTCCGTAAT	TGGATCTGTTCTTGTGAATG
Cluster of differentiation 36	CD36	CTTTGCCTCTCCAGTTGAA	ACACAGGTCTCCCTTCTT
Reference genes			
TATA-binding protein	TBP	CCGAAACGCCGAATATAA	GGACTGTTCTTCACTCTTG
Peptidylprolyl Isomerase A	PPIA	GAGTTAAGAGTGTTGATGTAGG	CCTGGGACTGGAAAGTAA
Tyrosine 3-Monooxygenase/Tryptophan 5-Monooxygenase Activation Protein, Zeta	YWHAZ	TGACATTGGGTAGCATTAAC	GCACCTGACAAATAGAAAGA

7.2.4.4 RT-qPCR data analysis

Each reaction described in section 7.2.4.3 was performed in triplicate (technical replicates) for day 0, day 14 NI, and day 14 I for each biological replicate. The standard deviation (SD) for the C_q values of triplicates were determined using the LightCycler® 480 software (Roche, Basel, Switzerland, v1.5.1). Only samples with SD $\leq$ 0.5 from the mean were used in the data analysis. In samples with SD > 0.5 from the mean, outlier replicates (within 2 SD of the mean) were excluded. Furthermore, qPCR reactions described in 7.2.4.3 were done using NoRT controls described in 7.2.4.2 as the template to investigate the presence of genomic DNA (gDNA) in the RNA samples. Amplification in NoRT controls (where no reverse transcriptase was added) would indicate the presence of gDNA contaminants, as dsDNA but not RNA should amplify in a PCR reaction. NoRT amplification was detected at C_q = 33 and subsequently a $C_q \leq 33$ was set for target gene expression. Target gene C_q values > 33 may be amplification resulting from gDNA present in the sample(s). Samples whose NoRT reactions had a Cq ≤ 33 were excluded from data analysis.

Relative gene expression was calculated using the comparative C_T method described in 7.2.4. Due to a limited amount of RNA, efficiency of amplification could not be determined using a standard curve for each gene, as proposed by Rao and colleagues (204). Therefore, amplification efficiency of 100% was assumed when calculating the relative fold increase (RFI) using Equation 5. YWHAZ, PPIA, and TBP were used as reference genes as described in 7.2.4.

$$\text{RFI} = 2^{-\Delta\Delta\text{Ct}}$$

Equation 5

The relative fold increase calculation can be used to determine relative gene expression levels between samples relative to a reference sample using the C_T values generated by the LightCycler 480 II system.

In this study, the fold change expression of the target adipogenic genes was calculated relative to the control (non-induced) samples using the comparative C_T method shown in equation 4 and the RFI calculation in equation 5 to determine the change in

adipogenic target gene expression (up-or down-regulation). All C_T values were normalised to the chosen reference genes.

7.3 Results

The different combinations of cryopreserved hASC cultures and media supplements (biological replicates) used in the flow cytometry, microscopy, and RT-qPCR evaluations of adipogenic potential are summarised in Table 7.4. RT-qPCR crossed out biological replicates were completed, but were excluded from analysis due to the exclusion criteria discussed in section 7.2.4.

Table 7.4: Summary of biological replicates (Total (n)) for microscopy (M), flow cytometry (F), and RT-qPCR (P) evaluation of adipogenesis.

	A071016			A091019			A100717			A091018-01A			A150817-01A			A311019-01A			A311019-02T			Total (n)		
	F	M	P	F	M	P	F	M	P	F	M	P	F	M	P	F	M	P	F	M	P	F	M	P
FBS	✓	✓		✓	✓	✓										✓	✓	✓	✓	✓	✓	4	4	3
pHPL	✓	✓		✓	✓	✓	✓	✓	✓		✓	~~✓~~	✓	✓								4	5	2
PRP 1	✓	✓		✓	✓	✓	✓	✓	✓									✓						
PRP 2	✓	✓		✓	✓	✓	✓	✓	~~✓~~									✓				9	9	6
PRP 3	✓	✓		✓	✓	~~✓~~	✓	✓	✓									~~✓~~						

Results are shown as mean ± standard error on day 14 for induced and non-induced samples.

7.3.1 Adipogenesis microscopy results

Visual confirmation of intracellular lipid droplets in hASCs undergoing adipogenesis was done using fluorescent microscopy. Figure 7.4 contains representative fluorescent microscopy images for FBS NI (A) and I (B), pHPL NI (C) and I (D), and PRP NI (E) and I (F) on day 14. Visible lipid droplets were present in nucleated cells in all induced samples across all media on day 14. The non-induced samples did not show the same visible lipid droplets.

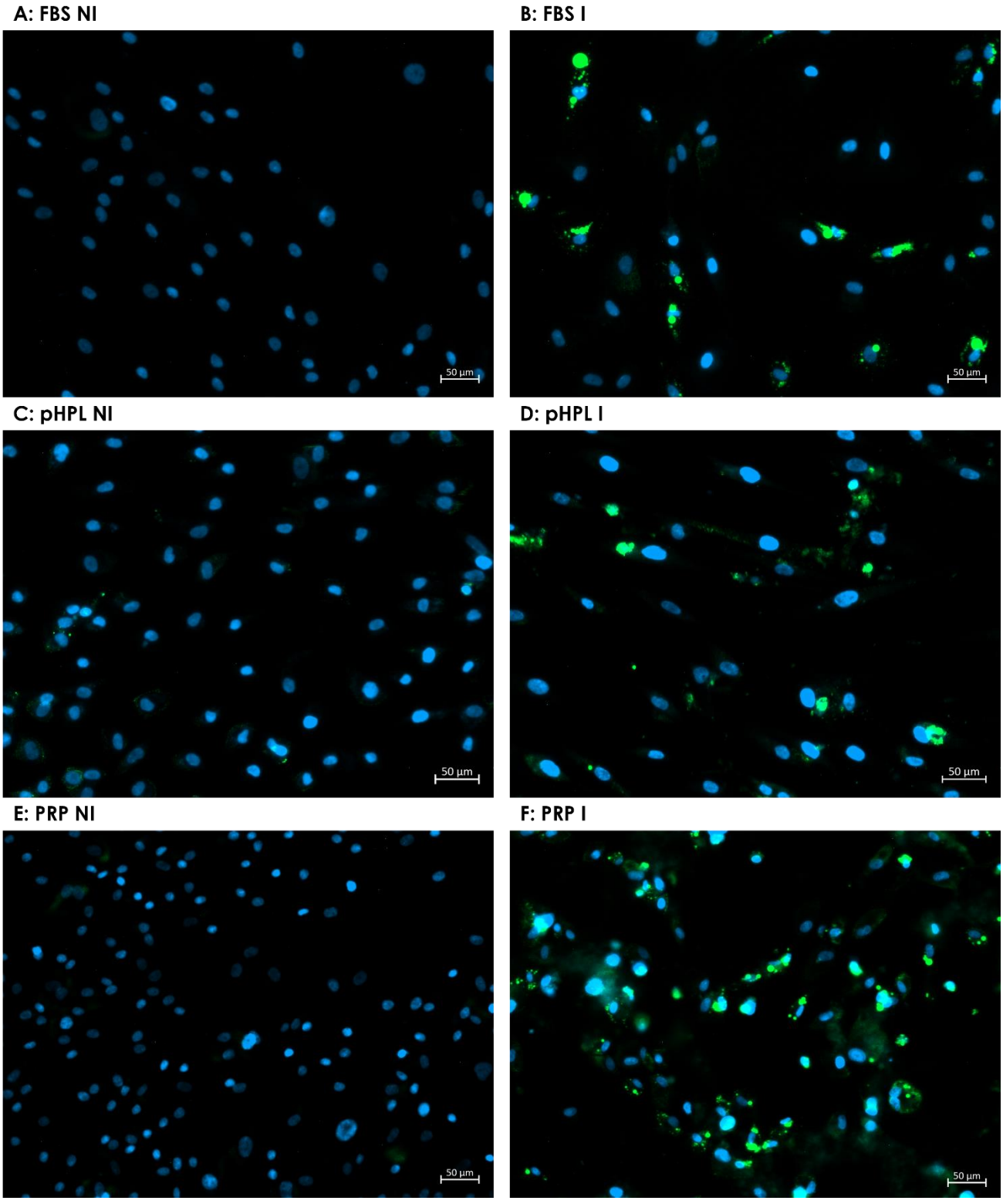

Figure 7.4 Representative fluorescent microscopy images for day 14 non-induced and induced samples in various media.
A: FBS Non-induced; B: FBS Induced; C: pHPL Non-induced; D: pHPL Induced; E: PRP Non-induced; F: PRP Induced. Scale bars = 50 µM. Green represents Nile Red staining of lipids; blue represents DAPI staining of hASC nuclei. Table 7.4 shows n = 4 for FBS, n = 9 for PRP, and n = 5 for pHPL. No analysis for statistical significance was completed as fluorescent microscopy was considered a qualitative assay.

7.3.2 Adipogenesis flow cytometry results

Flow cytometry was done as a quantitative measure of the adipogenic differentiation potential in the various media. The percentage of Nile Red positive (NR^+) hASCs at day 14 after adipogenic induction indicates the percentage of hASCs that contain intracellular lipid droplets. Debris and free-floating lipid droplets were excluded from data analysis using a nucleic fluorescent dye, as described in the previous section.

The percentage of NR^+ cells increased from day 0 to day 14 in all three media and differentiation conditions. There was also an increase in NR^+ cells in the induced cells compared to the non induced cells across all media. FBS supplemented medium had the highest percentage NR^+ cells, followed by PRP with pHPL medium showing the lowest NR^+ percentage. The NR^+ cell populations showed that the hASCs retain the ability to differentiate into adipocytes in all three media. No statistically significant differences were found in the percentage of NR^+ cells between the various media on day 0 or 14.

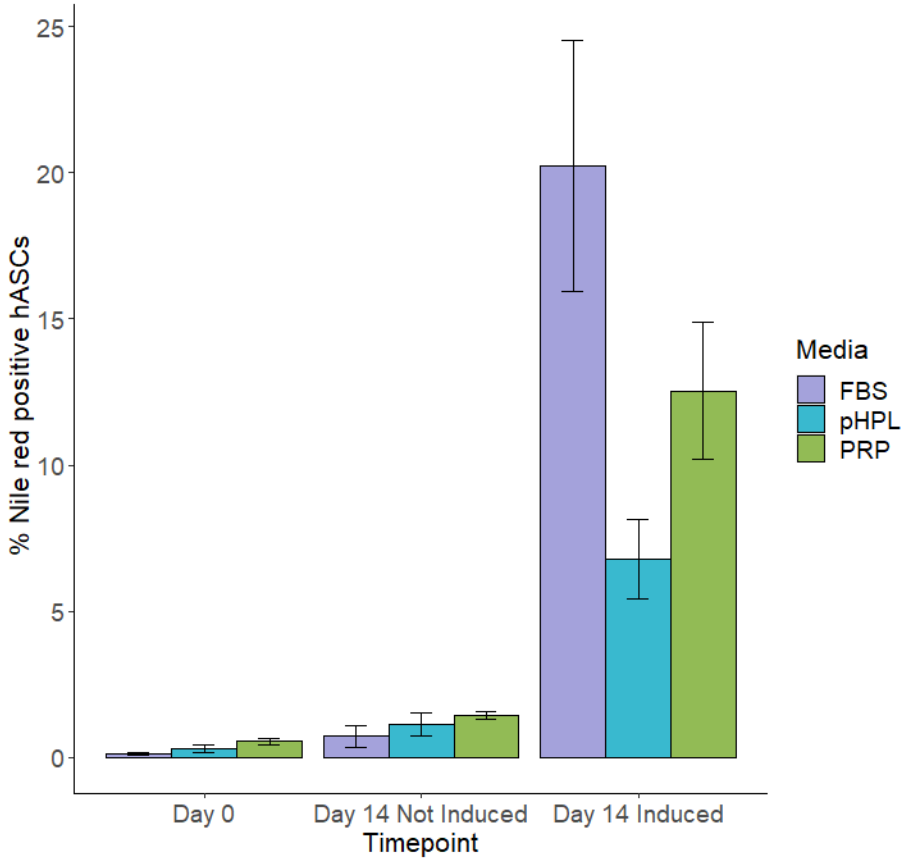

Figure 7.5 The percentage of NR^+ hASCs in the various media on days 0 and 14 obtained by flow cytometry.

No statistically significant differences were found between any of the groups on day 0, or 14. Table 7.4 summarises that n = 4 for FBS, n = 4 for pHPL, and n = 4 for PRP.

7.3.3 Adipogenesis gene expression results

Microscopy and flow cytometry results generated from this study clearly demonstrate that hASCs retain their capacity for adipogenic differentiation regardless of the type of serum supplementation. Gene expression analysis was done to confirm the expression of genes associated with adipogenic differentiation. For each gene investigated across the various media, three technical replicates were included. The biological replicates are shown in Table 7.4. Data points were excluded based on gDNA contamination observed in the NoRT controls ($C_q \leq 33$) and an SD > 0.5 between technical replicates.

The relative fold-change expression of C/EBPβ, PPARγ, and CD36 is shown in Figure 7.6. Relative fold-change expression was calculated using the comparative C_T method as described previously in section 7.2.4. C/EBPβ was down-regulated (relative fold-change expression < 1) in hASCs that underwent adipogenic differentiation in FBS and pHPL but was up-regulated (relative fold-change expression >1) in PRP compared to the NI control. In all three media, PPARγ was up-regulated. Lastly, CD36 was up-regulated in FBS and PRP but down-regulated in pHPL. No statistically significant differences were found in the gene expression results for the six adipogenic genes investigated.

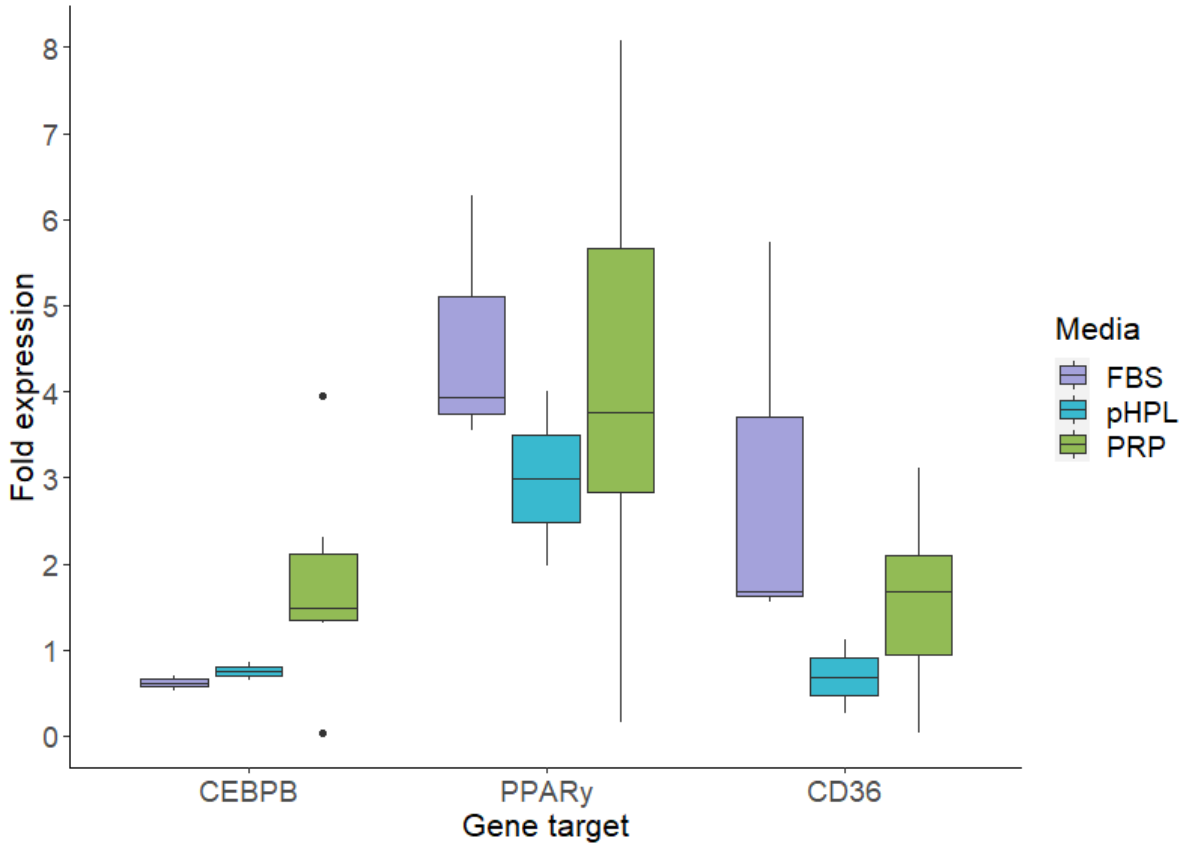

Figure 7.6 Fold expression ($2^{-\Delta\Delta CT}$) of three gene targets calculated using the ΔΔCT method. Fold expression < 1 indicates down-regulation. C/EBPβ in FBS and pHPL is down-regulated along with CD36 expression in pHPL medium. No statistically significant differences were found between any of the groups on day 0, or 14. Table 7.4 summarises that n = 3 for FBS, n = 2 for pHPL, and n = 6 for PRP.

C/EBPα, FABP4 and AdipoQ expression was also investigated. Across all time points and media conditions, no C/EBPα expression was observed as all samples had either C_q > 33 or the gene was not expressed at levels high enough to generate a detectable C_q. For day 14 induced samples, FABP4 and AdipoQ were both expressed in all media; however, it was not possible to determine the fold change expression (RFI) using the ΔΔCT method in all the samples, because in some instances, there was no amplification of FABP4 or AdipoQ in non-induced control samples. Table 7.5 displays the average C_q values of each condition and the fold expression ($2^{-\Delta\Delta CT}$) relative to the non-induced control where both non-induced and induced C_q values were obtained and subsequently used to calculate the relative fold change expression of these target genes.

Table 7.5 C_q and fold expression values for FABP4 and AdipoQ in all media on day 14.

		FABP4		AdipoQ	
Media	I/NI	C_q value	RFI	C_q value	RFI
FBS	I	17,1	-	20,6	-
	NI	x		x	
	I	15,3	73 458	20,1	-
	NI	31,4		x	
	I	16,2	7 301	21,2	3 280
	NI	29,0		32,8	
pHPL	I	15,6	26 891	18,6	-
	NI	30,3		x	
	I	17,4	9 340	20,2	-
	NI	30,6		x	
PRP	I	20,6	34	22,7	71
	NI	25,7		28,9	
	I	19,2	-	20,5	
	NI	x		x	
	I	19,0	-	20,6	-
	NI	x		x	
	I	14,8	6 231	17,6	15 458
	NI	27,4		31,5	
	I	18,3	-	19,8	-
	NI	x		x	
	I	16,1	6 332	18,9	8 550
	NI	28,7		32,0	

7.4 Discussion and conclusion

Adipogenic differentiation was observed in all media, indicating that neither of the two human alternatives alters the ability of hASCs to undergo adipogenesis relative to cells differentiated in FBS. These results align with published MSC criteria (16,17). The increase in the percentage of hASCs that stained positive for NR from day 0 to day 14 NI was expected because hASC cell membranes contain lipids, resulting in a low level of NR positivity in all samples that increased as cell number increased from day 0 to 14. The increase in cell number from day 0 to day 14 in the NI samples accounts for the rise in NR staining observed, although the percentage of NR^+ cells was still low (< 3%). The percentage of NR staining observed across the different media for control samples followed the same trend seen in the proliferation study and absolute count in chapters 5 and 6, further strengthening the trend between cell number and NR^+ staining.

The morphology of the differentiating hASCs across all media was not the expected single large intracellular lipid droplet. In this study, the cells contained multiple smaller lipid droplets indicative of premature adipocytes. This morphology may be explained by the earlier timepoint used in this study, similar to results found by Felthaus et al., 2017 and as suggested by Ambele and colleagues (105).

The adipogenic potential seen in hASCs differentiatied in pHPL-supplemented medium contradicts work by Witzeneder et al., 2013, but supports results by others that found adipogenic differentiation is possible in pHPL containing medium (171,186). Adipogenesis in hASCs cultured in PRP-supplemented medium seen in this study is also corroborated findings published previously (30,173,187), showing that hASCs can differentiate into adipocytes in PRP medium *in vitro*. However, contradictory studies found no or reduced adipogenic differentiation in PRP medium (176,205).

The average C_q value for C/EBPα expression was 39.47 for all non-induced controls and 39.28 for all induced samples, and it was therefore deemed not expressed due to the C_q cut-off determined after the NoRTs were amplified to investigate for gDNA contamination. The lack of expression of C/EBPα is contradictory to most published literature as it is a transcription factor involved in adipogenesis, usually co-expressed

with PPARγ. It is described as an inducer of adipogenic differentiation (91,93,105,116). While contradictory to findings in literature, this is not necessarily surprising as only 20% of hASCs differentiated. The apparent lack of C/EBPα expression could therefore be due to low quantities present in total RNA isolates resulting in expression insufficient to amplify past the C_q threshold. However, there is evidence that adipogenesis is possible without C/EBPα expression since PPARγ is the primary regulator of adipogenic differentiation (116), which may explain why intracellular fat droplet accumulation is observed despite the lack of C/EBPα expression in this study.

Furthermore, C/EBPα is regarded as a later timepoint adipogenic gene (105). It may be that the expression of C/EBPα in this instance was initiated but was still at low levels, and the inclusion of a later time point could reveal higher, detectable levels of expression. According to Wu and colleagues (116), C/EBPα expression is seen after PPARγ expression, but before observing a mature adipocyte morphology similar to that observed in this study. Nevertheless, future studies should be conducted to investigate the apparent absence of C/EBPα expression.

The down-regulation of C/EBPβ in hASCs differentiated in pHPL- and FBS-supplemented media may result from RNA isolation at a later timepoint. C/EBPβ expression was included as it is the transcription factor that initiates the adipogenic gene cascade (91) and plays a role in mitotic clonal expansion as well as PPARγ induction which activates downstream adipogenic differentiation (91,116). It may be that C/EBPβ expression in hASCs differentiated in pHPL- and FBS-supplemented media decreased to undetectable levels by day 14. The up-regulation of C/EBPβ in the PRP-supplemented medium was expected as the cells could differentiate; however, it was not highly up-regulated, indicating that C/EBPβ expression in PRP had decreased by day 14. No previous studies comparing C/EBPα and C/EBPβ expression in human alternative-supplemented media under adipogenic differentiation conditions could be found. Thus, the expression of these two genes in the adipogenic gene pathway in human alternative-supplemented media should be investigated further for clarity.

The up-regulated expression of PPARγ across all media was expected as the primary regulator of adipogenesis, and fat accumulation was observed across all media (206). The up-regulation of PPARγ expression in PRP was contradictory to previous studies

(176,205) that found PPARγ was down-regulated compared to FBS. Other studies (187,206) found that PRP did not significantly down-regulate PPARγ expression compared to cells grown in FBS, similar to what was seen in this study. Expression of PPARγ in pHPL-supplemented adipogenesis observed was also reported in previous studies (127,207).

The lack of or low expression levels of FABP4 and AdipoQ in non-induced controls, and up-regulation and expression in induced samples, was expected since FABP4 and AdipoQ are adipokines expressed by adipocytes (93,106,115). These results were also observed in a previous study (206). The absence of noticeable lipid droplets in the non-induced controls was supported by the lack of adipocyte marker gene expression.

The up-regulation of AdipoQ in pHPL-grown hASCs seen in this study contradicts literature that found pHPL significantly down-regulated AdipoQ expression (207) but supports work by Oikonomopoulos and colleagues (127). FABP4 expression in pHPL-grown hASCs was observed when antibody staining was used to detect expression (171). In PRP medium, Chignon-Sicard and colleagues (205) saw AdipoQ and FABP4 expression; however, it was reduced compared to controls, similar to results in this study and elsewhere (176).

The lower level of lipid accumulation observed in pHPL-grown hASCs may be due to the down-regulation of CD36 observed. Christiaens et al., 2012 found that down-regulation of CD36 results in decreased adipogenic differentiation *in vitro*. CD36 plays a role in the uptake of long-chain fatty acids; therefore, fatty-acid uptake in pHPL-supplemented hASCs may be sub-optimal, resulting in the lower levels of differentiation observed. The up-regulation of CD36 expression seen in FBS- and PRP-supplemented hASCs is in line with the percentage of intracellular lipids seen in the flow cytometry results. Cells grown in FBS showed the highest percentage of NR^+ positivity followed by PRP-supplemented cells, similar to CD36 expression.

When considering the fluorescent microscopy and flow cytometry results, adipogenesis is possible in all three media tested in this study. This study confirms that terminal adipogenic potential in PRP and pHPL may be reduced compared to FBS, although the difference is not significant as reported elsewhere (205,207). It is possible that the growth factors present in PRP and pHPL media may impact adipogenesis, as

reported by Chignon-Sicard et al., 2017, who found that PRP has a significant anti-adipogenic effect through activation of the TGFβ pathway, and this warrants further investigation.

The contradictory results when investigating adipogenesis in human alternatives in the literature and this study may be due to the inherent biological variance when working with primary cells such as the hASCs as was the case in this study, as well as autologous blood products such as PRP. As mentioned in section 4.4, there is also no global standardised collection procedure or quality criteria for blood products. There is little consensus regarding the adipogenic gene expression profile in the various media in published literature which further complicates a definitive conclusion regarding gene expression and adipogenic differentiation potential in hASCs differentiated in human alternatives. Future studies investigating the effect of human alternatives on adipogenic differentiation potential of hASCs should include other contributing factors, such as hASC collection protocols and time in culture with the various medium supplements which may affect future therapeutic products. The RT-qPCR gene expression results in this study contradict previous literature when considering only the functions of C/EBPα and C/EBPβ in the adipogenic gene pathway. It must be noted that currently, no studies have looked at their expression in pHPL- and PRP-cultured hASCs, and a direct comparison is therefore not possible. Still, the main question of whether adipogenesis is possible in the three media was answered.

Further recommendations for future studies include treating isolated RNA with DNAse I treatment to reduce gDNA contamination and ensure more accurate results. More time points (days 0, 1, 3, 7, 14, and 21) may shed better light on the gene expression from earlier to later progression through adipogenesis in pHPL-and PRP-supplemented medium. To avoid total RNA isolation from cultures with differentiated and undifferentiated cells, one might consider plating single hASCs into a 384-well plate and only isolating RNA from wells where hASCs have differentiated into adipocytes. Other human alternatives studied in previous sections of this study and growth factors present in the current chosen media supplements should also be investigated for a more complete picture regarding factors that might influence the adipogenic potential of hASCs maintained human alternative-supplemented media. A correlation study regarding the faster proliferation seen earlier in this study, the

composition of media containing humanalternatives, and the adipogenic differentiation of hASCs in human alternative-supplemented media should also be considered.

In conclusion, adipogenic differentiation is possible in PRP-supplemented medium, and thus it is a suitable autologous replacement for FBS in adipogenic medium. Differentiation into adipocytes in pHPL medium was also achieved, making pHPL a suitable allogeneic human alternative to FBS in adipogenesis settings.

Chapter 8: Conclusion and future perspectives

hASCs as a potential cell-based therapeutic product in regenerative medicine has generated widespread interest due to characteristics such as multipotency and immunomodulation (17). Furthermore, large numbers of hASCs can be isolated from adipose tissue with minor donor site morbidity and expanded *in vitro* to clinically relevant cell numbers (12,15,17). Subsequently, numerous clinical trials are underway using hASCs to treat various diseases (1,2).

Before hASCs can be produced as a therapeutic product, a crucial consideration is their compliance to GMP to ensure high quality, safe treatment (25,160,171,208). Currently, *ex vivo* hASC expansion and maintenance to obtain clinically relevant cell numbers rely on cell culture media containing xenogeneic FBS (21,24,25,122). FBS in culture media of hASCs intended for clinical use poses multiple safety concerns such as zoonotic disease transfer and ethical considerations regarding animal suffering (19,26,27). This study, therefore, aimed to determine the best alternative to FBS from human blood products. The proposed human alternatives produced from whole blood were pHPL, HS, FFP, PPP, and PRP. To the author's knowledge, this dissertation represents the first time all five proposed human alternatives were used in a simultaneous head-to-head comparison with FBS. The focus was on the effects of human alternatives on the proliferation, morphology, viability, immunophenotype, and retention of adipogenic differentiation potential of hASCs. This study contributes to the current body of knowledge considering alternatives to FBS towards a GMP compliant cell therapeutic product.

The results confirmed that all human alternatives adhered to quality criteria (investigated in objective one and discussed in Chapter 4: and sustained hASCs *in vitro* without altering the immunophenotype or negatively affecting viability, as discussed in Chapters 5 and 6 for objectives two and three. Two human alternatives, PRP and pHPL, significantly increased cell proliferation of hASCs, which is advantageous in a clinical setting as it reduces the time required to reach clinically sufficient cell numbers. Based on these results, for the fourth objective, retention of adipogenic differentiation potential was investigated in pHPL, PRP, and FBS which is

discussed in Chapter 7. Adipogenesis was achieved in all three of these culture media, indicating no loss of adipogenic potential due to the medium supplements compared to FBS.

Fast proliferation was, however, not the only important aspect when considering a human alternative to FBS. When choosing a human alternative in a clinical *ex vivo* setting, blood products' autologous or allogeneic nature will have to be carefully considered as well as the availability, accessibility, and cost of production of the various human alternative options, as some allogeneic blood products such as FFP and HS may be more easily accessible as they are routine products manufactured by blood banks. Autologous blood products offer advantages from histocompatibility and infectious disease screening perspectives. There are, however, disadvantages when using autologous products, such as PRP, as they can be highly variable due to inherent biological variance. Subsequently, inconsistent research and clinical outcomes may be seen. In contrast, allogeneic products can be more standardised but will require intensive disease screening and quality control steps to ensure a high-quality product (28).

Future studies could include adipogenesis in PPP, FFP, and HS supplemented media, as these were not investigated in this study. Furthermore, osteogenesis and chondrogenic differentiation of hASCs in the various human alternatives could be investigated. Assessment of the immunomodulatory characteristics of hASCs in the various human alternatives could also be considered. Synthetic medium would be the ideal for a therapeutic setting as it is fully customisable, however it is costly and time consuming to produce (27). Therefore, feasibility, cost, hASC proliferation, differentiation, and similar characteristics as were investigated in this study could also be studied in synthetic, serum-free medium. Serum-free medium may be an option where complete control of medium composition and exposure of hASCs to reagents is required in a therapeutic setting.

In conclusion, an FBS substitute may have to be chosen not only for its ability to promote proliferation but based on the intended application or hASC treatment envisioned.

Chapter 9: References

1. National Library of Medicine. Mesenchymal stem cells - List Results - ClinicalTrials.gov [Internet]. 2021 [cited 2021 Jul 26]. Available from: https://clinicaltrials.gov/ct2/results?cond=&term=mesenchymal+stem+cells&country=&state=&city=&dist=

2. Blau HM, Daley GQ. Stem cells in the treatment of disease. N Engl J Med. 2019;380(18):1748–60.

3. Orozco L, Soler R, Morera C, Alberca M, Sánchez A, García-Sancho J. Intervertebral Disc Repair by Autologous Mesenchymal Bone Marrow Cells: A Pilot Study. Transplantation [Internet]. 2011 Oct 15 [cited 2021 Aug 18];92(7):822–8. Available from: https://pubmed.ncbi.nlm.nih.gov/21792091/

4. Shakoori P, Zhang Q, Le AD. Applications of Mesenchymal Stem Cells in Oral and Craniofacial Regeneration. Oral Maxillofac Surg Clin North Am [Internet]. 2017;29(1):19–25. Available from: http://dx.doi.org/10.1016/j.coms.2016.08.009

5. Freitag J, Bates D, Boyd R, Shah K, Barnard A, Huguenin L, et al. Mesenchymal stem cell therapy in the treatment of osteoarthritis: Reparative pathways, safety and efficacy - A review. BMC Musculoskelet Disord [Internet]. 2016;17(1):1–13. Available from: http://dx.doi.org/10.1186/s12891-016-1085-9

6. Squillaro T, Peluso G, Galderisi U. Clinical Trials With Mesenchymal Stem Cells: An Update. Cell Transplant [Internet]. 2016;25(5):829–48. Available from: http://www.ncbi.nlm.nih.gov/pubmed/26423725

7. Feins S, Kong W, Williams EF, Milone MC, Fraietta JA. An introduction to chimeric antigen receptor (CAR) T-cell immunotherapy for human cancer. Am J Hematol. 2019;94(S1):S3–9.

8. Lipowska-Bhalla G, Gilham DE, Hawkins RE, Rothwell DG. Targeted immunotherapy of cancer with CAR T cells: Achievements and challenges. Cancer Immunol Immunother. 2012;61(7):953–62.

9. Zhang YS, Yue K, Aleman J, Mollazadeh-Moghaddam K, Bakht SM, Yang J, et al. 3D Bioprinting for Tissue and Organ Fabrication. Ann Biomed Eng.

2017;45(1):148–63.

10. Bieback K, Brinkman I. Mesenchymal stromal cells from human perinatal tissues: From biology to cell therapy. World J Stem Cells [Internet]. 2010 Aug 26;2(4):81–92. Available from: http://www.wjgnet.com/1948-0210/full/v2/i4/81.htm

11. Kimbrel EA, Lanza R. Pluripotent stem cells: the last 10 years. Regen Med [Internet]. 2016 Dec;11(8):831–47. Available from: https://www.futuremedicine.com/doi/10.2217/rme-2016-0117

12. Gazit Z, Pelled G, Sheyn D, Yakubovich DC, Gazit D. Mesenchymal Stem Cells. In: Atala A, Lanza R, Mikos AG, Nerem R, editors. Principles of Regenerative Medicine [Internet]. Third Edit. Elsevier; 2019. p. 205–18. Available from: http://dx.doi.org/10.1016/B978-0-12-809880-6.00014-X

13. Lanza R, Gearhart J, Hogan B, Melton D, Pedersen R, Thomas ED, et al. Essentials of Stem Cell Biology [Internet]. Third. Lanza R, Atala A, editors. Elsevier; 2009. 665 p. Available from: https://linkinghub.elsevier.com/retrieve/pii/C20090000786

14. Bora P, Majumdar AS. Adipose tissue-derived stromal vascular fraction in regenerative medicine: a brief review on biology and translation. Stem Cell Res Ther [Internet]. 2017 Jun 15 [cited 2021 Sep 8];8(1). Available from: /pmc/articles/PMC5472998/

15. Baer PC, Geiger H. Adipose-Derived Mesenchymal Stromal/Stem Cells: Tissue Localization, Characterization, and Heterogeneity. Stem Cells Int [Internet]. 2012;2012:1–11. Available from: http://www.hindawi.com/journals/sci/2012/812693/

16. Dominici M, Le Blanc K, Mueller I, Slaper-Cortenbach I, Marini F., Krause DS, et al. Minimal criteria for defining multipotent mesenchymal stromal cells. The International Society for Cellular Therapy position statement. Cytotherapy [Internet]. 2006;8(4):315–7. Available from: http://dx.doi.org/10.1080/14653240600855905

17. Bourin P, Bunnell BA, Casteilla L, Dominici M, Katz AJ, March KL, et al. Stromal

cells from the adipose tissue-derived stromal vascular fraction and culture expanded adipose tissue-derived stromal/ stem cells: a joint statement of the International Federation for Adipose Therapeutics (IFATS) and Science and the International S. Cytotherapy [Internet]. 2013 Jun;15(6):641–8. Available from: http://dx.doi.org/10.1016/j.jcyt.2013.02.006

18. van der Valk J, Gstraunthaler G. Fetal Bovine Serum (FBS) — A Pain in the Dish? Altern to Lab Anim [Internet]. 2017 Dec 1;45(6):329–32. Available from: http://journals.sagepub.com/doi/10.1177/026119291704500611

19. van der Valk J, Bieback K, Buta C, Cochrane B, Dirks WG, Fu J, et al. Fetal bovine serum (FBS): Past – present – future. ALTEX [Internet]. 2018;35(1):99–118. Available from: https://www.altex.org/index.php/altex/article/view/101

20. Gottipamula S, Muttigi MS, Kolkundkar U, Seetharam RN. Serum-free media for the production of human mesenchymal stromal cells: a review. Cell Prolif [Internet]. 2013 Dec;46(6):608–27. Available from: https://onlinelibrary.wiley.com/doi/10.1111/cpr.12063

21. Sensebé L, Gadelorge M, Fleury-Cappellesso S. Production of mesenchymal stromal/stem cells according to good manufacturing practices: A review. Stem Cell Res Ther. 2013;4(3).

22. EudraLex. The Rules Governing Medicinal Products in the European Union, Volume 4; Annex 2: Manufacture of Biological active substances and Medicinal Products for Human Use. 2018. p. 25.

23. EudraLex. The Rules Governing Medicinal Products in the European Union, Volume 4, Good Manufacturing Practice. Brussels; 2017. p. 82.

24. Pamies D, Bal-Price A, Simeonov A, Tagle D, Allen D, Gerhold D, et al. Good Cell Culture Practice for stem cells and stem-cell-derived models. Toxicol Lett [Internet]. 2017;34(1):95–132. Available from: http://www.altex.org/index.php/altex/article/view/76

25. Patrikoski M, Juntunen M, Boucher S, Campbell A, Vemuri MC, Mannerström B, et al. Development of fully defined xeno-free culture system for the preparation

and propagation of cell therapy-compliant human adipose stem cells. Stem Cell Res Ther [Internet]. 2013;4(2):27. Available from: http://stemcellres.com/content/4/2/27

26. Yang Z, Xiong H. Culture Conditions and Types of Growth Media for Mammalian Cells. In: Ceccherini-Nelli L, Matteoli B, editors. Biomedical Tissue Culture [Internet]. InTech; 2012. p. 3–18. Available from: http://www.intechopen.com/books/biomedical-tissue-culture/culture-conditions-and-types-of-growth-media-for-mammalian-cells

27. Dessels C, Potgieter M, Pepper MS. Making the Switch: Alternatives to Fetal Bovine Serum for Adipose-Derived Stromal Cell Expansion. Front Cell Dev Biol [Internet]. 2016;4(October):1–10. Available from: http://journal.frontiersin.org/article/10.3389/fcell.2016.00115/full

28. Shih DTB, Burnouf T. Preparation, quality criteria, and properties of human blood platelet lysate supplements for ex vivo stem cell expansion. N Biotechnol [Internet]. 2015 Jan;32(1):199–211. Available from: http://dx.doi.org/10.1016/j.nbt.2014.06.001

29. Gersch RP, Glahn J, Tecce MG, Wilson AJ, Percec I. Platelet rich plasma augments adipose-Derived stem cell growth and differentiation. Aesthetic Surg J. 2017;37(6):723–9.

30. Atashi F, Jaconi MEE, Pittet-Cuénod B, Modarressi A. Autologous Platelet-Rich Plasma: A Biological Supplement to Enhance Adipose-Derived Mesenchymal Stem Cell Expansion. Tissue Eng Part C Methods [Internet]. 2015 Mar;21(3):253–62. Available from: http://online.liebertpub.com/doi/abs/10.1089/ten.tec.2014.0206

31. Kocaoemer A, Kern S, Klüter H, Bieback K. Human AB Serum and Thrombin-Activated Platelet-Rich Plasma Are Suitable Alternatives to Fetal Calf Serum for the Expansion of Mesenchymal Stem Cells from Adipose Tissue. Stem Cells [Internet]. 2007;25(5):1270–8. Available from: http://doi.wiley.com/10.1634/stemcells.2006-0627

32. Gstraunthaler G, Rauch C, Wechselberger J, Feifel E. Human Platelet Lysates

Successfully Replace Fetal Bovine Serum in Adipose-Derived Adult Stem Cell Culture. J Adv Biotechnol Bioeng. 2014;2(1):1–11.

33. Bieback K, Hecker A, Kocaömer A, Lannert H, Schallmoser K, Strunk D, et al. Human Alternatives to Fetal Bovine Serum for the Expansion of Mesenchymal Stromal Cells from Bone Marrow. Stem Cells Transl Clin Res [Internet]. 2009 Sep;27(9):2331–41. Available from: https://onlinelibrary.wiley.com/doi/10.1002/stem.139

34. Witzeneder K, Lindenmair A, Gabriel C, Höller K, Theiß D, Redl H, et al. Human-derived alternatives to fetal bovine serum in cell culture. Transfus Med Hemotherapy. 2013;40(6):417–23.

35. Nimura A, Muneta T, Koga H, Mochizuki T, Suzuki K, Makino H, et al. Increased proliferation of human synovial mesenchymal stem cells with autologous human serum. Arthritis Rheum. 2008;58(2):501–10.

36. Baer PC, Griesche N, Luttmann W, Schubert R, Luttmann A, Geiger H. Human adipose-derived mesenchymal stem cells in vitro: evaluation of an optimal expansion medium preserving stemness. Cytotherapy [Internet]. 2010 Jan;12(1):96–106. Available from: http://dx.doi.org/10.3109/14653240903377045

37. Müller I, Kordowich S, Holzwarth C, Spano C, Isensee G, Staiber A, et al. Animal serum-free culture conditions for isolation and expansion of multipotent mesenchymal stromal cells from human BM. Cytotherapy. 2006;8(5):437–44.

38. Burnouf T, Strunk D, Koh MBC, Schallmoser K. Human platelet lysate: Replacing fetal bovine serum as a gold standard for human cell propagation? Biomaterials [Internet]. 2016 Jan;76:371–87. Available from: http://dx.doi.org/10.1016/j.biomaterials.2015.10.065

39. Mishra A, Tummala P, King A, Lee B, Kraus M, Tse V, et al. Buffered Platelet-Rich Plasma Enhances Mesenchymal Stem Cell Proliferation and Chondrogenic Differentiation. Tissue Eng Part C Methods [Internet]. 2009;15(3):431–5. Available from: http://www.liebertonline.com/doi/abs/10.1089/ten.tec.2008.0534

40. Schallmoser K, Bartmann C, Rohde E, Reinisch A, Kashofer K, Stadelmeyer E, et al. Human platelet lysate can replace fetal bovine serum for clinical-scale expansion of functional mesenchymal stromal cells. Transfusion [Internet]. 2007 Aug;47(8):1436–46. Available from: http://doi.wiley.com/10.1111/j.1537-2995.2007.01220.x

41. Veronique Serre FA. Platelet Rich Plasma Promotes Proliferation of Adipose Derived Mesenchymal Stem Cells via Activation of AKT and Smad2 Signaling Pathways. J Stem Cell Res Ther [Internet]. 2015;05(08):1–10. Available from: https://www.omicsonline.org/open-access/platelet-rich-plasma-promotes-proliferation-of-adipose-derived-mesenchymal-stem-cells-via-activation-of-akt-and-smad2-signaling-pathways-2157-7633-1000301.php?aid=59490

42. Smith AG. Embryo-derived stem cells: of mice and men. Annu Rev Cell Dev Biol [Internet]. 2001;17:435–62. Available from: http://www.ncbi.nlm.nih.gov/pubmed/11687496

43. Zhang X, Stojkovic P, Przyborski S, Cooke M, Armstrong L, Lako M, et al. Derivation of Human Embryonic Stem Cells from Developing and Arrested Embryos. Stem Cells [Internet]. 2006 Dec;24(12):2669–76. Available from: http://doi.wiley.com/10.1634/stemcells.2006-0377

44. Volarevic V, Markovic BS, Gazdic M, Volarevic A, Jovicic N, Arsenijevic N, et al. Ethical and safety issues of stem cell-based therapy. Int J Med Sci. 2018;15(1):36–45.

45. Takahashi K, Yamanaka S. Induction of Pluripotent Stem Cells from Mouse Embryonic and Adult Fibroblast Cultures by Defined Factors. Cell [Internet]. 2006 Aug;126(4):663–76. Available from: https://linkinghub.elsevier.com/retrieve/pii/S0092867406009767

46. Mason C, Dunnill P. A brief definition of regenerative medicine. Regen Med [Internet]. 2008;3(1):1–5. Available from: http://www.futuremedicine.com/doi/10.2217/17460751.3.1.1

47. Cossu G, Birchall M, Brown T, De Coppi P, Culme-Seymour E, Gibbon S, et al. Lancet Commission: Stem cells and regenerative medicine. Lancet [Internet].

2018;391(10123):883–910. Available from: http://dx.doi.org/10.1016/S0140-6736(17)31366-1

48. Gupta PK, Chullikana A, Parakh R, Desai S, Das A, Gottipamula S, et al. A double blind randomized placebo controlled phase I/II study assessing the safety and efficacy of allogeneic bone marrow derived mesenchymal stem cell in critical limb ischemia. J Transl Med [Internet]. 2013 Dec 10 [cited 2021 Aug 18];11(1):143. Available from: https://pubmed.ncbi.nlm.nih.gov/23758736/

49. Jang YO, Kim YJ, Baik SK, Kim MY, Eom YW, Cho MY, et al. Histological improvement following administration of autologous bone marrow-derived mesenchymal stem cells for alcoholic cirrhosis: a pilot study. Liver Int [Internet]. 2014 Jan 1 [cited 2021 Aug 18];34(1):33–41. Available from: https://onlinelibrary.wiley.com/doi/full/10.1111/liv.12218

50. Kucharzewski M, Rojczyk E, Wilemska-Kucharzewska K, Wilk R, Hudecki J, Los MJ. Novel trends in application of stem cells in skin wound healing. Eur J Pharmacol [Internet]. 2019;843(December 2018):307–15. Available from: https://doi.org/10.1016/j.ejphar.2018.12.012

51. Duscher D, Barrera J, Wong VW, Maan ZN, Whittam AJ, Januszyk M, et al. Stem Cells in Wound Healing: The Future of Regenerative Medicine? A Mini-Review. Gerontology. 2016;62(2):216–25.

52. Le Blanc K, Frassoni F, Ball L, Locatelli F, Roelofs H, Lewis I, et al. Mesenchymal stem cells for treatment of steroid-resistant, severe, acute graft-versus-host disease: a phase II study. Lancet [Internet]. 2008 May 10 [cited 2021 Aug 18];371(9624):1579–86. Available from: https://linkinghub.elsevier.com/retrieve/pii/S014067360860690X

53. Auletta JJ, Lazarus HM. Immune restoration following hematopoietic stem cell transplantation: an evolving target. Bone Marrow Transplant [Internet]. 2005 May 21;35(9):835–57. Available from: http://www.nature.com/articles/1704966

54. Herrmann R, Sturm M, Shaw K, Purtill D, Cooney J, Wright M, et al. Mesenchymal stromal cell therapy for steroid-refractory acute and chronic graft versus host disease: a phase 1 study. Int J Hematol [Internet]. 2012 Feb 20 [cited 2021 Aug

18];95(2):182–8. Available from: https://link.springer.com/article/10.1007/s12185-011-0989-2

55. Hirsch T, Rothoeft T, Teig N, Bauer JW, Pellegrini G, De Rosa L, et al. Regeneration of the entire human epidermis using transgenic stem cells. Nature. 2017;551(7680):327–32.

56. Fernandes S, Chong JJH, Paige SL, Iwata M, Torok-Storb B, Keller G, et al. Comparison of Human Embryonic Stem Cell-Derived Cardiomyocytes, Cardiovascular Progenitors, and Bone Marrow Mononuclear Cells for Cardiac Repair. Stem Cell Reports [Internet]. 2015 Nov 10 [cited 2021 Jul 31];5(5):753–62. Available from: http://www.cell.com/article/S2213671115002738/fulltext

57. Gussoni E, Pavlath GK, Lanctot AM, Sharma KR, Miller RG, Steinman L, et al. Normal dystrophin transcripts detected in Duchenne muscular dystrophy patients after myoblast transplantation. Nature [Internet]. 1992 Apr [cited 2021 Jul 31];356(6368):435–8. Available from: https://www.nature.com/articles/356435a0

58. Charville GW, Cheung TH, Yoo B, Santos PJ, Lee GK, Shrager JB, et al. Ex Vivo Expansion and In Vivo Self-Renewal of Human Muscle Stem Cells. Stem Cell Reports [Internet]. 2015 Oct 13 [cited 2021 Jul 31];5(4):621–32. Available from: https://pubmed.ncbi.nlm.nih.gov/26344908/

59. Relaix F, Bencze M, Borok MJ, Der Vartanian A, Gattazzo F, Mademtzoglou D, et al. Perspectives on skeletal muscle stem cells. Nat Commun [Internet]. 2021 Dec 29 [cited 2021 Aug 18];12(1):692. Available from: https://www.nature.com/articles/s41467-020-20760-6

60. Sugimura R, Jha DK, Han A, Soria-Valles C, da Rocha EL, Lu Y-F, et al. Haematopoietic stem and progenitor cells from human pluripotent stem cells. Nature [Internet]. 2017 May 25 [cited 2021 Aug 18];545(7655):432–8. Available from: https://pubmed.ncbi.nlm.nih.gov/28514439/

61. Feng Q, Shabrani N, Thon JN, Huo H, Thiel A, Machlus KR, et al. Scalable Generation of Universal Platelets from Human Induced Pluripotent Stem Cells. Stem Cell Reports [Internet]. 2014 Nov [cited 2021 Aug 18];3(5):817–31.

Available from: https://pubmed.ncbi.nlm.nih.gov/25418726/

62. Moreau T, Evans AL, Vasquez L, Tijssen MR, Yan Y, Trotter MW, et al. Large-scale production of megakaryocytes from human pluripotent stem cells by chemically defined forward programming. Nat Commun [Internet]. 2016 Sep 1 [cited 2021 Aug 18];7(1):11208. Available from: https://www.nature.com/articles/ncomms11208

63. Doulatov S, Vo LT, Chou SS, Kim PG, Arora N, Li H, et al. Induction of Multipotential Hematopoietic Progenitors from Human Pluripotent Stem Cells via Respecification of Lineage-Restricted Precursors. Cell Stem Cell [Internet]. 2013 Oct 3 [cited 2021 Aug 18];13(4):459–70. Available from: https://pubmed.ncbi.nlm.nih.gov/24094326/

64. Chicha L, Feki A, Boni A, Irion O, Hovatta O, Jaconi M. Human Pluripotent Stem Cells Differentiated in Fully Defined Medium Generate Hematopoietic CD34+ and CD34− Progenitors with Distinct Characteristics. Milstone DS, editor. PLoS One [Internet]. 2011 Feb 25 [cited 2021 Aug 18];6(2):e14733. Available from: https://dx.plos.org/10.1371/journal.pone.0014733

65. Kunkanjanawan T, Carter R, Ahn K, Yang J, Parnpai R, Chan AWS. Induced Pluripotent HD Monkey Stem Cells Derived Neural Cells for Drug Discovery. SLAS Discov Adv Life Sci R&D [Internet]. 2017 Jul 27;22(6):696–705. Available from: http://journals.sagepub.com/doi/10.1177/2472555216685044

66. Marks P, Gottlieb S. Balancing Safety and Innovation for Cell-Based Regenerative Medicine. N Engl J Med [Internet]. 2018 Mar 8;378(10):954–9. Available from: http://www.nejm.org/doi/10.1056/NEJMsr1715626

67. Riis S, Zachar V, Boucher S, Vemuri MC, Pennisi CP, Fink T. Critical steps in the isolation and expansion of adipose-derived stem cells for translational therapy. Expert Rev Mol Med [Internet]. 2015 Jun 8;17(Table 1):e11. Available from: http://www.journals.cambridge.org/abstract_S1462399415000101

68. Möller EM, Bahnweg G, Sandermann H, Geiger HH. A simple and efficient protocol for isolation of high molecular weight DNA from filamentous fungi, fruit bodies, and infected plant tissues. Nucleic Acids Res. 1992;20(22):6115–6.

69. Bianco P, Robey PG, Simmons PJ. Mesenchymal Stem Cells: Revisiting History, Concepts, and Assays. Cell Stem Cell [Internet]. 2008 Apr 7;2(4):313–9. Available from: https://linkinghub.elsevier.com/retrieve/pii/S1934590908001148

70. Samsonraj RM, Raghunath M, Nurcombe V, Hui JH, van Wijnen AJ, Cool SM. Concise Review: Multifaceted Characterization of Human Mesenchymal Stem Cells for Use in Regenerative Medicine. Stem Cells Transl Med [Internet]. 2017 Dec;6(12):2173–85. Available from: https://onlinelibrary.wiley.com/doi/10.1002/sctm.17-0129

71. Friedenstein AJ, Petrakova K V, Kurolesova AI, Frolova GP. Heterotopic of bone marrow. Analysis of precursor cells for osteogenic and hematopoietic tissues. Transplantation [Internet]. 1968 Mar;6(2):230–47. Available from: http://www.ncbi.nlm.nih.gov/pubmed/5654088

72. Andrzejewska A, Lukomska B, Janowski M. Concise Review: Mesenchymal Stem Cells: From Roots to Boost. Stem Cells [Internet]. 2019 Jul;37(7):855–64. Available from: https://onlinelibrary.wiley.com/doi/10.1002/stem.3016

73. Kallmeyer K, Pepper MS. Homing properties of mesenchymal stromal cells. Expert Opin Biol Ther. 2015;15(4):477–9.

74. Ortiz LA, DuTreil M, Fattman C, Pandey AC, Torres G, Go K, et al. Interleukin 1 receptor antagonist mediates the antiinflammatory and antifibrotic effect of mesenchymal stem cells during lung injury. Proc Natl Acad Sci [Internet]. 2007 Jun 26 [cited 2021 Jul 31];104(26):11002–7. Available from: https://www.pnas.org/content/104/26/11002

75. Shabbir A, Zisa D, Suzuki G, Lee T. Heart failure therapy mediated by the trophic activities of bone marrow mesenchymal stem cells: A noninvasive therapeutic regimen. Am J Physiol - Hear Circ Physiol [Internet]. 2009 Jun [cited 2021 Jul 31];296(6):H1888–97. Available from: https://pubmed.ncbi.nlm.nih.gov/19395555/

76. Hong HS, Kim YH, Son Y. Perspectives on mesenchymal stem cells: Tissue repair, immune modulation, and tumor homing. Arch Pharm Res [Internet]. 2012 Feb 28 [cited 2021 Jul 31];35(2):201–11. Available from:

https://pubmed.ncbi.nlm.nih.gov/22370775/

77. Merck. Dulbecco's Modified Eagle's Medium (DME) Formulation | Sigma-Aldrich [Internet]. [cited 2018 Mar 13]. Available from: https://www.sigmaaldrich.com/life-science/cell-culture/learning-center/media-formulations/dme.html

78. Freshney RI. Culture of Animal Cells [Internet]. 6th ed. Hoboken, NJ, USA: John Wiley & Sons, Inc.; 2010. 732 p. Available from: http://doi.wiley.com/10.1002/9780470649367

79. Björklund M. Cell size homeostasis: Metabolic control of growth and cell division. Biochim Biophys Acta - Mol Cell Res [Internet]. 2019 Mar 1 [cited 2021 Mar 23];1866(3):409–17. Available from: https://linkinghub.elsevier.com/retrieve/pii/S0167488918302544

80. Alberts B, Johnson A, Lewis J, Morgan D, Raff M, Roberts K, et al. Molecular Biology of the Cell [Internet]. 6th ed. Bochicchio A, Granum Lewis S, Zayatz E, editors. New York: Garland Science, Taylor & Francis Group, LLC; 2017. Available from: https://www.taylorfrancis.com/books/9781317563754

81. Alenzi FQB. Links between apoptosis, proliferation and the cell cycle. Br J Biomed Sci [Internet]. 2004 Jan 23;61(2):99–102. Available from: https://www.tandfonline.com/doi/full/10.1080/09674845.2004.11732652

82. Terzi MY, Izmirli M, Gogebakan B. The cell fate: senescence or quiescence. Mol Biol Rep [Internet]. 2016 Nov 1 [cited 2021 Dec 13];43(11):1213–20. Available from: https://pubmed.ncbi.nlm.nih.gov/27558094/

83. Bertoli C, Skotheim JM, de Bruin RAM. Control of cell cycle transcription during G1 and S phases. Nat Rev Mol Cell Biol [Internet]. 2013 Aug 23;14(8):518–28. Available from: http://www.nature.com/articles/nrm3629

84. Fink SL, Cookson BT. Apoptosis, Pyroptosis, and Necrosis: Mechanistic Description of Dead and Dying Eukaryotic Cells. Infect Immun [Internet]. 2005 Apr;73(4):1907–16. Available from: https://iai.asm.org/content/73/4/1907

85. D'Arcy MS. Cell death: a review of the major forms of apoptosis, necrosis and

autophagy. Cell Biol Int [Internet]. 2019 Jun 25;43(6):582–92. Available from: https://onlinelibrary.wiley.com/doi/10.1002/cbin.11137

86. Wyllie AH, Kerr JFR, Currie AR. Cell Death: The Significance of Apoptosis. In: International Review of Cytology [Internet]. 1980. p. 251–306. Available from: https://linkinghub.elsevier.com/retrieve/pii/S0074769608623128

87. Kerr JFR, Wyllie AH, Currie AR. Apoptosis: A Basic Biological Phenomenon with Wideranging Implications in Tissue Kinetics. Br J Cancer [Internet]. 1972 Aug [cited 2021 Apr 24];26(4):239–57. Available from: /pmc/articles/PMC2008650/?report=abstract

88. Khalid N, Azimpouran M. Necrosis. Lancet [Internet]. 2021 Mar 16 [cited 2021 Jul 27];80(2046):547–8. Available from: https://www.ncbi.nlm.nih.gov/books/NBK557627/

89. Sarjeant K, Stephens JM. Adipogenesis. Cold Spring Harb Perspect Biol [Internet]. 2012 Sep 1;4(9):1–20. Available from: http://cshperspectives.cshlp.org/lookup/doi/10.1101/cshperspect.a008417

90. Rosen ED, MacDougald OA. Adipocyte differentiation from the inside out. Nat Rev Mol Cell Biol. 2006;7(12):885–96.

91. Tang QQ, Lane MD. Adipogenesis: From Stem Cell to Adipocyte. Annu Rev Biochem [Internet]. 2012 Jul 7;81(1):715–36. Available from: http://www.annualreviews.org/doi/10.1146/annurev-biochem-052110-115718

92. Scheja L, Heeren J. The endocrine function of adipose tissues in health and cardiometabolic disease. Nat Rev Endocrinol [Internet]. 2019;15(9):507–24. Available from: http://dx.doi.org/10.1038/s41574-019-0230-6

93. de Sá PM, Richard AJ, Hang H, Stephens JM. Transcriptional Regulation of Adipogenesis. In: Comprehensive Physiology [Internet]. Hoboken, NJ, USA: John Wiley & Sons, Inc.; 2017. p. 635–74. Available from: http://doi.wiley.com/10.1002/cphy.c160022

94. Nawrocki AR, Rajala MW, Tomas E, Pajvani UB, Saha AK, Trumbauer ME, et al. Mice Lacking Adiponectin Show Decreased Hepatic Insulin Sensitivity and

Reduced Responsiveness to Peroxisome Proliferator-activated Receptor γ Agonists. J Biol Chem [Internet]. 2006 Feb 3 [cited 2021 Jul 30];281(5):2654–60. Available from: https://pubmed.ncbi.nlm.nih.gov/16326714/

95. Christiaens V, Van Hul M, Lijnen HR, Scroyen I. CD36 promotes adipocyte differentiation and adipogenesis. Biochim Biophys Acta [Internet]. 2012 Jul;1820(7):949–56. Available from: http://dx.doi.org/10.1016/j.bbagen.2012.04.001

96. Prentice KJ, Saksi J, Hotamisligil GS. Adipokine FABP4 integrates energy stores and counterregulatory metabolic responses. J Lipid Res. 2019;60(4):734–40.

97. Ali AT, Hochfeld WE, Myburgh R, Pepper MS. Adipocyte and adipogenesis. Eur J Cell Biol [Internet]. 2013 Jun;92(6–7):229–36. Available from: http://dx.doi.org/10.1016/j.ejcb.2013.06.001

98. Lynes MD, Tseng Y-H. Deciphering adipose tissue heterogeneity. Ann N Y Acad Sci [Internet]. 2018 Jan;1411(1):5–20. Available from: http://doi.wiley.com/10.1111/nyas.13398

99. Scott MA, Nguyen VT, Levi B, James AW. Current Methods of Adipogenic Differentiation of Mesenchymal Stem Cells. Stem Cells Dev [Internet]. 2011 Oct;20(10):1793–804. Available from: https://www.liebertpub.com/doi/10.1089/scd.2011.0040

100. Styner M, Sen B, Xie Z, Case N, Rubin J. Indomethacin promotes adipogenesis of mesenchymal stem cells through a cyclooxygenase independent mechanism. J Cell Biochem [Internet]. 2010 Nov 1;111(4):1042–50. Available from: https://www.ncbi.nlm.nih.gov/pmc/articles/PMC3624763/pdf/nihms412728.pdf

101. Zhao X, Hu H, Wang C, Bai L, Wang Y, Wang W, et al. A comparison of methods for effective differentiation of the frozen-thawed 3T3-L1 cells. Anal Biochem [Internet]. 2019 Mar;568(September 2018):57–64. Available from: https://doi.org/10.1016/j.ab.2018.12.020

102. Sakoda H, Ogihara T, Anai M, Funaki M, Inukai K, Katagiri H, et al. Dexamethasone-induced insulin resistance in 3T3-L1 adipocytes is due to

inhibition of glucose transport rather than insulin signal transduction. Diabetes [Internet]. 2000 Oct 1 [cited 2021 Jul 30];49(10):1700–8. Available from: https://diabetes.diabetesjournals.org/content/49/10/1700

103. MacDougald OA, Cornelius P, Liu R, Lane MD. Insulin Regulates Transcription of the CCAAT/Enhancer Binding Protein (C/EBP) α, β, and δ Genes in Fully-differentiated 3T3-L1 Adipocytes. J Biol Chem. 1995 Jan 13;270(2):647–54.

104. Vater C, Kasten P, Stiehler M. Culture media for the differentiation of mesenchymal stromal cells. Acta Biomater [Internet]. 2011 Feb;7(2):463–77. Available from: https://linkinghub.elsevier.com/retrieve/pii/S1742706110003570

105. Ambele MA, Dessels C, Durandt C, Pepper MS. Genome-wide analysis of gene expression during adipogenesis in human adipose-derived stromal cells reveals novel patterns of gene expression during adipocyte differentiation. Stem Cell Res [Internet]. 2016 May;16(3):725–34. Available from: http://dx.doi.org/10.1016/j.scr.2016.04.011

106. Fang H, Judd RL. Adiponectin Regulation and Function. In: Comprehensive Physiology [Internet]. Wiley; 2018. p. 1031–63. Available from: https://onlinelibrary.wiley.com/doi/10.1002/cphy.c170046

107. Gao H, Volat F, Sandhow L, Galitzky J, Nguyen T, Esteve D, et al. CD36 Is a Marker of Human Adipocyte Progenitors with Pronounced Adipogenic and Triglyceride Accumulation Potential. Stem Cells. 2017;35(7):1799–814.

108. Kucharski M, Kaczor U. Fatty acid binding protein 4 (FABP4) and the body lipid balance. Folia Biol. 2017;65(4):181–6.

109. Lefterova MI, Zhang Y, Steger DJ, Schupp M, Schug J, Cristancho A, et al. PPARγ and C/EBP factors orchestrate adipocyte biology via adjacent binding on a genome-wide scale. Genes Dev [Internet]. 2008 Nov 1 [cited 2021 Jul 30];22(21):2941–52. Available from: http://genesdev.cshlp.org/content/22/21/2941.full

110. Lefterova MI, Haakonsson AK, Lazar MA, Mandrup S. PPARγ and the global map of adipogenesis and beyond. Trends Endocrinol Metab. 2014;25(6):293–302.

111. Mishkin S, Stein L, Gatmaitan Z, Arias IM. The binding of fatty acids to cytoplasmic proteins: Binding to Z protein in liver and other tissues of the rat. Biochem Biophys Res Commun. 1972 Jun 9;47(5):997–1003.

112. Ockner RK, Manning JA, Poppenhausen RB, Ho WKL. A Binding Protein for Fatty Acids in Cytosol of Intestinal Mucosa, Liver, Myocardium, and Other Tissues. Science (80-) [Internet]. 1972 Jul 7 [cited 2021 Jul 30];177(4043):56–8. Available from: https://science.sciencemag.org/content/177/4043/56

113. Pepino MY, Kuda O, Samovski D, Abumrad NA. Structure-Function of CD36 and Importance of Fatty Acid Signal Transduction in Fat Metabolism. Annu Rev Nutr [Internet]. 2014 Jul 17;34(1):281–303. Available from: http://www.annualreviews.org/doi/10.1146/annurev-nutr-071812-161220

114. Tang Q-Q, Zhang J-W, Daniel Lane M. Sequential gene promoter interactions by C/EBPβ, C/EBPα, and PPARγ during adipogenesis. Biochem Biophys Res Commun [Internet]. 2004 May 21 [cited 2021 Jul 30];318(1):213–8. Available from: https://pubmed.ncbi.nlm.nih.gov/15110775/

115. Wu LE, Samocha-Bonet D, Whitworth PT, Fazakerley DJ, Turner N, Biden TJ, et al. Identification of fatty acid binding protein 4 as an adipokine that regulates insulin secretion during obesity. Mol Metab [Internet]. 2014;3(4):465–73. Available from: http://dx.doi.org/10.1016/j.molmet.2014.02.005

116. Wu Z, Rosen ED, Brun R, Hauser S, Adelmant G, Troy AE, et al. Cross-regulation of C/EBPα and PPARγ controls the transcriptional pathway of adipogenesis and insulin sensitivity. Vol. 3, Molecular Cell. 1999. p. 151–8.

117. Durandt C, van Vollenstee FA, Dessels C, Kallmeyer K, de Villiers D, Murdoch C, et al. Novel flow cytometric approach for the detection of adipocyte subpopulations during adipogenesis. J Lipid Res [Internet]. 2016;57(4):729–42. Available from: http://www.ncbi.nlm.nih.gov/pubmed/26830859%5Cnhttp://www.pubmedcentral.nih.gov/articlerender.fcgi?artid=PMC4808761

118. Dessels C, Pepper MS. Reference Gene Expression in Adipose-Derived Stromal Cells Undergoing Adipogenic Differentiation. Tissue Eng - Part C Methods.

2019;25(6):353–66.

119. Sensebé L, Bourin P, Tarte K. Good manufacturing practices production of mesenchymal stem/stromal cells. Hum Gene Ther. 2011;22(1):19–26.

120. Van Der Valk J, Mellor D, Brands R, Fischer R, Gruber F, Gstraunthaler G, et al. The humane collection of fetal bovine serum and possibilities for serum-free cell and tissue culture. Toxicol Vitr. 2004;18(1):1–12.

121. Heger J, Pastuschek J, Fröhlich K, Görke LM, Peters S, Markert UR, et al. Human serum – An alternative growth supplement for cell culture? J Reprod Immunol [Internet]. 2016;115:78–9. Available from: http://linkinghub.elsevier.com/retrieve/pii/S0165037816303382

122. van der Valk J, Brunner D, De Smet K, Fex Svenningsen Å, Honegger P, Knudsen LE, et al. Optimization of chemically defined cell culture media - Replacing fetal bovine serum in mammalian in vitro methods. Toxicol Vitr [Internet]. 2010;24(4):1053–63. Available from: http://dx.doi.org/10.1016/j.tiv.2010.03.016

123. Basu D, Kulkarni R. Overview of blood components and their preparation. Indian J Anaesth. 2014;58(5):529–37.

124. Hoffbrand, A.V; Moss PA. Essential Haematology. 6th ed. WILEY-BLACKWELL; 2011. 454 p.

125. American Society of Hematology. Hematology Glossary [Internet]. 2021 [cited 2021 Dec 8]. Available from: https://www.hematology.org/education/patients/blood-basics

126. Koellensperger E, von Heimburg D, Markowicz M, Pallua N. Human Serum from Platelet-Poor Plasma for the Culture of Primary Human Preadipocytes. Stem Cells [Internet]. 2006;24(5):1218–25. Available from: http://doi.wiley.com/10.1634/stemcells.2005-0020

127. Oikonomopoulos A, van Deen WK, Manansala A, Lacey PN, Tomakili TA, Ziman A, et al. Optimization of human mesenchymal stem cell manufacturing: the effects of animal/xeno-free media. Sci Rep [Internet]. 2015 Dec 13;5(1):16570.

Available from: http://dx.doi.org/10.1038/srep16570

128. Pham P Van, Bui KH, Ngo DQ, Vu NB, Truong NH, Phan NL, et al. Activated platelet-rich plasma improves adipose-derived stem cell transplantation efficiency in injured articular cartilage. Stem Cell Res Ther. 2013;4(91):1–11.

129. Simon CD, Perkins J, Barras P, Eastridge B, Blackbourne LH. Fresh frozen plasma. US Army Med Dep J [Internet]. 2009;64–7. Available from: http://www.ncbi.nlm.nih.gov/pubmed/20088049

130. Trojahn Kølle SF, Oliveri RS, Glovinski P V., Kirchhoff M, Mathiasen AB, Elberg JJ, et al. Pooled human platelet lysate versus fetal bovine serum-investigating the proliferation rate, chromosome stability and angiogenic potential of human adipose tissue-derived stem cells intended for clinical use. Cytotherapy [Internet]. 2013;15(9):1086–97. Available from: http://dx.doi.org/10.1016/j.jcyt.2013.01.217

131. Bieback K, Hecker A, Schlechter T, Hofmann I, Brousos N, Redmer T, et al. Replicative aging and differentiation potential of human adipose tissue-derived mesenchymal stromal cells expanded in pooled human or fetal bovine serum. Cytotherapy [Internet]. 2012 May;14(5):570–83. Available from: https://linkinghub.elsevier.com/retrieve/pii/S1465324912706709

132. Bernardo ME, Avanzini MA, Perotti C, Cometa AM, Moretta A, Lenta E, et al. Optimization of in vitro expansion of human multipotent mesenchymal stromal cells for cell-therapy approaches: Further insights in the search for a fetal calf serum substitute. J Cell Physiol [Internet]. 2007 Apr;211(1):121–30. Available from: http://doi.wiley.com/10.1002/jcp.20911

133. Bernardo ME, Cometa AM, Pagliara D, Vinti L, Rossi F, Cristantielli R, et al. Ex vivo expansion of mesenchymal stromal cells. Best Pract Res Clin Haematol [Internet]. 2011;24(1):73–81. Available from: http://dx.doi.org/10.1016/j.beha.2010.11.002

134. Chieregato K, Castegnaro S, Madeo D, Astori G, Pegoraro M, Rodeghiero F. Epidermal growth factor, basic fibroblast growth factor and platelet-derived growth factor-bb can substitute for fetal bovine serum and compete with human

platelet-rich plasma in the ex vivo expansion of mesenchymal stromal cells derived from adipose tiss. Cytotherapy [Internet]. 2011;13(8):933–43. Available from: http://dx.doi.org/10.3109/14653249.2011.583232

135. Vogel A, Ross R, Raines E. Role of serum components in density-dependent inhibition of growth of cells in culture: J Cell Biol. 1980;85(2):377–85.

136. O'Shaughnessy DF, Atterbury C, Bolton Maggs P, Murphy M, Thomas D, Yates S, et al. Guidelines for the use of fresh-frozen plasma, cryoprecipitate and cryosupernatant. Br J Haematol [Internet]. 2004 Jul;126(1):11–28. Available from: http://doi.wiley.com/10.1111/j.1365-2141.2004.04972.x

137. Bieback K, Fernandez-Muñoz B, Pati S, Schäfer R. Gaps in the knowledge of human platelet lysate as a cell culture supplement for cell therapy: a joint publication from the AABB and the International Society for Cell & Gene Therapy. Transfusion. 2019;59(11):3448–60.

138. Alves R, Grimalt R. A Review of Platelet-Rich Plasma: History, Biology, Mechanism of Action, and Classification. Ski Appendage Disord [Internet]. 2018;4(1):18–24. Available from: https://www.karger.com/Article/FullText/477353

139. Schallmoser K, Strunk D. Generation of a Pool of Human Platelet Lysate and Efficient Use in Cell Culture. In: Helgason CD, Miller CL, editors. Methods in Molecular Biology [Internet]. Springer Science; 2014. p. 349–62. Available from: http://www.verlag-hanshuber.com/zeitschriften/doi.php?doi=10.1027/0838-1925.17.6.228

140. Hassis ME, Niles RK, Braten MN, Albertolle ME, Ewa Witkowska H, Hubel CA, et al. Evaluating the effects of preanalytical variables on the stability of the human plasma proteome. Anal Biochem [Internet]. 2015 Jun;478:14–22. Available from: http://linkinghub.elsevier.com/retrieve/pii/S0003269715001001

141. Cates NC, Oakley DJ, Onwuemene OA. Therapeutic white blood cell and platelet depletions using the spectra OPTIA system continuous mononuclear cell protocol. J Clin Apher [Internet]. 2018 Oct;33(5):580–5. Available from: https://linkinghub.elsevier.com/retrieve/pii/S0031938416312148

142. Wolmarans E. Characterisation of adipose-derived stromal cell heterogeneity. 2019. 240 p.

143. Schallmoser K, Strunk D. Preparation of Pooled Human Platelet Lysate (pHPL) as an Efficient Supplement for Animal Serum-Free Human Stem Cell Cultures. J Vis Exp [Internet]. 2009 Oct 30;(32):20–3. Available from: http://www.jove.com/index/Details.stp?ID=1523

144. Rapodile T, van den Berg K. South African National Blood Service Guidelines for Medical Assessment of Blood Donors [Internet]. 2019. p. 148. Available from: https://sanbs.org.za/wp-content/uploads/2019/04/48545-SANBS-Guidelines-for-Medical-Assessent-of-blood-March.pdf

145. Pavlovic V, Ciric M, Jovanovic V, Stojanovic P. Platelet Rich Plasma: a short overview of certain bioactive components. Open Med [Internet]. 2016 Jan 1;11(1):242–7. Available from: https://www.degruyter.com/view/j/med.2016.11.issue-1/med-2016-0048/med-2016-0048.xml

146. Sultan A. Five-minute preparation of platelet-poor plasma for routine coagulation testing. East Mediterr Heal J. 2010 Feb;16(2):233–6.

147. Simon TL, McCullough J, Snyder EL, Solheim BG, Strauss RG, editors. Rossi's Principles of Transfusion Medicine [Internet]. 5th ed. Oxford: WILEY-BLACKWELL; 2016. 754 p. Available from: https://www.wiley.com/en-us/Rossi%27s+Principles+of+Transfusion+Medicine%2C+5th+Edition-p-9781119012993

148. Acebes-Huerta A, Arias-Fernández T, Bernardo Á, Muñoz-Turrillas MC, Fernández-Fuertes J, Seghatchian J, et al. Platelet-derived bio-products: Classification update, applications, concerns and new perspectives. Transfus Apher Sci [Internet]. 2020 Feb;59(1):102716. Available from: https://doi.org/10.1016/j.transci.2019.102716

149. Snyder EL. Prevention of HLA alloimmunization: Role of leukocyte depletion and UV-B irradiation. Yale J Biol Med. 1990;63(5):419–27.

150. Schmidt M, Spengler H, Lambrecht B, Hourfar MK, Seifried E, Tonn T. A new one-platform flow cytometric method for residual cell counting in platelet concentrates. Transfusion [Internet]. 2009 Jul 22;49(12):2604–11. Available from: http://doi.wiley.com/10.1111/j.1537-2995.2009.02326.x

151. Lambrecht B, Spengler H-PP, Nauwelaers F, Bauerfeind U, Mohr H, Muller TH, et al. Flow cytometric assay for the simultaneous determination of residual white blood cells, red blood cells, and platelets in fresh-frozen plasma: Validation and two years' experience. Transfusion. 2009 Jun;49(6):1195–204.

152. Loza-Correa M, Perkins H, Kumaran D, Kou Y, Qaisar R, Geelhood S, et al. Noninvasive pH monitoring for bacterial detection in platelet concentrates. Transfusion [Internet]. 2016 Jun;56(6):1348–55. Available from: http://doi.wiley.com/10.1111/trf.13557

153. Adan A, Alizada G, Kiraz Y, Baran Y, Nalbant A. Flow cytometry: basic principles and applications. Crit Rev Biotechnol [Internet]. 2017 Feb 17;37(2):163–76. Available from: https://www.tandfonline.com/doi/full/10.3109/07388551.2015.1128876

154. BioLegend. Spectra Analyzer [Internet]. [cited 2021 Mar 8]. Available from: https://www.biolegend.com/en-us/spectra-analyzer

155. Roy J Carver Biotechnology Center Univerity of Illinois. Flow Cytometry Protocols: Cell Counting [Internet]. [cited 2021 Mar 11]. Available from: https://biotech.illinois.edu/flowcytometry/protocols/cell-counting

156. Ramström S, Södergren A, Tynngård N, Lindahl T. Platelet Function Determined by Flow Cytometry: New Perspectives? Semin Thromb Hemost [Internet]. 2016 Feb 17;42(03):268–81. Available from: http://www.thieme-connect.de/DOI/DOI?10.1055/s-0035-1570082

157. Dessels C, Durandt C, Pepper MS. Comparison of human platelet lysate alternatives using expired and freshly isolated platelet concentrates for adipose-derived stromal cell expansion. Platelets [Internet]. 2018 Apr 3;30(3):356–67. Available from: https://www.tandfonline.com/doi/full/10.1080/09537104.2018.1445840

158. South African National Blood Service. Clinical guidelines for the use of blood products in South Africa [Internet]. 2014. p. 87. Available from: https://www.wcbs.org.za/village/wpbnew/sites/default/files/clinical_guidelines_5th Edition_2014.pdf

159. Kobolak J, Dinnyes A, Memic A, Khademhosseini A, Mobasheri A. Mesenchymal stem cells: Identification, phenotypic characterization, biological properties and potential for regenerative medicine through biomaterial micro-engineering of their niche. Methods [Internet]. 2016;99:62–8. Available from: http://dx.doi.org/10.1016/j.ymeth.2015.09.016

160. Bieback K. Platelet Lysate as Replacement for Fetal Bovine Serum in Mesenchymal Stromal Cell Cultures. Transfus Med Hemotherapy [Internet]. 2013;40(5):326–35. Available from: https://www.karger.com/Article/FullText/354061

161. Pu LLQ, Coleman SR, Cui X, Ferguson REH, Vasconez HC. Autologous fat grafts harvested and refined by the coleman technique: A comparative study. Plast Reconstr Surg. 2008;122(3):932–7.

162. ThermoFisher Scientific. TrypLE™ Express Enzyme (1X), no phenol red [Internet]. [cited 2021 Feb 11]. Available from: https://www.thermofisher.com/order/catalog/product/12604021#/12604021

163. D'Agostino RBS, Sullivan LM, Beiser AS. Introductory Applied Biostatistics. Crockett C, editor. Belmont: Brooks/Cole Cengage learning; 2006. 1–628 p.

164. Glen S. "Dunn's test: Definition" From StatisticsHowTo.com: Elementary Statistics for the rest of us! [Internet]. [cited 2021 Mar 11]. Available from: https://www.statisticshowto.com/dunns-test/

165. Skehan P, Storeng R, Scudiero D, Monks A, McMahon J, Vistica D, et al. New Colorimetric Cytotoxicity Assay for Anticancer-Drug Screening. JNCI J Natl Cancer Inst [Internet]. 1990 Jul 4 [cited 2018 Mar 19];82(13):1107–12. Available from: https://academic.oup.com/jnci/article-lookup/doi/10.1093/jnci/82.13.1107

166. Vichai V, Kirtikara K. Sulforhodamine B colorimetric assay for cytotoxicity

screening. Nat Protoc [Internet]. 2006 Aug 17;1(3):1112–6. Available from: http://www.nature.com/articles/nprot.2006.179

167. Orellana E, Kasinski A. Sulforhodamine B (SRB) Assay in Cell Culture to Investigate Cell Proliferation. Bio-Protocol [Internet]. 2016;6(21):1–7. Available from: http://www.bio-protocol.org/e1984

168. Vitro Vivo Biotechnology. SRB Cell Growth Assay Kit [Internet]. p. 1–2. Available from: www.vitrovivo.com

169. Needleman SB, Romberg RW. Limits of linearity and detection for some drugs of abuse. J Anal Toxicol. 1990;14(1):34–8.

170. Oldekop M-L. Estimating the linear range: Validation of liquid chromatography mass spectrometry (LC-MS) methods (analytical chemistry) course [Internet]. [cited 2021 Feb 26]. Available from: https://sisu.ut.ee/lcms_method_validation/33-estimating-linear-range

171. Czapla J, Matuszczak S, Kulik K, Wiśniewska E, Pilny E, Jarosz-Biej M, et al. The effect of culture media on large-scale expansion and characteristic of adipose tissue-derived mesenchymal stromal cells. Stem Cell Res Ther. 2019;10(1):1–11.

172. Choi J, Chung JH, Kwon GY, Kim KW, Kim S, Chang H. Effectiveness of autologous serum as an alternative to fetal bovine serum in adipose-derived stem cell engineering. Cell Tissue Bank. 2013;14(3):413–22.

173. Felthaus O, Prantl L, Skaff-Schwarze M, Klein S, Anker A, Ranieri M, et al. Effects of different concentrations of Platelet-rich Plasma and Platelet-Poor Plasma on vitality and differentiation of autologous Adipose tissue-derived stem cells. Clin Hemorheol Microcirc [Internet]. 2017 May 5;66(1):47–55. Available from: 0

174. Riis S, Nielsen FM, Pennisi CP, Zachar V, Fink T. Comparative Analysis of Media and Supplements on Initiation and Expansion of Adipose-Derived Stem Cells. Stem Cell Transl Med [Internet]. 2016 Mar;5(3):314–24. Available from: http://doi.wiley.com/10.5966/sctm.2015-0127

175. Majd H, Quinn TM, Wipff P-J, Hinz B. Dynamic Expansion Culture for

Mesenchymal Stem Cells. In: Methods in molecular biology (Clifton, NJ) [Internet]. 2011. p. 175–88. Available from: http://link.springer.com/10.1007/978-1-60761-999-4_12

176. Liao HT, James IB, Marra KG, Rubin JP. The Effects of Platelet-Rich Plasma on Cell Proliferation and Adipogenic Potential of Adipose-Derived Stem Cells. Tissue Eng - Part A. 2015;21(21–22):2714–22.

177. Schafer KA. The Cell Cycle: A Review. Vet Pathol [Internet]. 1998 Nov 26;35(6):461–78. Available from: http://journals.sagepub.com/doi/10.1177/030098589803500601

178. Liu L, Michowski W, Kolodziejczyk A, Sicinski P. The cell cycle in stem cell proliferation, pluripotency and differentiation. Nat Cell Biol [Internet]. 2019;21(9):1060–7. Available from: http://dx.doi.org/10.1038/s41556-019-0384-4

179. Kanduc D, Mittelman A, Serpico R, Sinigaglia E, Sinha A, Natale C, et al. Cell death: Apoptosis versus necrosis (Review). Int J Oncol [Internet]. 2002 Jul 1;21(1):165–70. Available from: http://www.spandidos-publications.com/10.3892/ijo.21.1.165

180. ThermoFisher Scientific. Vybrant® DyeCycle™ Ruby stain | Thermo Fisher Scientific - ZA [Internet]. 2008 [cited 2021 Mar 24]. Available from: https://www.thermofisher.com/za/en/home/references/protocols/cell-and-tissue-analysis/flow-cytometry-protocol/cell-cycle-analysis/vybrant-dyecycle-ruby-stain.html

181. Donnenberg AD, Meyer EM, Rubin JP, Donnenberg VS. The cell-surface proteome of cultured adipose stromal cells. Cytom Part A. 2015;87(7):665–74.

182. Chazotte B. Labeling Nuclear DNA Using DAPI. Cold Spring Harb Protoc [Internet]. 2011 Jan 1 [cited 2021 May 18];80–2. Available from: www.cshprotocols.orghttp://cshprotocols.cshlp.org/Downloadedfromwww.cshprotocols.org

183. Tanious FA, Veal JM, Buczak H, Ratmeyer LS, Wilson WD. DAPI (4',6-diamidino-

2-phenylindole) binds differently to DNA and RNA: minor-groove binding at AT sites and intercalation at AU sites. Biochemistry [Internet]. 1992 Mar 31 [cited 2021 May 19];31(12):3103–12. Available from: https://pubs.acs.org/doi/abs/10.1021/bi00127a010

184. Invitrogen. FITC Annexin V/Dead Cell Apoptosis Kit with FITC annexin V and PI, for Flow Cytometry [Internet]. 2010. Available from: https://www.thermofisher.com/order/catalog/product/V13242#/V13242

185. Willemsen JCN, Spiekman M, Stevens HPJ, Van Der Lei B, Harmsen MC. Platelet-Rich Plasma Influences Expansion and Paracrine Function of Adipose-Derived Stromal Cells in a Dose-Dependent Fashion. Plast Reconstr Surg. 2016;137(3):554e-565e.

186. Cowper M, Frazier T, Wu X, Curley J, Ma M, Mohiuddin O, et al. Human Platelet Lysate as a Functional Substitute for Fetal Bovine Serum in the Culture of Human Adipose Derived Stromal/Stem Cells. Cells. 2019;8(7):724.

187. D'Esposito V, Passaretti F, Perruolo G, Ambrosio MR, Valentino R, Oriente F, et al. Platelet-Rich Plasma Increases Growth and Motility of Adipose Tissue-Derived Mesenchymal Stem Cells and Controls Adipocyte Secretory Function. J Cell Biochem. 2015;116(10):2408–18.

188. Laner-Plamberger S, Oeller M, Mrazek C, Hartl A, Sonderegger A, Rohde E, et al. Upregulation of mitotic bookmarking factors during enhanced proliferation of human stromal cells in human platelet lysate. J Transl Med [Internet]. 2019 Dec 30;17(1):432. Available from: https://translational-medicine.biomedcentral.com/articles/10.1186/s12967-019-02183-0

189. Kakudo N, Morimoto N, Ma Y, Kusumoto K. Differences between the Proliferative Effects of Human Platelet Lysate and Fetal Bovine Serum on Human Adipose-Derived Stem Cells. Cells. 2019;8(10).

190. Lindroos B, Aho KL, Kuokkanen H, Räty S, Huhtala H, Lemponen R, et al. Differential gene expression in adipose stem cells cultured in allogeneic human serum versus fetal bovine serum. Tissue Eng - Part A. 2010;16(7):2281–94.

191. Liumbruno G, Bennardello F, Lattanzio A, Piccoli P, Rossetti G. Recommendations for the transfusion of plasma and platelets. Blood Transfus. 2009;7(2):132–50.

192. Rieger AM, Nelson KL, Konowalchuk JD, Barreda DR. Modified Annexin V/Propidium Iodide Apoptosis Assay For Accurate Assessment of Cell Death. J Vis Exp [Internet]. 2011 [cited 2021 Mar 26];(50):3–6. Available from: http://www.jove.com/index/Details.stp?ID=2597

193. Cholewa D, Stieh T, Schellenberg A, Bokermann G, Joussen S, Koch C, et al. Expansion of adipose mesenchymal stromal cells is affected by human platelet lysate and plating density. Cell Transplant. 2011;20(9):1409–22.

194. Sanderson MJ, Smith I, Parker I, Bootman MD. Fluorescence Microscopy. Cold Spring Harb Protoc [Internet]. 2014 Oct 1;2014(10):pdb.top071795-pdb.top071795. Available from: http://www.cshprotocols.org/cgi/doi/10.1101/pdb.top071795

195. Greenspan P, Mayer EP, Fowler SD. Nile red: a selective fluorescent stain for intracellular lipid droplets. J Cell Biol [Internet]. 1985 Mar 1;100(3):965–73. Available from: https://rupress.org/jcb/article/100/3/965/21349/Nile-red-a-selective-fluorescent-stain-for

196. Ma X, Wang D, Zhao W, Xu L. Deciphering the roles of PPARγ in adipocytes via dynamic change of transcription complex. Vol. 9, Frontiers in Endocrinology. 2018.

197. Aldridge A, Kouroupis D, Churchman S, English A, Ingham E, Jones E. Assay validation for the assessment of adipogenesis of multipotential stromal cells—a direct comparison of four different methods. Cytotherapy [Internet]. 2013 Jan;15(1):89–101. Available from: http://dx.doi.org/10.1016/j.jcyt.2012.07.001

198. Fowler SD, Greenspan P. Application of Nile Red, a Fluorescent Hydrophobic Probe, for the Detection of Neutral Lipid Deposits in Tissue Sections: Comparison with Oil Red O. J Histochem Cytochem. 1985;33(8):883–836.

199. Arya M, Shergill IS, Williamson M, Gommersall L, Arya N, Patel HRH. Basic

principles of real-time quantitative PCR. Expert Rev Mol Diagn [Internet]. 2005 Mar 9;5(2):209–19. Available from: http://www.tandfonline.com/doi/full/10.1586/14737159.5.2.209

200. Cao H, Shockey JM. Comparison of TaqMan and SYBR Green qPCR Methods for Quantitative Gene Expression in Tung Tree Tissues. J Agric Food Chem [Internet]. 2012 Dec 19;60(50):12296–303. Available from: https://pubs.acs.org/doi/10.1021/jf304690e

201. Schneeberger C, Speiser P, Kury F, Zeillinger R. Quantitative detection of reverse transcriptase-PCR products by means of a novel and sensitive DNA stain. Genome Res [Internet]. 1995 Feb 1;4(4):234–8. Available from: http://www.genome.org/cgi/doi/10.1101/gr.4.4.234

202. Fink T, Lund P, Pilgaard L, Rasmussen J, Duroux M, Zachar V. Instability of standard PCR reference genes in adipose-derived stem cells during propagation, differentiation and hypoxic exposure. BMC Mol Biol [Internet]. 2008;9(1):98. Available from: http://bmcmolbiol.biomedcentral.com/articles/10.1186/1471-2199-9-98

203. Li X, Yang Q, Bai J, Xuan Y, Wang Y. Identification of appropriate reference genes for human mesenchymal stem cell analysis by quantitative real-time PCR. Biotechnol Lett [Internet]. 2015 Jan 2;37(1):67–73. Available from: http://link.springer.com/10.1007/s10529-014-1652-9

204. Rao X, Huang X, Zhou Z, Lin X. An improvement of the 2ˆ(-delta delta CT) method for quantitative real-time polymerase chain reaction data analysis. Biostat Bioinforma Biomath [Internet]. 2013 Aug;3(3):71–85. Available from: http://www.ncbi.nlm.nih.gov/pubmed/25558171%0Ahttp://www.pubmedcentral.nih.gov/articlerender.fcgi?artid=PMC4280562

205. Chignon-Sicard B, Kouidhi M, Yao X, Delerue-Audegond A, Villageois P, Peraldi P, et al. Platelet-rich plasma respectively reduces and promotes adipogenic and myofibroblastic differentiation of human adipose-derived stromal cells via the TGFβ signalling pathway. Sci Rep [Internet]. 2017 Dec 7;7(1):2954. Available from: http://www.nature.com/articles/s41598-017-03113-0

206. Bieback K, Ha VA-T, Hecker A, Grassl M, Kinzebach S, Solz H, et al. Altered Gene Expression in Human Adipose Stem Cells Cultured with Fetal Bovine Serum Compared to Human Supplements. Tissue Eng Part A [Internet]. 2010 Nov;16(11):3467–84. Available from: https://www.liebertpub.com/doi/10.1089/ten.tea.2009.0727

207. Mangum LH, Natesan S, Stone R, Wrice NL, Larson DA, Florell KF, et al. Tissue Source and Cell Expansion Condition Influence Phenotypic Changes of Adipose-Derived Stem Cells. Stem Cells Int. 2017;2017.

208. Lim MH, Ong WK, Sugii S. The current landscape of adipose-derived stem cells in clinical applications. Expert Rev Mol Med [Internet]. 2014 May 7;16(4):e8. Available from: http://www.liebertonline.com/doi/abs/10.1089/ten.tea.2010.0661

209. Bustin SA, Benes V, Garson JA, Hellemans J, Huggett J, Kubista M, et al. The MIQE Guidelines: Minimum Information for Publication of Quantitative Real-Time PCR Experiments. 2009 [cited 2021 Aug 7]; Available from: http://www.mibbi.org

210. Thermo Fisher Scientific - NanoDrop Products. Technical Bulletin: Assessment of Nucleic Acid Purity [Internet]. Wilmington; [cited 2021 Aug 10]. p. 2. Available from: www.nanodrop.com

211. Taylor S, Wakem M, Dijkman G, Alsarraj M, Nguyen M. A practical approach to RT-qPCR—Publishing data that conform to the MIQE guidelines. Methods. 2010 Apr 1;50(4):S1–5.

212. Padhi BK, Singh M, Rosales M, Pelletier G, Cakmak S. A PCR-based quantitative assay for the evaluation of mRNA integrity in rat samples. Biomol Detect Quantif [Internet]. 2018 May 1 [cited 2021 Aug 10];15:18–23. Available from: https://linkinghub.elsevier.com/retrieve/pii/S2214753517302176

213. Andersen CL, Jensen JL, Ørntoft TF. Normalization of Real-Time Quantitative Reverse Transcription-PCR Data: A Model-Based Variance Estimation Approach to Identify Genes Suited for Normalization, Applied to Bladder and Colon Cancer Data Sets. Cancer Res [Internet]. 2004 Aug 1 [cited 2021 Aug 10];64(15):5245–50. Available from: https://cancerres.aacrjournals.org/content/64/15/5245

Appendix A: MIQE Guidelines

A. Introduction

The Minimal Information for Publications of Quantitative Real-Time PCR Experiments (MIQE) is a set of guidelines to ensure publishing of accurate, reliable, and reproducible qPCR data. The MIQE guidelines should be included in any manuscript that contains qPCR data which contains a set of essential and desired criteria (209). The MIQE guidelines arose from necessity as misleading, irreproducible, and inconsistent results were published which had a negative impact on drug developments, disease monitoring, and research.

In this study RT-qPCR was used to determine the expression of six target genes: C/EBPα and β, PPARγ, FABP4, AdipoQ, and CD36 involved in adipogenesis. The MIQE guidelines checklist was used to assess the quality of the results.

B. Experimental design

Cryopreserved hASCs were seeded at a density of 5000 cells/cm^2 in 75 cm^2 (T75) cell culture flasks and expanded in the various supplemented CGM (FBS, pHPL, PRP) to 50-60% confluence. On induction day, the CGM was aspirated and discarded. Fresh CGM of each supplemented medium was added to the corresponding control group (referred to as the non-induced group). Adipogenic induction medium of the supplemented media was added to the corresponding experimental (induced group) group. The control/non-induced groups were maintained in CGM in parallel with the experimental/induced groups. Adipogenic potential was assessed on induction day (day 0) and day 14 post induction.

Three hASC biological replicates were used for each medium supplement resulting in n=3 for FBS, n=3 for pHPL, and n=9 for PRP (PRP 1, PRP 2, and PRP 3 supplemented media added to three biological hASC replicates, thus 3 × 3).

Table A 1: Experimental layout of flasks for RT-qPCR RNA extraction.

	PRP 3			PRP 2			PRP 1			pHPL			FBS		
hASC	1	2	3	1	2	3	1	2	3	1	2	3	1	2	3
Day 0	1×T75	1×T75	1×T75	1×T75	1×T75	1×T75	1×T75	1×T75	1×T75	1×T75	1×T75	1×T75	1×T75	1×T75	1×T75
Day 14	NI: 1×T75 I: 2×T75	NI: 1×T75 I: 2×T75	NI: 1×T75 I: 2×T75	NI: 1×T75 I: 2×T75	NI: 1×T75 I: 2×T75	NI: 1×T75 I: 2×T75	NI: 1×T75 I: 2×T75	NI: 1×T75 I: 2×T75	NI: 1×T75 I: 2×T75	NI: 1×T75 I: 2×T75	NI: 1×T75 I: 2×T75	NI: 1×T75 I: 2×T75	NI: 1×T75 I: 2×T75	NI: 1×T75 I: 2×T75	NI: 1×T75 I: 2×T75
Total (n)	9									3			3		

C. Samples

C.1. Description

RNA was extracted from induced and non-induced cells for all supplemented media on days 0 and 14.

The day 0 samples were untreated, non-induced hASCs expanded in either FBS, pHPL, or PRP until 50-60% confluence.

The day 14 induced samples were hASCs expanded to 50-60% confluence in the various media before induction with adipogenic media containing the respective supplements and maintained for 14 days.

They day 14 non-induced samples were hASCs expanded to 50-60% confluence in the various media and left to expand parallel to induced cultures as controls. The medium was complete medium containing the same concentration of the respective supplements as the adipogenic medium without the adipogenic cocktail.

C.2. Microdissection or macrodissection

No microdissection or microdissection were done on samples

C.3. Processing

The samples were processed as described in Chapter 7, section 7.2.1and 7.2.4.

C.4. If frozen – how and how quickly?

hASCs were frozen in liquid nitrogen after isolation from lipoaspirate before expansion. All hASCs used in this study were cryopreserved for long term storage in liquid nitrogen. None of the samples were subjected to freeze-thawing during expansion and differentiation.

C.5. If fixed – how and how quickly?

The samples were not fixed.

C.6. Storage

The samples were not stored prior to RNA isolation. The RNA was isolated from hASCs directly after dissociation on day 0 and 14 and then stored at -80°C until used for cDNA synthesis.

D. Nucleic acid extraction

Total RNA was extracted as described in Chapter 7 section 7.2.4.1.

D.1. DNase or RNase treatment

No DNase or RNase treatment was performed.

D.2. Contamination assessment

Genomic DNA (gDNA) contamination was assessed using the no reverse transcription controls (NoRTs) generated during cDNA synthesis as described in Chapter 7, section 7.2.4.4. The reference gene YWHAZ was used and a positive control for all NoRT amplification reactions was included containing a cDNA synthesis where reverse transcriptase was added. Amplification was detected in some of the samples and subsequently a Cq cut-off = 33 was determined

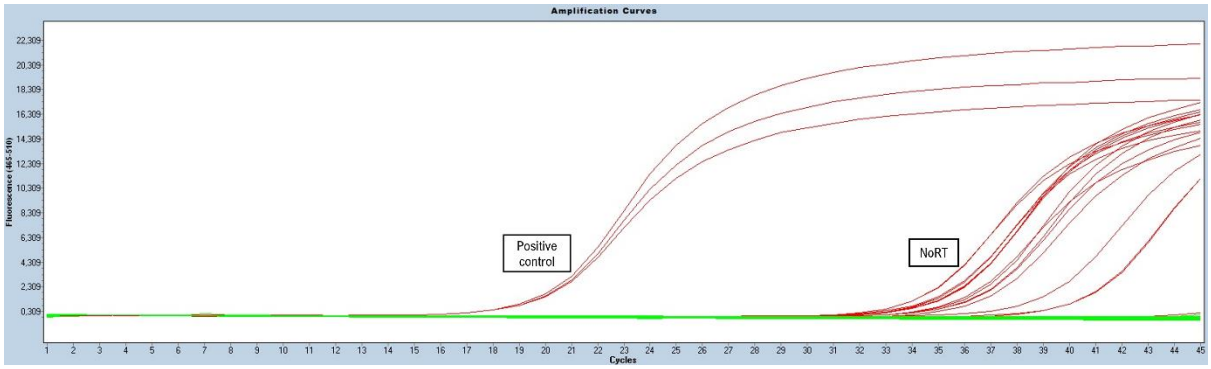

Figure A 1: Representative amplification plot for NoRT controls.
The reference gene YWAZ was used as a positive control with 20ng/µL template, using a total of 40ng per reaction (Mean Cq = 19.86, n=3). Some amplification was detected in the NoRT controls after which a Cq = 33 cut-off was determined. Samples with a NoRT Cq value < 33 were excluded from analysis as any amplification may be due to gDNA contamination.

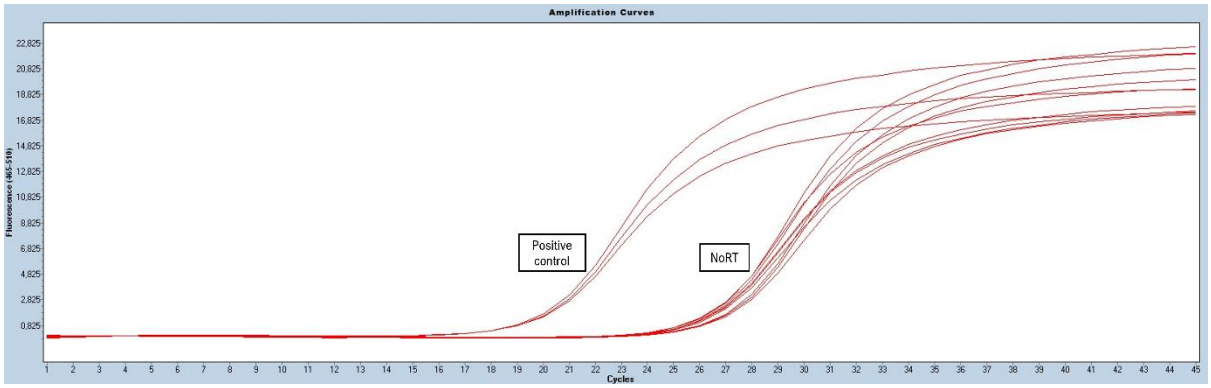

Figure A 2: Representative amplification plot for NoRT controls of a sample that was excluded due to gDNA contamination.
Samples with a NoRT Cq < 33 were excluded from analysis as amplification of target genes may be as a result of gDNA contamination. YWHAZ was used with a positive control Cq value = 19.86.

D.3. Nucleic acid quantification and purity

A Nanodrop ND 1000 spectrophotometer (Thermo Fisher Scientific, Waltham, MA, USA) was used to measure RNA concentration (ng/µL) and quality (A260/280). RNA quality (A260/280) ratio of 1.8-2.1 is accepted as pure for downstream applications (210,211). An A260/280 ratio outside the 1.8-2.1 range suggests contaminants in the sample. All extracted RNA samples had a A260/280 ratio within the 1.8-2.1 range.

Table A 2: RNA quality (A260/280) and quantity (ng/µL) for two hASC cultures.

	Supplement	Timepoint	Quality (A260/280)	Concentration (ng/µL)
Culture 1	FBS	Day 0	1.94	48.12
		Day 14 NI	2.04	347.1
		Day 14 I	2.06	343.1
	pHPL	Day 0	2.04	369.26
		Day 14 NI	2.08	329.12
		Day 14 I	2.06	647.69
	PRP1	Day 0	2.02	393
		Day 14 NI	2.05	409.75
		Day 14 I	2.06	710.06
	PRP2	Day 0	2.05	351.83
		Day 14 NI	2.08	309.84
		Day 14 I	2.06	594.72
	PRP3	Day 0	2.05	255.7
		Day 14 NI	2.1	812
		Day 14 I	2.01	476.5

	Supplement	Timepoint	Quality (A260/280)	Concentration (ng/µL)
Culture 2	FBS	Day 0	2.06	102.32
		Day 14 NI	2.04	380.1
		Day 14 I	2.04	385.1
	pHPL	Day 0	2.08	182.2
		Day 14 NI	2.05	204.25
		Day 14 I	2.09	632.53
	PRP1	Day 0	2.07	248.8
		Day 14 NI	2.05	325.59
		Day 14 I	2.09	616.19
	PRP2	Day 0	2.05	291.63
		Day 14 NI	2.08	805.21
		Day 14 I	2.06	313.62
	PRP3	Day 0	2.07	258.7
		Day 14 NI	2.08	274.7
		Day 14 I	2.04	622.38

Table A 3: RNA quality (A260/280) and quantity (ng/µL) for the third hASC culture.

	Supplement	Timepoint	Quality (A260/280)	Concentration (ng/µL)
Culture 3	FBS	Day 0	2.03	57.12
		Day 14 NI	2.02	436.5
		Day 14 I	2.06	321.2
	pHPL	Day 0	2.07	177.8
		Day 14 NI	2.04	395.9
		Day 14 I	2.08	648.3
	PRP1	Day 0	2.08	140.9
		Day 14 NI	2.01	795.4
		Day 14 I	2.08	461.9
	PRP2	Day 0	2.06	184.7
		Day 14 NI	2.09	1022.7
		Day 14 I	2.08	541.7
	PRP3	Day 0	2.09	149.6
		Day 14 NI	2.1	578.9
		Day 14 I	2.1	958.3

D.4. RNA integrity

Isolated RNA integrity was determined using a TapeStation® 2200 platform (Agilent Technologies, CA, USA) along with the RNA Screen Tape® (Agilent Technologies, CA, USA) and sample buffer (Agilent Technologies, CA, USA). A RINe value ≥ 8 indicates intact, high-quality RNA (212).

The manufacturer instruction for sample preparation was followed. Briefly, 5 µL sample buffer was added to 1 µL of RNA with a concentration between 25-500 ng/µL as specified by the manufacturer. The sample was then transferred to a thermal cycler (Gene Amp® PCR 28 syster 9700, Applied Biosystems, Life Technologies®, Thermo Fisher Scientific, CA, USA) where it was heated for 3 min at 72°C and cooled on ice for 2 min before analysis in the TapeStation® 2200.

Table A 4: RNA integrity values (RINe).

	Supplement	Timepoint	RINe		Supplement	Timepoint	RINe		Supplement	Timepoint	RINe
Culture 1	FBS	Day 0	9.5	Culture 2	FBS	Day 0	10	Culture 3	FBS	Day 0	9.7
		Day 14 NI	9.8			Day 14 NI	9.9			Day 14 NI	10
		Day 14 I	9.5			Day 14 I	9.8			Day 14 I	9.7
	pHPL	Day 0	9.9		pHPL	Day 0	9.9		pHPL	Day 0	9.9
		Day 14 NI	9.9			Day 14 NI	10			Day 14 NI	9.9
		Day 14 I	9.6			Day 14 I	9.7			Day 14 I	10
	PRP1	Day 0	9.9		PRP1	Day 0	9.9		PRP1	Day 0	10
		Day 14 NI	9.4			Day 14 NI	9.7			Day 14 NI	9.5
		Day 14 I	9.4			Day 14 I	9.7			Day 14 I	9.5
	PRP2	Day 0	9.9		PRP2	Day 0	9.9		PRP2	Day 0	10
		Day 14 NI	9.5			Day 14 NI	9.7			Day 14 NI	9.5
		Day 14 I	9.5			Day 14 I	9.9			Day 14 I	9.7
	PRP3	Day 0	9.9		PRP3	Day 0	9.9		PRP3	Day 0	9.5
		Day 14 NI	9.5			Day 14 NI	9.7			Day 14 NI	9.6
		Day 14 I	9.3			Day 14 I	9.8			Day 14 I	9.7

D.5. Inhibition testing

No inhibition testing was performed.

E. Reverse Transcription

Reverse transcription was performed as described in Chapter 7 section 7.2.4.2. No information is given for the reverse transcriptase by the kit manufacturer except: “One unit catalyzes the incorporation of 1 nmol of dTTP into acid-insoluble material in 10 minutes at 37 ºC in 50 mM Tris-HCl, pH 8.6, 40 mM KCl, 1 mM MnSO4, 1 mM DTT, and 0.5 mM [3H]TTP, using 200 µM oligo(dT)12-18-primed poly(A)n as template.”

E.1. cDNA quantification and purity

The total cDNA quantity (ng) and quality (A260/280) was measured using a Nanodrop ND 1000 spectrophotometer. An A260/280 ratio of ~1.8 is accepted as pure for DNA (210,211).

Table A 5: cDNA quantity and purity

	Supplement	Timepoint	cDNA 260/280	Total cDNA (ng)
Culture 1	pHPL	D0	1.79	1460
		D14 NI	1.79	1200
		D14 I	1.81	1033.6
	PRP1	D0	1.81	1366.1
		D14 NI	1.84	1167.5
		D14 I	1.8	1386.4
	PRP2	D0	1.82	1141.7
		D14 NI	1.8	1336.6
		D14 I	1.79	1269.6
	PRP3	D0	1.76	1014
		D14 NI	1.84	1163.4
		D14 I	1.83	1179.5
	FBS	D0	1.84	894.1
		D14 NI	1.87	1147.2
		D14 I	1.85	1174.5
Culture 2	pHPL	D0	1.84	1074.6
		D14 NI	1.84	1114.7
		D14 I	1.85	1097.6
	PRP1	D0	1.83	1305.7
		D14 NI	1.81	1180.7
		D14 I	1.82	1198.7
	PRP2	D0	1.85	1048.5
		D14 NI	1.8	1489.9
		D14 I	1.81	1286.5
	PRP3	D0	1.83	1528.8
		D14 NI	1.8	1178.8
		D14 I	1.83	1357.7
	FBS	D0	1.83	908
		D14 NI	1.85	1386.6
		D14 I	1.87	1082.1

	Supplement	Timepoint	cDNA 260/280	Total cDNA (ng)
Culture 3	pHPL	D0	1.82	1090.6
		D14 NI	1.83	995.7
		D14 I	1.84	1280.3
	PRP1	D0	1.83	1200.2
		D14 NI	1.85	1055.6
		D14 I	1.81	1117.3
	PRP2	D0	1.82	1127.9
		D14 NI	1.82	1553.6
		D14 I	1.81	1558.4
	PRP3	D0	1.8	1625
		D14 NI	1.81	1307.1

	D14 I	1.83	1188.6
	D0	1.86	1110.8
FBS	D14 NI	1.83	1076.3
	D14 I	1.86	1102.1

E.2. Quantitation cycle (Cq) values with and without reverse transcriptase (RT)

Table A 6: Quantitation cycle values of NoRT controls.

NRT	Cq	Excluded?	NRT	Cq	Excluded?	NRT	Cq	Excluded?
A1	0		B1	38.09		C1	28.41	Excluded
A2	0		B2	0		C2	29.20	Excluded
A3	0		B3	0		C3	28.43	Excluded
A4	0		B4	0		C4	34.16	
A5	0		B5	40		C5	34.89	
A6	0		B6	0		C6	35.53	
A7	34.49		B7	0		C7	33.39	
A8	0		B8	40		C8	37.67	
A9	36.49		B9	0		C9	34.62	
A10	34.67		B10	35.24		C10	34.69	
A11	0		B11	28.65	Excluded	C11	27.43	Excluded
A12	0		B12	30.80	Excluded	C12	28.67	Excluded
D1	36.94		B13	36.93		C13	35.47	
D2	35.06		B14	35.44		C14	35.50	
D3	35.61		B15	35.96		C15	33.57	
Positive Control						19.86		

gDNA contamination is present in some of the samples. Samples with a NoRT Cq < 33 were excluded from analysis resulting in the total biological replicates summarised in Table 7.4, Chapter 7, section 7.3. NoRTs of samples that were included amplified more than 10 cycles later after the positive control (YWHAZ, mean Cq = 19.86).

E.3. cDNA storage

The cDNA was stored at -20°C until it was used in RT-qPCR reactions.

F. qPCR target information

The target genes and reference genes accession numbers and amplicon locations and lengths are listed in Table A 7.

Table A 7: Target and reference gene accession numbers and amplicon information.

Genes of interest					
Gene name		Accession number	Amplicon length	Start	Stop
CCAAT/Enhancer-binding protein alpha	C/EBPα	NM_001285829	119	2235	2353
CCAAT/Enhancer-binding protein beta	C/EBPβ	NM_005194.4	104	1423	1526
Peroxisome proliferator-activated receptor gamma	PPARγ	NM_001354666.3	124	441	564
Fatty-acid binding protein 4	FABP4	NM_001442.3	126	369	494
Adiponectin	AdipoQ	NM_001177800.2	135	3346	3480
Cluster of differentiation 36	CD36	NM_001001548.3	122	1185	1306
TATA-binding protein	TBP	NM_001172085.2	130	602	731
Peptidylprolyl Isomerase A	PPIA	NM_001300981.2	116	918	1033
Tyrosine 3-Monooxygenase/Tryptophan 5-Monooxygenase Activation Protein, Zeta	YWHAZ	NM_001135699.2	126	2237	2362

F.1. In silico specificity screen

The specificity of the primers was tested using the *in silico* website NCBI BLAST® software. Primers were excluded if they returned a match other than the target sequence.

F.2. Primer locations

The primer locations were visualised using NCBI Primer-BLAST® (website) and are seen in Figure A 3.

F.3. Splice variants targeted

No splice variants were targeted.

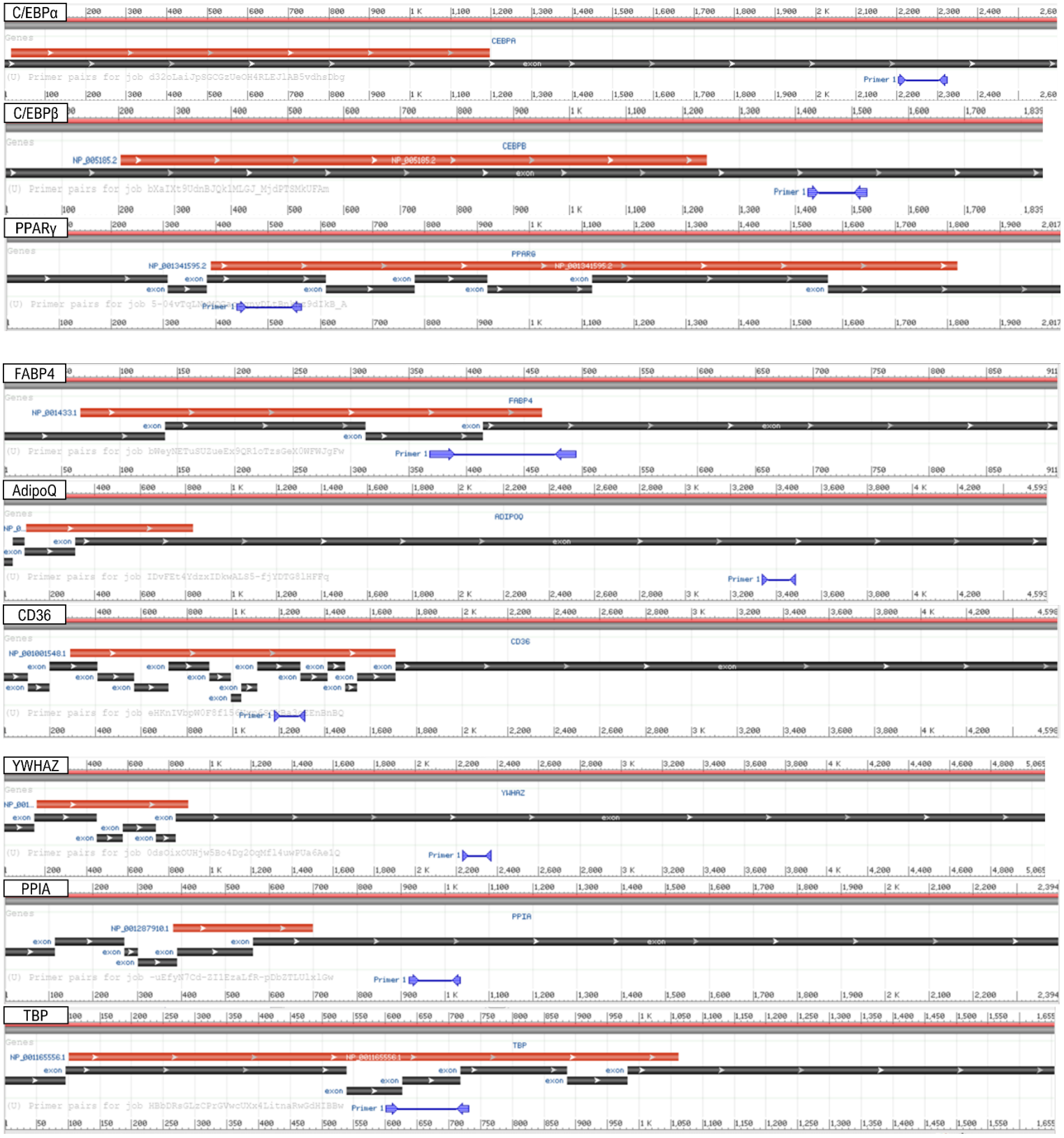

Figure A 3: Primer locations of genes of interest and reference genes.

G. qPCR oligonucleotides

The primer sequences of the target and reference genes are listed in Table 7.3 in Chapter 7, section 7.2.4.3.

G.1. Location and identity of any modifications

No modifications were made.

G.2. Manufacturer of oligonucelotides

The oligonucleotides were manufactured by Integrated DNA Technologies (IDT, Coralville, IA, USA).

H. RT-qPCR protocol

RT-qPCR was performed as described in Chapter 7, section 7.2.4.3.

H.1. Polymerase identity and concentration

The LightCycler® 480 SYBR Green I Master Mix was used which contains the FastStart™ Taq DNA Polymerase (Roche, Basel, Switzerland). No concentration was provided.

H.2. Buffer/kit identity and manufacturer

The LightCycler® 480 SYBR Green I Master Mix (Roche, Basel, Switzerland; catalogue number: 04887352001) was used in all qPCR reactions.

H.3. Additives

No additives were used

H.4. Manufacturer of plates/tubes and catalogue numbers

LightCycler® 480 Multiwell Plate 96 white plates (Roche, Basel, Switzerland; Catalogue number: 0472962001) were used for all qPCR reactions.

H.5. Munfacturer of qPCR instrument

All qPCR reactions were performed on the LightCycler® 480 II instrument (Roche, Basel, Switzerland).

I. qPCR Validation

I.1. Specificity

The specificity of the qPCR reactions was determined using melt curves performed at the end of each run. Melt curves will show primer dimers, secondary product, and contamination as additional peaks before or after the melting temperature (T_m) peak. Primer dimers will result in a shoulder before the main T_m peak with gDNA contamination showing as a shoulder after the main T_m peak. Representative images of the melt curves are displayed in Figure A 4.

C/EBPβ

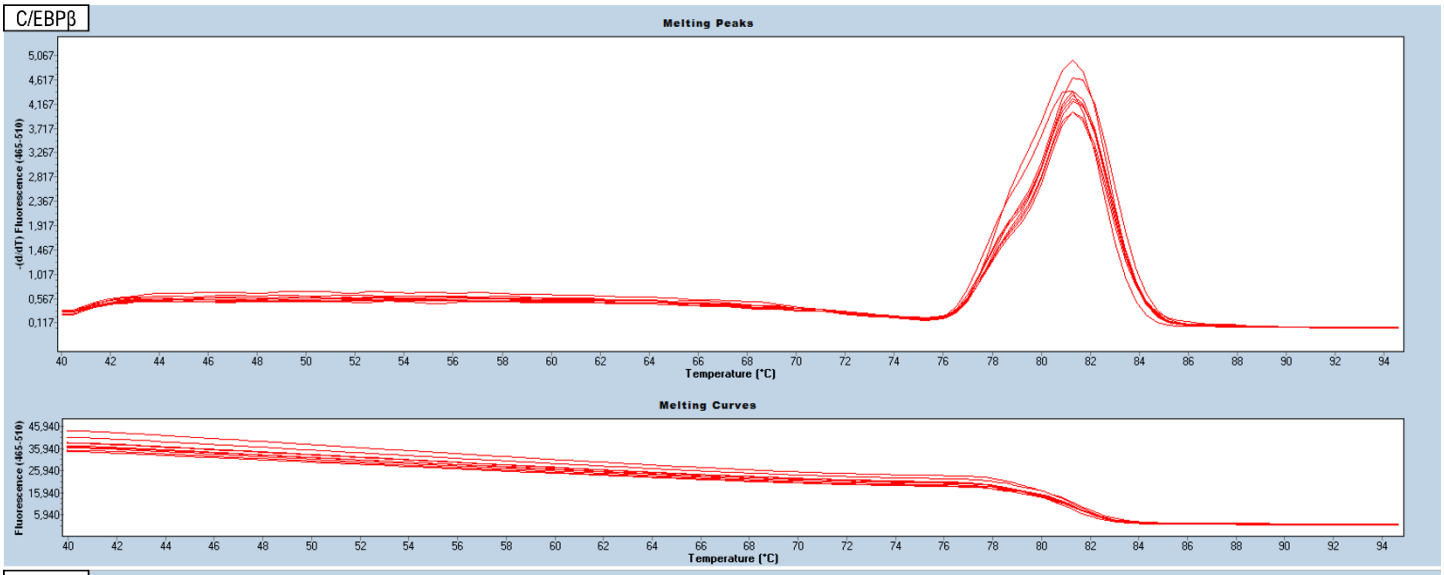

PPARγ

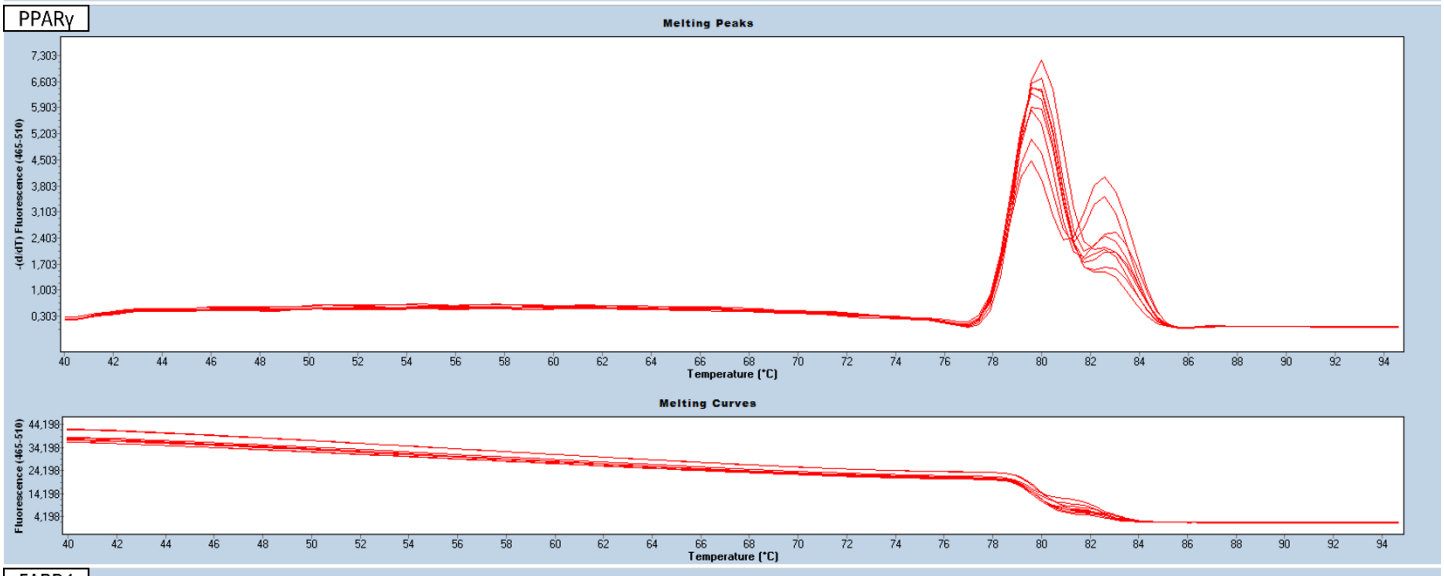

FABP4

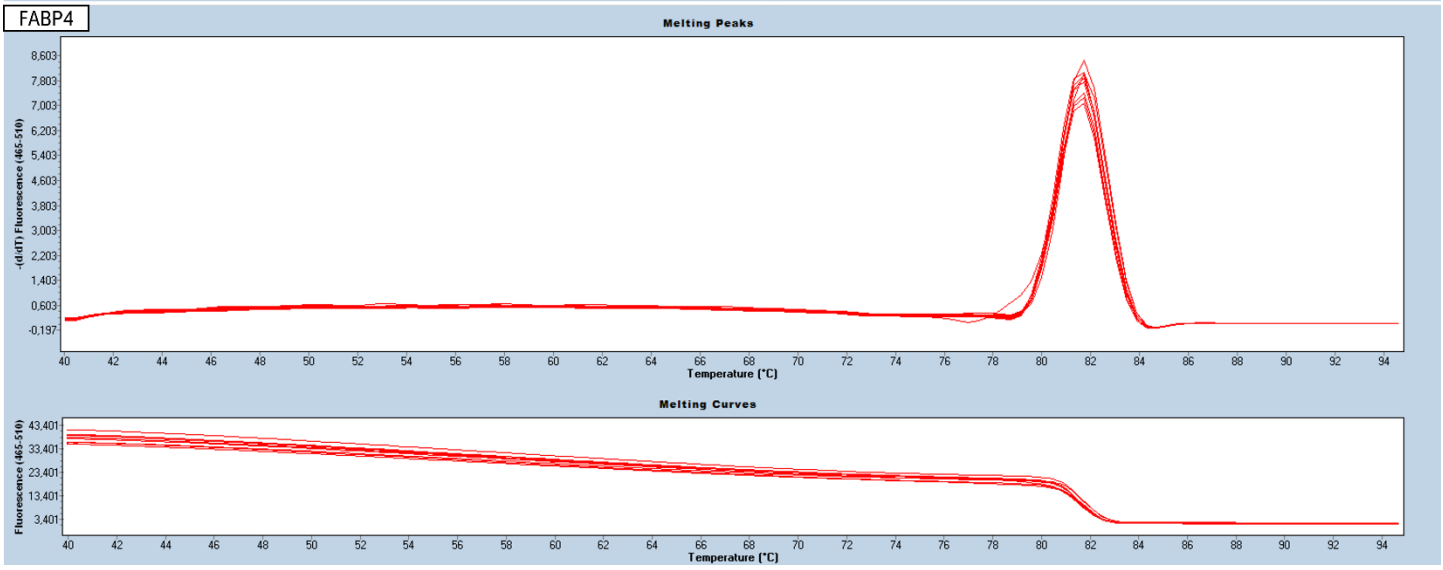

AdipoQ

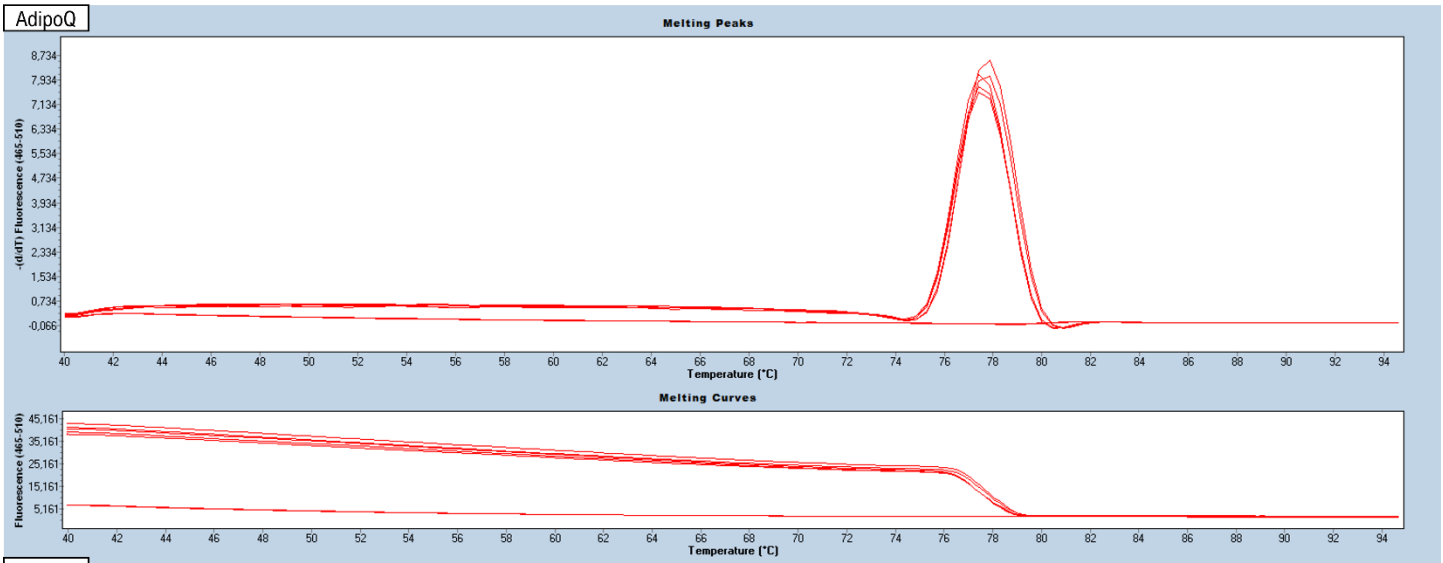
Melting Peaks
-(d/dT) Fluorescence (465-510)
8,734
7,934
7,134
6,334
5,534
4,734
3,934
3,134
2,334
1,534
0,734
-0,066
40 42 44 46 48 50 52 54 56 58 60 62 64 66 68 70 72 74 76 78 80 82 84 86 88 90 92 94
Temperature (°C)

Melting Curves
Fluorescence (465-510)
45,161
35,161
25,161
15,161
5,161
40 42 44 46 48 50 52 54 56 58 60 62 64 66 68 70 72 74 76 78 80 82 84 86 88 90 92 94
Temperature (°C)

CD36

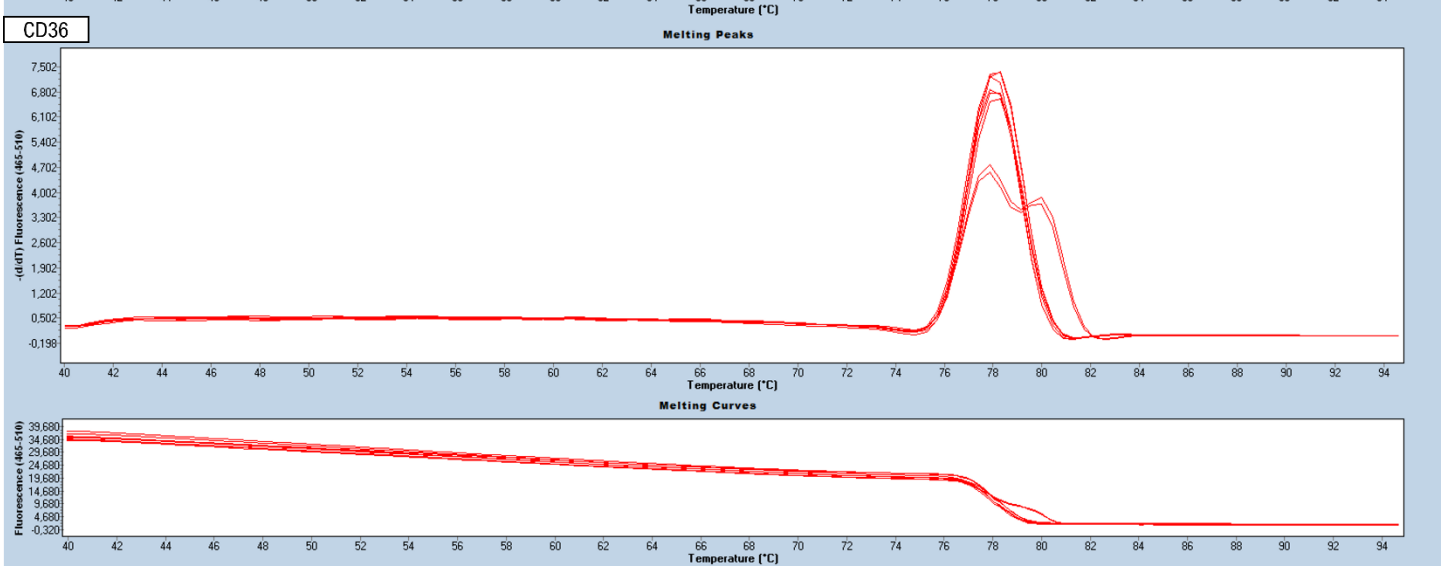
Melting Peaks
-(d/dT) Fluorescence (465-510)
7,502
6,802
6,102
5,402
4,702
4,002
3,302
2,602
1,902
1,202
0,502
-0,198
40 42 44 46 48 50 52 54 56 58 60 62 64 66 68 70 72 74 76 78 80 82 84 86 88 90 92 94
Temperature (°C)

Melting Curves
Fluorescence (465-510)
39,680
34,680
29,680
24,680
19,680
14,680
9,680
4,680
-0,320
40 42 44 46 48 50 52 54 56 58 60 62 64 66 68 70 72 74 76 78 80 82 84 86 88 90 92 94
Temperature (°C)

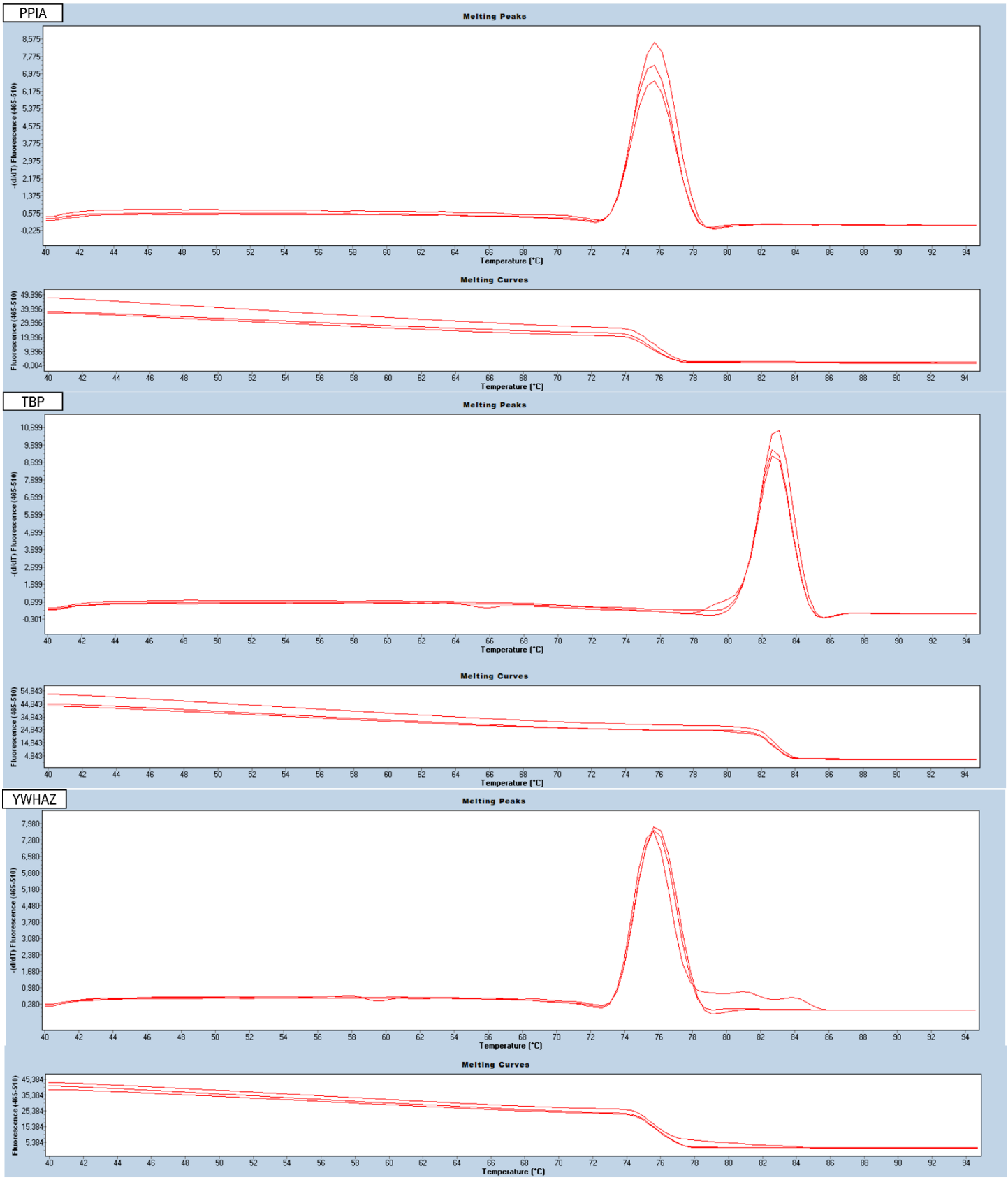

Figure A 4: Representative images of melt curves and melt peaks for genes of interest and reference genes.
Melt curves (bottom) and melt peaks (top) were used to test the specificity of the reactions by determining the presence of secondary products, contamination of primer dimers.

No template controls (NTCs)

For each target gene NTCs (three technical replicates) were included on each plate. If amplification was detected in NTCs, the plate was rerun.

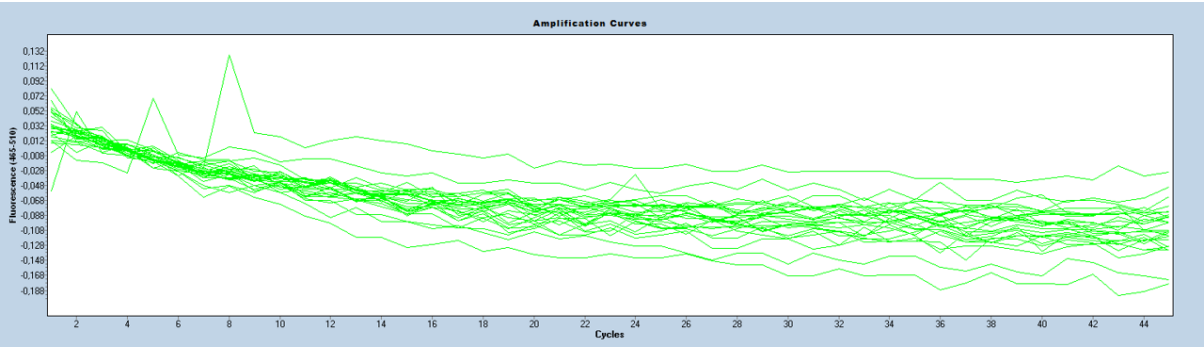

Figure A 5: Representative image of amplification in NTC reactions.

I.2. Standard curves

Standard curves for each primer could not be completed due to insufficient RNA.

I.3. Linear dynamic range

Linear dynamic range was not determined as no standard curves could be completed.

I.4. Quantitation cycle values variation at lower limit

The variation for the lower limit (lowest concentration on the standard curve) was not determined as standard curves could not be completed.

I.5. Evidence of limit of detection

Limit of detection was not performed. Cq values ≤ 33 were viewed as acceptable. Cq values > 33 were excluded as it was not deemed trustworthy.

I.6. If multiplex, efficiency and LOD for each assay

No multiplexing was performed in this study.

J. Data analysis

J.1. qPCR analysis program

The LightCycler® Software (version 1.5.1; Roches, Basel, Switzerland) was used for data analysis.

J.2. Quantitiation cycle (Cq) method determination

Cq values were determind using the second derivative maximum method according to the LightCycler® Software and algorithms.

J.3. Results of no template controls (NTCs)

NTC reactions had a Cq value of zero. Representative image for NTCs can be seen in Figure A 5.

J.4. Justification of number and choice of reference genes

This study used three reference genes (TBP, PPIA, and YWHAZ) previously identified as suitable for the experimental conditions in this study (118,202,203) as well as independent studies completed by members of the ICMM (Ms Carla Dessels, Ms Carina da Silva, and Dr Chrisna Durandt).

The stability of the three reference genes was confirmed in PRP-supplemented medium using NormFinder for R, version 5 (213). Three PRP-supplemented medium biological replicates were used and reactions for day 0, day 14 non-induced, and day 14 induced were done in triplicate for all three chosen reference genes. NormFinder returned the stability values for TBP, YWHAZ, PPIA as 0.45, 0.49, and 1.08 respectively. Stability values closer to zero are indicative of more stable expression. PPIA is the least stably expressed reference gene but was deemed suitable for this study. One might consider including more timepoints and biological replicates to further investigate the stable expression of the three reference genes in PRP-supplemented medium under adipogenesis conditions.

J.5. Normalisation method

The Cq values of the target genes were normalised by subtracting the geometric mean of the Cq values of the three reference genes from both the experimental and control group Cq values. The experimental group samples were then normalised to the control

group samples by subtracting the Cq values of the not induced (control group) samples from the Cq values of the induced (experimental group).

J.6. Number of biological replicates

A complete layout of the biological replicates can be found in Table 7.4 in Chapter 7, section 7.3.

J.7. Number and stage (RT or qPCR) of technical replicates

Three technical repeats (three separate wells) were done for each reaction on the qPCR plate using the samples cDNA.

J.8. Repeatability (intra-assay variation)

A standard deviation of 1 or less between technical replicates was considered repeatable.

J.9. Statistics

Statistical analysis was performed using R (version 4.0.3) and RStudio (version 1.4.1103). The significance level was set at $\alpha = 0.05$. The Kruskal-Wallis test was used to test for significance between groups. If significance was found, the Dunn's post-hoc test with Bonferroni correction for multiple sampling was performed.

Appendix B: Ethics documentation

UNIVERSITEIT VAN PRETORIA
UNIVERSITY OF PRETORIA
YUNIBESITHI YA PRETORIA

Faculty of Health Sciences

Institution: The Research Ethics Committee, Faculty Health Sciences, University of Pretoria complies with ICH-GCP guidelines and has US Federal wide Assurance.

- FWA 00002567, Approved dd 22 May 2002 and Expires 03/20/2022.
- IORG #: IORG0001762 OMB No. 0990-0279 Approved for use through February 28, 2022 and Expires: 03/04/2023.

22 January 2021

Approval Certificate
Annual Renewal

Ethics Reference No.: 424/2018
Title: Human alternatives to foetal bovine serum for the expansion of human adipose-derived stem cells

Dear Ms AR Gerber

The **Annual Renewal** as supported by documents received between 2021-01-05 and 2021-01-20 for your research, was approved by the Faculty of Health Sciences Research Ethics Committee on 2021-01-20 as resolved by its quorate meeting.

Please note the following about your ethics approval:

- Renewal of ethics approval is valid for 1 year, subsequent annual renewal will become due on 2022-01-22.
- Please remember to use your protocol number (424/2018) on any documents or correspondence with the Research Ethics Committee regarding your research.
- Please note that the Research Ethics Committee may ask further questions, seek additional information, require further modification, monitor the conduct of your research, or suspend or withdraw ethics approval.

Ethics approval is subject to the following:

- The ethics approval is conditional on the research being conducted as stipulated by the details of all documents submitted to the Committee. In the event that a further need arises to change who the investigators are, the methods or any other aspect, such changes must be submitted as an Amendment for approval by the Committee.

We wish you the best with your research.

Yours sincerely

Dr R Sommers
MBChB MMed (Int) MPharmMed PhD
Deputy Chairperson of the Faculty of Health Sciences Research Ethics Committee, University of Pretoria

The Faculty of Health Sciences Research Ethics Committee complies with the SA National Act 61 of 2003 as it pertains to health research and the United States Code of Federal Regulations Title 45 and 46. This committee abides by the ethical norms and principles for research, established by the Declaration of Helsinki, the South African Medical Research Council Guidelines as well as the Guidelines for Ethical Research: Principles Structures and Processes, Second Edition 2015 (Department of Health)

Research Ethics Committee
Room 4-60, Level 4, Tswelopele Building
University of Pretoria, Private Bag x323
Gezina 0031, South Africa
Tel +27 (0)12 356 3084
Email: deepeka.behari@up.ac.za
www.up.ac.za

Fakulteit Gesondheidswetenskappe
Lefapha la Disaense tša Maphelo

Postal Address: Private Bag X14, Weltevreden Park, 1715
Tel: 011 761 9000 **Email**: customerservice@sanbs.org.za

SOUTH AFRICAN NATIONAL BLOOD SERVICE NPC

NPO Number: 049066NPO
NPC Registration No. 2000/026390/08

Human Research Ethics Committee

OHRP Number : IORG0006278
FWA Registration Number : IRB00007553
SA NHREC Registration Number : REC-270606-013

Secretariat: Tel: 011 761 9033 | Valencia.Simmadari@sanbs.org.za

24th March 2020

To : Prof. M Pepper

E-mail : michael.pepper@up.ac.za

Dear Prof. Pepper,

ACKNOWLEDGEMENT OF RECEIPT OF NOTIFICATION

HREC REFERENCE NUMBER : 2013/17

PROTOCOL TITLE : Expansion of human mesenchymal stromal cells: human alternatives to foetal bovine serum

SANBS HREC hereby acknowledges receipt of your email dated 23rd March 2020, in which HREC was notified of the proposed changes to the above-named protocol.

The amendments to be made to the protocol are as per respective supporting documentation.

Your requests for the above changes were accompanied by the following documents

1. SANBS Protocol Extension Pepper UP Cover Letter
2. SANBS Protocol Extension Pepper UP

These documents were reviewed by the Chairman of SANBS HREC who accepted and approved the proposed changes.

Yours sincerely

VJSimmadari

Valencia Simmadari
SANBS HREC Secretariat

Universal Blood Type
O-
Donates to ..... Everyone
Receives from .....

SOUTH AFRICAN NATIONAL BLOOD SERVICE NPC

Human Research Ethics Committee

OHRP Number : IORG0006278
FWA Registration Number : IRB00007553
SA NHREC Registration Number : REC-270606-013

SANBS
South African National Blood Service
Association Incorporated Under Section 21
Registration No: 2000/028390/08

Secretariat: Tel: 011 761 9135 | Fax: 011 761 9137 | Cell: 082 523 8523 | felicity.lew@sanbs.org.za

8 February 2018

Dr Michael Peper
Email : Michael.pepper@up.ac.za

Dear Dr Pepper,

ACKNOWLEDGEMENT OF RECEIPT OF NOTIFICATION AND APPROVAL

HREC REFERENCE NUMBER : 2013/17

PROTOCOL TITLE : Expansion of human adipose-derived stem cells: Human Alternatives to foetal bovine serum.

SANBS HREC hereby acknowledges receipt of your email dated 19 January 2018 in which HREC was notified of the proposed changes to the above-named protocol:-

Amendment: Addition of two new Investigators

Your requests for the below changes were accompanied by the following documents:

1. CV for Anastasios Athanasiadis; and
2. CV Aurono Gerber.

These documents were reviewed by the Chairman of SANBS HREC who accepted and approved the proposed changes.

The proposed changes are necessary and approved and can be implemented immediately.

Yours sincerely

Felicity Lew
SANBS HREC Secretariat

Human Research Ethics Committee

OHRP Number : IORG0006278
FWA Registration Number : IRB00007553
SA NHREC Registration Number : REC-270606-013

SANBS
South African National Blood Service

Secretariat: Tel: 011 761 9135 | Fax: 011 761 9137 | Cell: 082 523 8523 | felicity.lew@sanbs.org.za

15 October 2017

Prof Michael Peper
University of Pretoria
Email : Michael.pepper@up.ac.za

Dear Pepper,

ACKNOWLEDGEMENT OF RECEIPT OF NOTIFICATION AND APPROVAL

HREC REFERENCE NUMBER : 2013/17

PROTOCOL TITLE : Expansion of human adipose-derived stem cells: Human Alternatives to foetal bovine serum.

SANBS HREC hereby acknowledges receipt of your email dated 12 October 2017 in which HREC was notified of the proposed changes to the above-named protocol:-

Amendment: Human Alternative Production

The human products will be collected and manufactured with the collaboration of the of the Specialized Therapeutics Services (STS) division of the South African National Blood Service (SANBS).

The pHPL product was previously obtained from the blood of healthy donors supplied by SANBS. This was performed as a MSc project undertaken by Ms. Carla Dessels (UP Ethics number 421/2013 and SANBS ethics approval number 2013/17). The remaining pHPL product is stored at the laboratories of the Institute for Cellular and Molecular Medicine (ICMM) and will be made use of during this study.

FFP is a product routinely made by SANBS and will be purchased from them. The line manager will ensure feasibility of all products and will send through all results from their in-house quality control checks. The products obtained from SANBS will be frozen at -25°C and stored until future use.

The HS, PRP and PPP will be obtained from healthy blood donors, who have given informed consent with the help of the Specialized Therapeutics Services (STS) division of SANBS. The donors that adhere to the project selection criteria (males, blood groups O- and AB-) will be recruited by SANBS from the SANBS donor list. Every donor will be assigned a reference number by SANBS that will be used to identify the sample thereby providing anonymity. All patient information will be kept confidential.

Prior to the collection of the products, the donors will be invited to attend an information session in which the research project, for which their blood donations will be used, will be explained. The collection procedure of the blood products will also be explained during this session. After the information session, all donors will complete the standard SANBS blood donation questionnaire and a blood sample will be taken from each donor by a trained SANBS nurse. This will also allow the SANBS nurse to do a peripheral vein assessment. The blood sample and the peripheral vein assessment will be used to determine the suitability of the donor for the study. The blood samples will be tested for HIV, hepatitis B and C and any other infectious diseases that the investigators might deem necessary.

All blood samples and blood donations will be taken at the University of Pretoria's Clinical Research Unit (CRU); Room 2-54, Floor 2, Pathology Building, Prishof Campus. The CRU will provide us with space and beds for the donors and will ensure that there will be oxygen and the necessary resuscitation equipment available in case of emergencies. There will also be a doctor on stand-by at all times during the collection procedure. The donors will be allowed to withdraw from the study at any time point.

For the collection of HS, the donors will be required to donate a standard whole blood unit (approximate 200 mL), which will be collected in a dry pack. For PRP and PPP, 200mL of blood products will be collected from each donor via the Spectra Optia® Apheresis System, which will be operated by a trained SANBS nurse. After collection, SANBS will do in-house quality control checks of all products obtained and will send through all results to the researchers.

Your requests for the above changes were accompanied by the following documents

1. Human Alternative Project Amendment doc (Stipulated above)
2. Feasibility letter Human Alternative MSC
3. Informed consent form Blood Donor.

These documents were reviewed by the Chairman of SANBS HREC who reviewed, accepted and approved the proposed changes.

The proposed changes are necessary and approved and can be implemented immediately.

Yours sincerely

Felicity Lew
SANBS HREC Secretariat